HAL
open science

# Contrôle d'une source d'énergie hybride : Pile à combustible-Supercondensateur

Cinda Luz Sandoval Torres

## To cite this version:

Cinda Luz Sandoval Torres. Contrôle d'une source d'énergie hybride : Pile à combustible-Supercondensateur. Automatique / Robotique. Ecole nationale supérieure d'arts et métiers - ENSAM; Centro Nacional de Investigación y Desarrollo Tecnológico (Cuernavaca, Mor., México), 2016. Français. NNT : 2016ENAM0067 . tel-01513109

**HAL Id: tel-01513109**

**https://pastel.hal.science/tel-01513109v1**

Submitted on 24 Apr 2017

**HAL** is a multi-disciplinary open access archive for the deposit and dissemination of scientific research documents, whether they are published or not. The documents may come from teaching and research institutions in France or abroad, or from public or private research centers.

L'archive ouverte pluridisciplinaire **HAL**, est destinée au dépôt et à la diffusion de documents scientifiques de niveau recherche, publiés ou non, émanant des établissements d'enseignement et de recherche français ou étrangers, des laboratoires publics ou privés.

2016-ENAM-0067

École doctorale n° 432 : Sciences des Métiers de l'ingénieur

# Doctorat ParisTech

# T H È S E

**pour obtenir le grade de docteur délivré par**

## l'École Nationale Supérieure d'Arts et Métiers

**Spécialité "Automatique "**

*présentée et soutenue publiquement par*

**Cinda Luz SANDOVAL TORRES**

Le 16 Décembre 2016

# Contrôle d'une source d'énergie hybride : Pile à combustible-Supercondensateur

Directeur de thèse : **Jean-Claude CARMONA**
Co-encadrement de la thèse : **Victor M. ALVARADO**

**Jury**

| | |
|---|---|
| **M. Abdelaziz HAMZAOUI**, Pr, IUT de Troyes | Rapporteur |
| **M. Ulises CANO CASTILLO**, Pr, INEEL, Cuernavaca | Rapporteur |
| **M. Jean-Claude CARMONA**, Pr, ENSAM | Examinateur |
| **M. Victor M. ALVARADO**, Pr, CENIDET, Cuernavaca | Examinateur |

T H È S E

**Arts et Métiers Paris Tech Campus de Aix-en-Provence**
**Nom de l'Unité de recherche**

# CONTROLE D'UNE SOURCE D'ENERGIE HYBRIDE : PILE A COMBUSTIBLE-SUPERCONDENSATEUR


## RESUME:

Cette thèse s'inscrit dans le cadre de conception d'une stratégie de gestion de l'énergie dans un système hybride de génération d'énergie électrique composé d'une pile à combustible (PC) et un module de supercondensateurs (SC). La source hybride fournit une puissance maximale de 1,2 kW et sa conception implique des décisions concernant la sélection de l'architecture du système hybride ainsi que le choix de la topologie et le dimensionnement d'une unité de convertisseurs. La stratégie de gestion vise à satisfaire la demande d'énergie électrique de la charge et favoriser la consommation énergétique efficiente ; sa performance est évaluée en développant un simulateur qui comprend la dynamique des éléments mis en jeu : deux sources et l'unité de convertisseurs. Le générateur hybride est supposé alimenter un profil de consommation correspondant à un véhicule électrique, de ce fait un cycle standard de conduite en ville en échelle est demandé lors des simulations, ce qui permet d'évaluer la performance du générateur hybride et plus spécifiquement de la stratégie de gestion énergétique.

Dans une première étape de cette thèse, un simulateur intégral a été construit avec des librairies de Simscape. Le simulateur est constitué des blocs de différents domaines, contenant des modèles fondamentaux des composants du système. Le block de pile à combustible modèle la dynamique d'un système BAHIA® (400 W - 1100 W, 0 A - 70 A nominale) et le block de supercondensateur modèle les cycles charge-décharge d'un module Maxwell de 400 F et 16 V. Un onduleur de tension pont complet avec convertisseur élévateur conditionne l'énergie délivrée par la pile à combustible et un convertisseur bidirectionnel (buck-boost) est connecté au module de supercondensateurs afin de conditionner les cycles de charge-décharge. L'unité des convertisseurs a été dimensionnée, puis, un modèle moyen de petits signaux a été formulé afin de décrire la dynamique de ces dispositifs. Les différents composants ont été intégrés dans l'environnement Simulink. Dans une deuxième étape, la stratégie de gestion énergétique a été conçue en considérant les caractéristiques et performances des sources ; le résultat est une stratégie de trois niveaux hiérarchiques, dont l'aspect principal est la définition des lois de commande locales et globale. Dans une troisième étape, le système complet est évalué en termes du niveau d'utilisation des sources, du domaine d'opération de la pile à combustible, et de l'accomplissement des objectifs des commandes locales et global, qui engagent notamment le SOC des supercondensateurs et la régulation de la tension du générateur hybride.



**Mots clés :** Système électrique hybride, Pile à combustible, Supercondensateur


ARTS ET MÉTIERS ParisTech

ParisTech INSTITUT DES SCIENCES ET TECHNOLOGIES PARIS INSTITUTE OF TECHNOLOGY

# CONTRIBUTION TO THE CONTROL OF A HYBRID ENERGY SOURCE BASED ON FUEL CELL UNIT COUPLED TO SUPERCAPACITORS


## ABSTRACT:

Energy generation from fossil fuels combustion is predicted to have severe future impacts in the world's economy and ecology. Fuel cells and supercapacitors are an alternative power source, environmentally friendly.

This dissertation presents a regulation architecture developed to coordinate a hybrid renewable source for typical solicitations of electric vehicles in a scaled operating range of 1 kW. The hybrid system is composed of a Polymer Electrolyte Membrane (PEM) fuel cell module, a supercapacitors bank and their respective power conditioning units. In order to optimize the overall operation, the proposed strategy is organized into three hierarchical levels, and the power demand for each energy source is determined in real time with a basis on a frequency distribution and a cutoff frequency, defined in accordance with the dynamical capabilities of the sources.

Even if numerous researches have been reported on the subject, few studies have taken into account the proper dynamics of each source in order to optimize the global performance of the hybrid power supply.

The goal of this work is to implement a complete simulator integrating not only dynamical models of each energy source, but also dynamical models of the power conditioning units. The control strategy consists of nested loops, arranged in three functional levels of hierarchy. The central idea is to find the optimal set point for each energy source, according to their own physical properties. Contrary to the existing control strategies, this strategy dynamically calculates the appropriate power demand for each energy source. Due to the complexity of the system, cascade control loops are proposed, organized into blocks, according to the system functionality and dynamics.

A functional simulation is obtained, where the system ensures the adequate supercapacitor state of charge and soft current demands to keep the fuel cell working in its safe operating region. Thus, lower fuel consumption and rapid response to load demands are guaranteed to improve efficiency.

Results demonstrate that the control strategy allows the regulation of the DC bus voltage under UDDS and ECE-15 driving cycles as load profiles. The fuel cell works within its maximum efficiency region, without falling in the degradation zone. In addition, the supercapacitor state of charge remains within the recommended range.



**Keywords** : Hybrid electrical system, Fuel Cell, Supercapacitor, Power converters


ARTS ET MÉTIERS ParisTech

ParisTech INSTITUT DES SCIENCES ET TECHNOLOGIES PARIS INSTITUTE OF TECHNOLOGY

# CONTRIBUCION AL CONTROL DE UNA FUENTE DE ENERGÍA HÍBRIDA BASADA EN CELDA DE COMBUSTIBLE ACOPLADA A SUPERCAPACITORES


## RESUMEN:

Es ampliamente conocido que la generación de energía a partir de combustibles fósiles tiene un grave impacto en la ecología, siendo en gran parte culpable del calentamiento global. A raíz de esto, hay que buscar energías de distinta naturaleza, las cuales sean amigables con el medio ambiente.

Esta tesis doctoral presenta la arquitectura de regulación desarrollada para coordinar una fuente de energía híbrida renovable que satisface las demandas de un vehículo eléctrico cuya demanda fue escalada a un rango de operación de 1 kW. El sistema híbrido se compone de una celda de combustible de membrana de intercambio protónico (PEM por sus siglas en inglés), un banco de supercapacitores y las respectivas unidades de acondicionamiento de potencia. Para optimizar la operación general, la estrategia propuesta se organiza en tres niveles jerárquicos mientras que la demanda de energía para cada fuente se determina en tiempo real a partir de la distribución de frecuencias, donde la frecuencia de corte se define de acuerdo a las capacidades dinámicas de las fuentes.

Aun cuando se han reportado numerosas investigaciones al respecto, son pocos los estudios que consideran las dinámicas propias de cada elemento (Celda de combustible, supercapacitor) para optimizar el desempeño global de la fuente de poder híbrida. El objetivo del presente trabajo es implementar un simulador de una fuente de energía híbrida basada en Celda de combustible, la cual integre no sólo los modelos dinámicos de cada fuente de energía, sino que también incluya los modelos dinámicos de las unidades de acondicionamiento de potencia. La estrategia de control consiste en ciclos anidados, organizados en tres niveles jerárquicos funcionales. La idea central es encontrar el punto de consigna central óptimo para cada fuente de energía, de acuerdo con sus propiedades físicas intrínsecas. A diferencia de las estrategias de control existentes, la estrategia propuesta calcula de forma dinámica la demanda de potencia exacta para cada fuente de energía. Debido a la complejidad del sistema, se proponen ciclos de control en cascada, las cuales se organizan en bloques, de acuerdo a la dinámica y funcionalidad del sistema. Se obtiene entonces una simulación funcional, donde el sistema garantiza un estado de carga adecuado para el supercapacitor y demandas de corriente suaves para la celda de combustible, que la mantengan funcionando en la región de operación segura. Así, se garantiza un bajo consumo de combustible y una respuesta rápida a las demandas de la carga para mejorar su eficiencia.

Los resultados demuestran que la estrategia de control permite la regulación del bus de Tensión en CD bajo los perfiles de ciclo de manejo UDDS y ECE-15. Lo anterior operando la celda de combustible en la región de máxima eficiencia y evitando caer en la zona de degradación. Adicionalmente, el estado de carga del capacitor se mantiene dentro del rango recomendado.



**Palabras clave:** Sistemas eléctricos híbridos, Celda de Combustible, Supercapacitor, Convertidores de potencia.



ARTS ET MÉTIERS ParisTech

ParisTech
INSTITUT DES SCIENCES ET TECHNOLOGIES
PARIS INSTITUTE OF TECHNOLOGY

*RÉSUMÉ EN FRANÇAIS*

# *Contrôle d'une source d'énergie hybride : Pile à combustible-Supercondensateur*

## 1. Introduction

Les piles à combustible sont des générateurs d'électricité et de chaleur qui offrent une densité d'énergie élevée et qui représentent une alternative renouvelable et propre aux énergies fossiles (gaz naturel, charbon et pétrole). Néanmoins, l'état de développement de cette technologie ne permet pas à ce jour de concurrencer avantageusement les machines à combustion interne à cause de leur coût élevé et leur capacité de puissance électrique basse [1].

Contrairement aux piles à combustible, l'électricité provenant des supercondensateurs n'est pas générée, mais stockée directement sous la forme d'un champ électrostatique, car ces dispositifs ne fonctionnent pas sur la base des réactions chimiques ; après, l'énergie est délivrée beaucoup plus rapidement que l'énergie des piles à combustible. Les supercondensateurs ont donc la capacité de produire une forte puissance électrique, mais offrent une densité d'énergie moins favorable que les piles à combustible.

La combinaison de haute densité d'énergie et de haute densité de puissance peut être obtenue avec un ensemble de pile à combustible-supercondensateur. L'hybridation d'un système d'alimentation de puissance électrique permet d'élargir le domaine d'opération, améliorer la réponse dynamique du système, ainsi que réduire le cout, étant donné que les sources sont dimensionnées en fonction de leur utilisation. Le fonctionnement efficace d'un système hybride de génération peut être assuré avec la mise en œuvre d'une stratégie de gestion de l'énergie. Cette stratégie doit en premier lieu, faire face à la distribution appropriée de la demande de puissance entre le générateur (pile à combustible) et l'accumulateur (supercondensateur) ; celle-ci doit également assurer un état de charge (SOC) convenable du module de supercondensateurs ; enfin, la stratégie de gestion doit comporter des lois de commande locale et garantir une tension constante.

Cette thèse s'inscrit dans le cadre de conception d'une stratégie de gestion de l'énergie dans un système hybride de génération d'énergie électrique composé d'une pile à combustible et une banque de supercondensateurs. La source hybride fournit une puissance maximale de 1,2 kW et sa conception implique des décisions concernant la sélection de l'architecture du système hybride ainsi que le choix de la topologie et le dimensionnement d'une unité de convertisseurs. La stratégie de gestion vise à satisfaire la demande d'énergie électrique de la charge et favoriser la consommation énergétique efficiente ; sa performance est évaluée en développant un simulateur qui comprend la dynamique des éléments mis en jeu : deux sources et l'unité de convertisseurs. Le générateur hybride est supposé alimenter un profil de consommation correspondant à un véhicule électrique, de ce fait un cycle standard de conduite en ville en petite échelle est demandé lors des simulations, ce qui permet d'évaluer la performance du générateur hybride et plus spécifiquement de la stratégie de gestion énergétique.

Dans une première étape, un simulateur intégral a été construit avec des librairies de Simscape/Simulink. Le simulateur est constitué des modules contenant des modèles mathématiques qui prédissent le comportement des différents dispositifs constituant le système hybride. Le module de la pile à combustible modèle la dynamique d'un système BAHIA® (400 W - 1100 W, 0 A - 70 A nominale) et le module de supercondensateur modèle les cycles charge-décharge d'une banque Maxwell de 400 F et 16 V. Un onduleur de tension pont complet avec convertisseur élévateur conditionne l'énergie délivrée par la pile à combustible et un convertisseur bidirectionnel (buck-boost) est connecté au module de supercondensateurs afin de conditionner les cycles de charge-décharge. L'unité des convertisseurs a été dimensionné, puis, un modèle moyen de petits signaux a été formulé afin de décrire la dynamique de ces dispositifs. Les différents composants ont été intégrés dans l'environnement Simulink. Dans une deuxième étape, la stratégie de gestion énergétique a été conçue en considérant les caractéristiques et performances des sources ; le résultat est une stratégie de trois niveaux hiérarchiques, dont l'aspect principal es la définition des lois de commande locales et globale. Dans une troisième étape, le système complet est évalué en termes du niveau d'utilisation des sources, du domaine d'opération de la pile à combustible, et de l'accomplissement des objectifs des commandes locales et global, qui engagent notamment l'état de charge des supercondensateurs et la régulation de la tension du générateur hybride.

## 2. Objectifs

### Objectif général

Concevoir et évaluer une stratégie de gestion de l'énergie délivrée par une source hybride, composée d'une pile à combustible et d'un module de supercondenasteurs, utilisée dans des applications portables et de véhicule électrique en échelle.

### Objectifs spécifiques

- Sélectionner l'architecture de la source hybride et la topologie de l'unité de convertisseurs de puissance connectés au bus CD de 48 V, en vissant la demande dynamique, caractéristique des applications des véhicules électriques.
- Simuler une source hybride composé d'un ensemble pile à combustible – banque de supercondensateurs, et d'un système de convertisseurs de puissance.
- Désigner les critères de distribution de la demande d'énergie entre les sources.
- Désigner les lois de commande locale de la pile à combustible et le convertisseur CD-CD associé.
- Désigner les lois de commande du module de supercondensaterurs et le convertisseur bidirectionnel associé.
- Concevoir l'algorithme de gestion globale du système.
- Evaluer, en simulation, la stratégie de gestion d'énergie proposée, en considérant un cycle standard de conduite en ville en échelle de 1 kW.

## 3. Architecture du générateur hybride et topologie des convertisseurs

La source hybride fournit une puissance maximale de 1,2 kW et sa conception implique des décisions concernant la sélection de l'architecture du système hybride ainsi que le choix de la topologie de l'unité de convertisseurs.

### Architectures de systèmes hybrides

Les études de Zhang [3], Erdinç et al. [4], [5], Thounthong et al. [2], [6] et Feroldi et al. [7] sont quelques exemples de l'utilisation de plusieurs topologies de convertisseur pour les applications de transport. La sélection de la topologie de l'unité de conditionnement de puissance du système hybride repose sur certains facteurs importants, le coût plus faible, une plus grande efficacité, l'isolation électrique, le fonctionnement fiable et sans ondulation.

Compte tenu des facteurs mentionnés ci-dessus, ainsi que des exigences caractéristiques de la charge, diverses topologies peuvent être utilisées afin d'interfacer les systèmes hybrides basés sur des PEMFC. La topologie plus récurrente qui est décrite dans la littérature pour des systèmes hybrides est composée de multiples convertisseurs continu / continu comme on le voit sur la Fig. 1. Thounthong et al. [8] et [9] sont des exemples d'application des systèmes pour cette structure hybride.

Cette topologie de conditionnement est proposée dans cette étude, car donne la possibilité de délivrer la valeur de consigne de la puissance à partir des sources d'énergie hybride tout en maintenant la tension du bus au niveau souhaité. Cette topologie a été appliquée dans différents domaines, et bien que plus complexe, implique une grande souplesse pour la conception de la stratégie de gestion de puissance. Le système de conditionnement dispose de deux convertisseurs qui peuvent réguler la tension de chaque source tout en protégeant efficacement la pile à combustible.

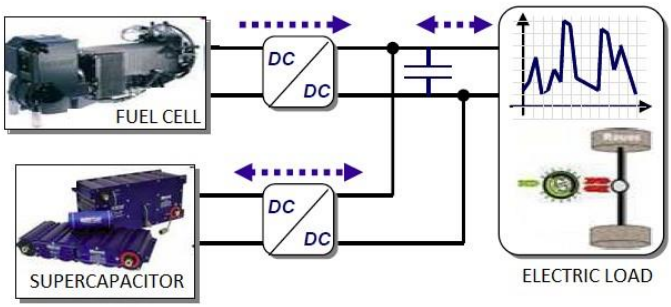


Figure 1 Structure avec deux convertisseurs

## Les approches de gestion de l'énergie

En raison du caractère multidisciplinaire des trains électriques avec sources multiples, l'efficacité et l'économie de carburant de ces systèmes hybrides dépendent essentiellement de l'efficacité de la stratégie de gestion de l'énergie (SGE). Il est largement admis que le fonctionnement ininterrompu et le comportement transitoire de la pile augmente les contraintes mécaniques à l'intérieur de la pile à combustible, et diminue par conséquent la durée de vie de la pile. D'autre part, la régulation continue des variables d'état (tels que le flux de réactif, la température de la pile, l'humidité, le débit et la pression) conduit directement à des exigences plus contraignantes des réponses dynamiques des actionneurs (vannes, moteurs, etc.) et des capteurs (pression, les débits, températures, humidité, etc.), et potentiellement augmenter le coût du système global.

Les stratégies de gestion de l'énergie sur la base de découplage de fréquence, pendant le fonctionnement quotidien d'un système, considèrent que les transitions de charge peuvent se produire fréquemment. Cela est particulièrement vrai pour les applications des véhicules. Les changements transitoires de la demande de charge peuvent se produire de façon répétée et

causer un stress dynamique sur la membrane de la PEMFC en raison des oscillations de pression et possibilité la privation d'oxygène, et donc de réduire la durée de vie du système. Ainsi, pour assurer la durée de vie de la pile à combustible en empêchant le système de travailler avec les hautes fréquences. L'approche de base pour ce problème est d'insérer un filtre passe-bas du premier ordre avec une valeur de coupure qui limite l'opération de la FC.

Le graphique de Ragone, Fig. 2, compare l'énergie spécifique et la puissance spécifique pour les systèmes de stockage de la production d'énergie [1].

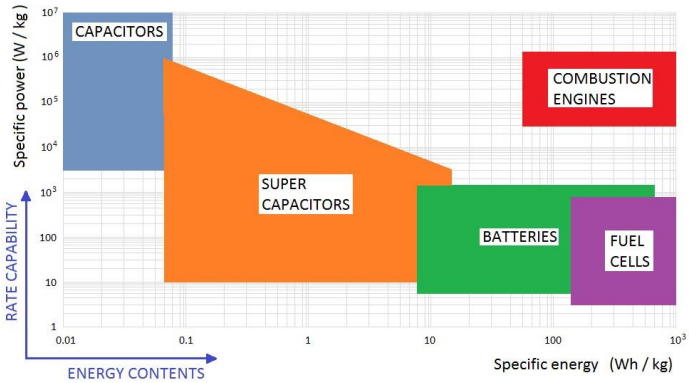


Figure 2 Ragone plot

## 4. La configuration de la gestion de l'énergie proposée

La conception du générateur hybride a démarré avec la sélection d'un bus de tension constant (CC) de 48 V, convenable aux structures de véhicules hybrides. Les éléments constitutifs du système ont été dimensionnés pour cette application en petite échelle de 1 kW. Le générateur hybride se compose d'une PEM FC Bahía® (400 W - 1100 W, 0 A - 70 A nominal), couplé avec une banque de supercondensateurs Maxwell (400 F, 16 V) fonctionnant comme la source auxiliaire, ainsi que leurs respectives unités de conditionnement de puissance. Un convertisseur élévateur CC / CC fait le conditionnement de puissance dans la pile à combustible, alors qu'un convertisseur CC / CC bidirectionnel gère la prestation et la récupération des cycles du supercondensateur. Les convertisseurs sont connectés en parallèle et régulent le bus CC, où la charge (une traction du véhicule électrique) est alimentée. La stratégie de gestion de l'énergie serve à coordonner tous les éléments dans le système avec l'objectif de fournir en permanence la puissance demandée par la charge, et en même temps, maintenir constante la tension du bus ($V_{bus}$) et assurer l'état de charge du supercondensateur.

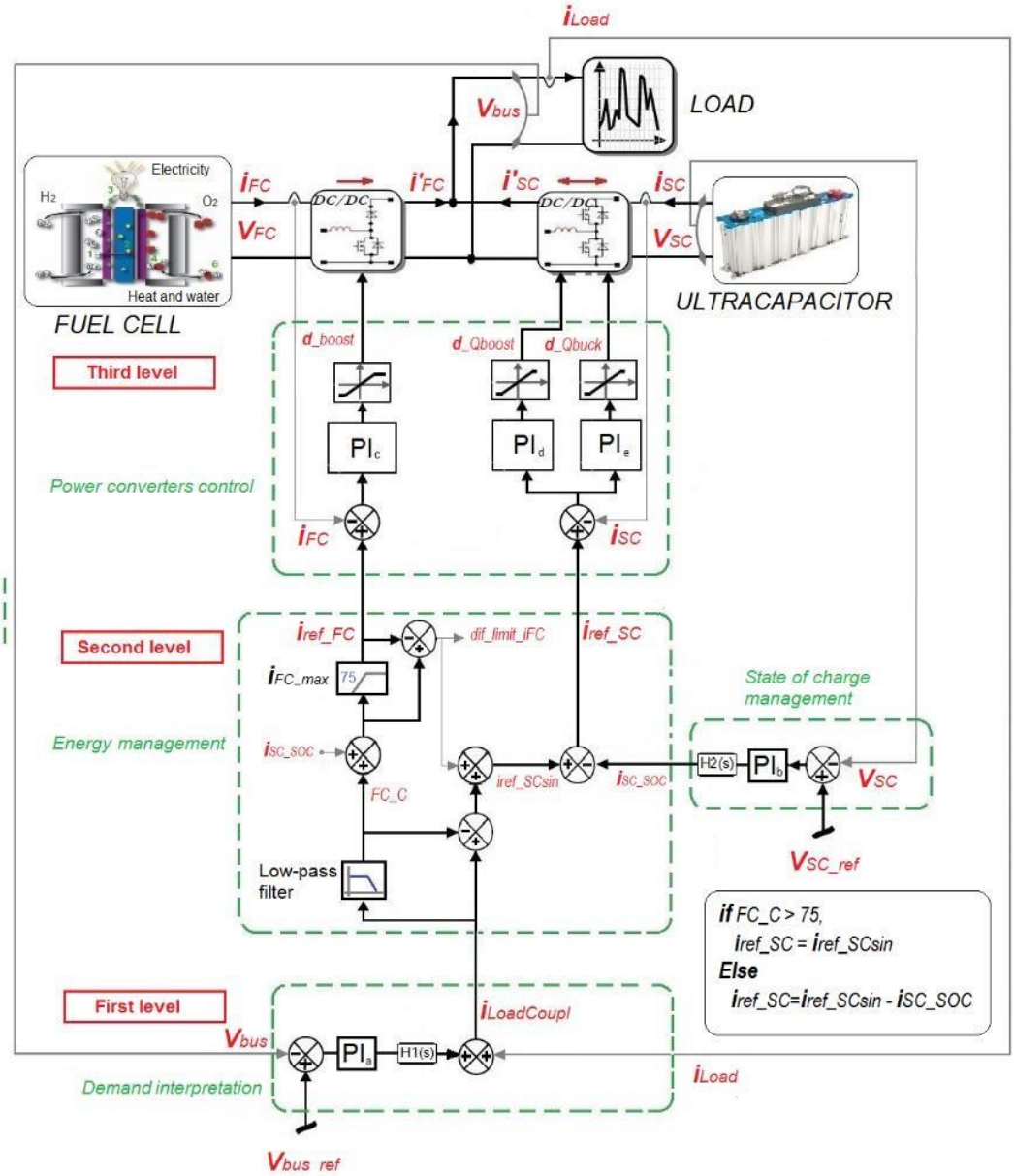


Fig. 3 Stratégie de gestion de l'énergie du générateur hybride.

La stratégie de gestion de l'énergie est organisée en trois niveaux hiérarchiques [10]. Le premier niveau est la régulation globale, nommé aussi module d'interprétation de la demande, ayant pour but la régulation de la tension sur le bus CC. Ici, la charge est le signal de perturbation. La sortie du module d'interprétation de la demande représente l'entrée des boucles de commande suivantes, comportant les niveaux hiérarchiques inférieurs. Le deuxième niveau comprend deux modules. Le module de commande interne est responsable de la régulation de l'état de charge du supercondensateur ; ensuite, le module de répartition de puissance entre la pile à combustible et le supercondensateur se base sur l'analyse de la réponse fréquentielle de la pila à combustible. Le troisième niveau comporte des boucles de

commande interne, qui gèrent l'interaction entre les unités de conditionnement de puissance et les sources (Fig.3).

L'évaluation de la stratégie proposée est décrite plus loin en utilisant des cycles de conduite à petite échelle.

## Boucle de régulation Global : Interprétation de la demande

La boucle de contrôle global a deux objectifs. Le premier objectif est de réguler la tension du bus ($V_{bus}$) à 48 V CC. Le second objectif consiste à obtenir le courant de référence ($I_{LoadCoupl}$) pour la pile à combustible et le supercondensateur, ce qui détermine par la suite, la demande d'énergie délivrée par chaque source.

Les sollicitations de la charge ne représentent pas l'énergie totale demandée au système. La demande globale doit être calculée à chaque instant compte tenu du déficit et de l'énergie supplémentaire dans le système complet.

La boucle de contrôle global est représentée dans la Fig. 4. Ce module reçoit deux entrées : la variable mesurée ($V_{bus}$) et l'exigence actuelle de la charge ($i_{load}$). La sortie du module est la courant de référence actuelle du niveau supérieur de gestion de l'énergie ou "Energy Management".

Ce module dispose d'un contrôleur interne PI de tension (contrôle maître). La variable $i_{Load}$ est considérée comme une perturbation et est ajoutée à la sortie du régulateur de $V_{bus}$. Les boucles de régulation locales (boîtes grises dans la Fig. 4) font partie des blocs hiérarchiques inférieurs.

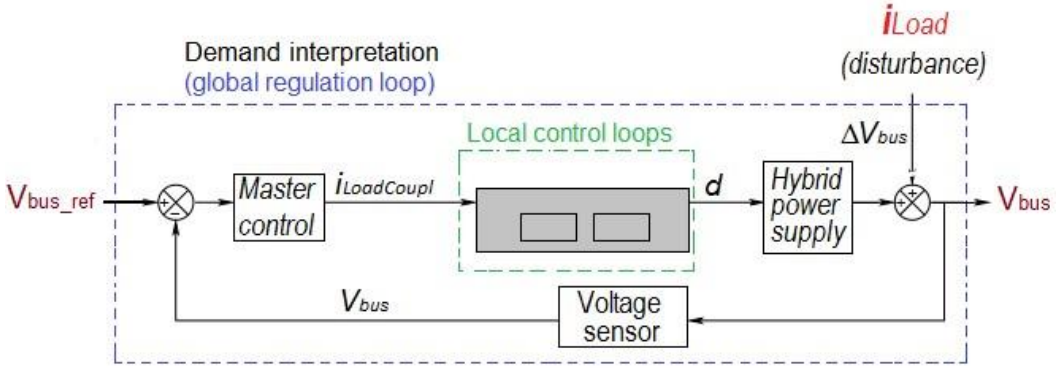


Fig. 4 Niveau d'interprétation de la demande.

## Deuxième niveau de hiérarchie : la gestion de l'énergie et l'état de charge (SOC)

Ce niveau est l'étape principale de la stratégie de gestion de l'énergie, et se compose de deux modules fonctionnels : le module de distribution d'énergie et celui de régulation de l'état de charge du supercondensateur (Fig. 5).

Le module de gestion de l'énergie détermine la répartition de puissance entre les sources afin de définir les références en courant de celles-ci. La conception de la stratégie de gestion est

basée sur la considération que le comportement dynamique des sources ne se tient pas dans la même gamme de fréquence, à savoir, les piles à combustibles sont des dispositifs à haute densité, mais ils ont des capacités de puissance plus faibles que les accumulateurs, et par conséquence des réponses plus lentes.

La fréquence de coupure de la pile est calculée à partir des mesures de signaux expérimentaux tension-courant, obtenues en ayant comme entrée un train d'échelons. On a observé que la fréquence de coupure est comprise entre 10 mHz et 50 mHz. A la fin, dans le but d'assurer une réponse adéquate de la pile à combustible, $f_{limit}$ a été fixée à la valeur la plus élevée obtenue (50 mHz).

L'apport du courant de charge fourni par la pile à combustible est déterminé de la façon suivante (Fig. 6) : les hautes fréquences sont fournies par le supercondensateur et les basses fréquences sont fournis par la pile à combustible. La fréquence de coupure détermine quelles sont les basses et les hautes fréquences.

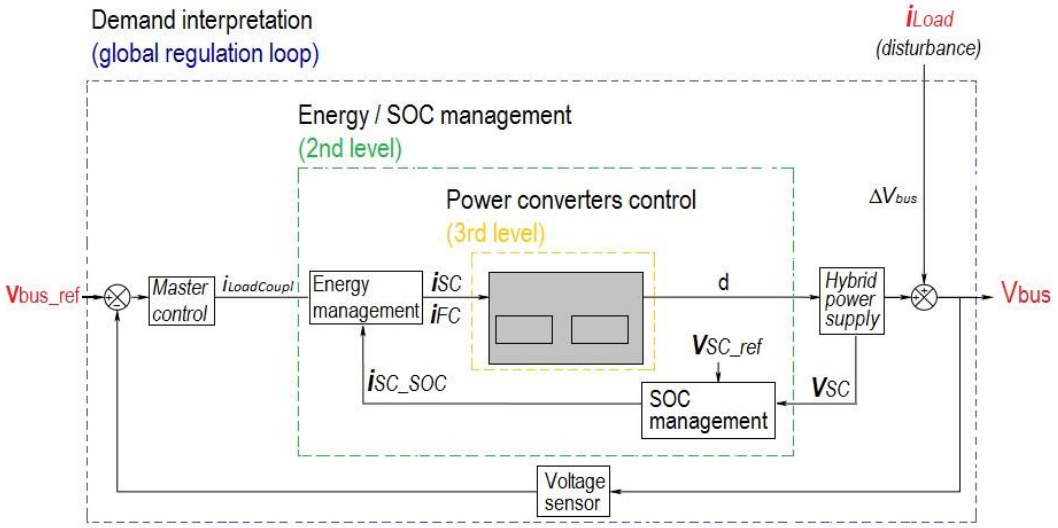


Fig. 5 Schéma de régulation fonctionnelle montrant deux niveaux.

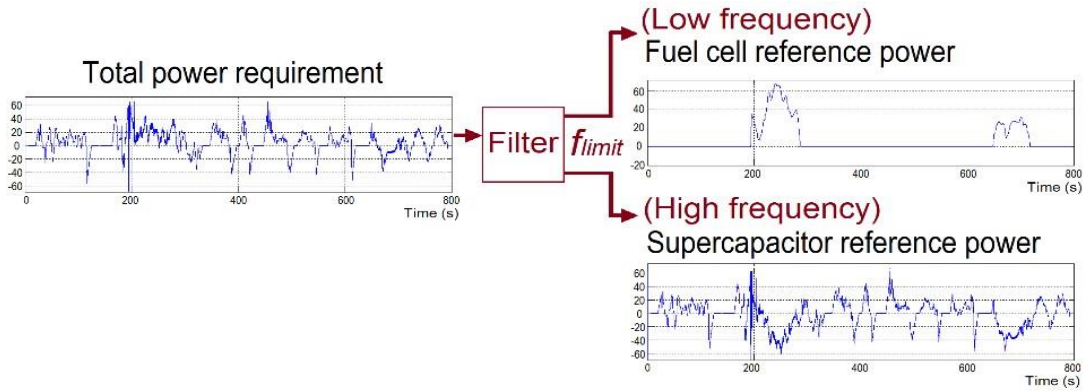


Fig. 6 Distribution dynamique de la demande globale demandé au générateur.

La sortie de tension n'est pas une mesure exacte de l'état de charge ; mais une approche simple consiste à contrôler la tension à un niveau correspondant à un état de charge convenable aux supercondensateurs avec la saturation du dispositif de commande aux limites de fonctionnement du supercondensateur. L'état de charge doit continuellement être supervisé afin de vérifier que le SOC de l'accumulateur reste dans les limites de sécurité. Le SOC a été évalué tel que l'indique (1) :

$$SOC = 100\left(\frac{Q_{init} - \int_0^t i(\tau)d\tau}{Q_T}\right)$$

où:

$Q_{init} = Initial\ charge\ (C)$
$Q_T = Total\ charge\ (C)$
$i(\tau) = Current\ (A)$

## Troisième niveau de la hiérarchie : le contrôle des convertisseurs de puissance

Ce module interagit directement avec les sources (Fig. 7) pour adapter la pile à combustible et les tensions de sortie du supercondensateur vers la tension $V_{bus}$ souhaitée, cela à l'aide de deux unités de conditionnement de puissance différentes.

La sortie du supercondensateur est conditionnée par un convertisseur bidirectionnel de demi-pont qui permet d'effectuer les cycles de livraison et de récupération. Le module de commande est alimenté avec les courants de référence des sources, qu'après sont comparés avec les courants des inductances mesurés de chaque convertisseur de puissance. Ensuite, un algorithme de commande de courant fournit le cycle correspondant de service (d) des signaux pour les deux convertisseurs CC / CC.

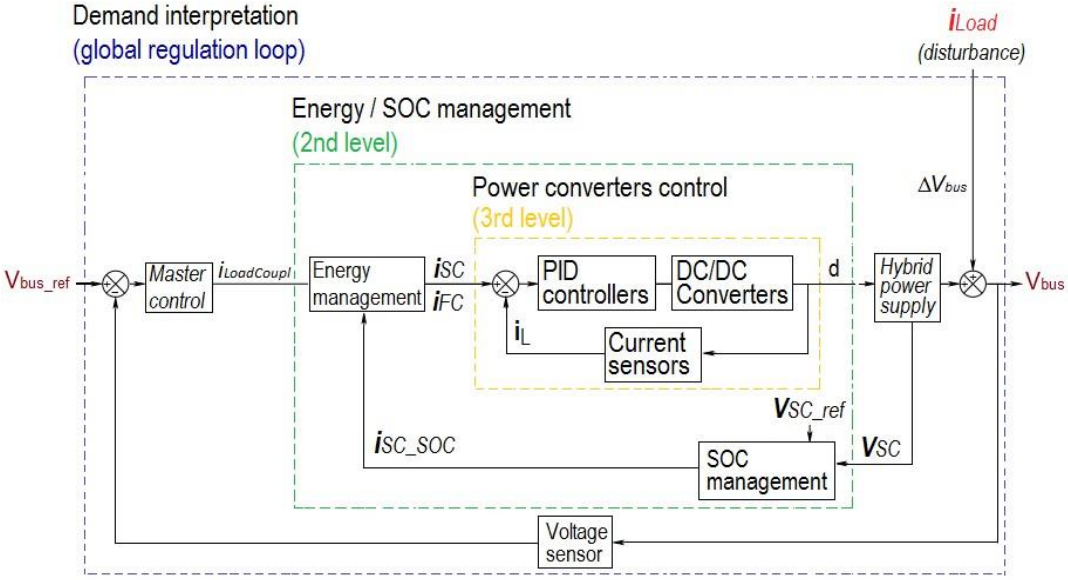


Fig. 7 Schéma de régulation fonctionnelle montrant trois niveaux.

## 5. Essais et résultats

Les séries de mesure tension-courant sont obtenues à partir des modules expérimentaux : une équipe d'alimentation Bahia PEMFC et une banque de supercondensateur Maxwell. Le module de puissance Bahia est une unité didactique industrielle composée d'un empilement de 24 cellules élémentaires PEM, qui génère une tension de 14-22 V et fournit un courant maximal de 75 A. L'équipe incorpore des collecteurs d'alimentation de réactants avec un humidificateur d'air et un circuit d'eau qui régule la température d'opération de la pile à combustible (Fig. 8). Le module comporte trois circuits : le circuit d'hydrogène, le circuit d'oxygène et le circuit d'eau de refroidissement (Fig. 9).

Fig. 8 Système expérimental Bahia.

La stœchiométrie d'oxygène peut être choisie dans une plage de 1,5 à 2,5. Toutes les expériences ont été réalisées avec un ratio de stœchiométrie égal à 1,5. Dans le second circuit, l'oxygène est obtenu à partir de l'air fourni par un ventilateur à canal latéral ; l'air passe à travers un humidificateur de la membrane avant d'alimenter la pile à combustible. L'air humide qui n'a pas réagi quitte la pile à combustible pour être réutilisée dans l'humidificateur et ensuite est libéré dans l'atmosphère. Les expériences ont été réalisées à une humidité relative de 80%.

Dans le troisième circuit, l'eau est utilisée dans un circuit de refroidissement pour réduire la chaleur produite par des réactions exothermiques. Le circuit de refroidissement comporte un régulateur de température toujours en fonctionnement. La température a été réglée à une valeur de référence de 65 °C.

La banque de supercondensateur Maxwell MOD0500 P016 B01 est composée de six supercondensateurs connectés en série (Fig. 10); des expériences ont été menées afin d'enregistrer le comportement de supercondensateur dans les cycles de livraison et de récupération. Les données ont été enregistrés à des valeurs de courant constant dans une gamme de 5 à 40 A, avec des incréments de 5 A. Le courant a été mesuré avec un capteur d'effet Hall fournissant 5 V / 50 A.

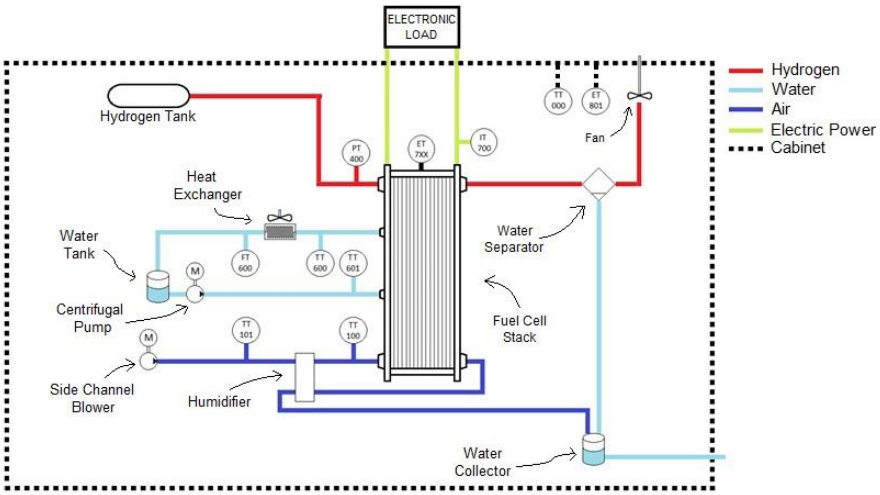


Fig. 9 Diagramme du système Bahia.

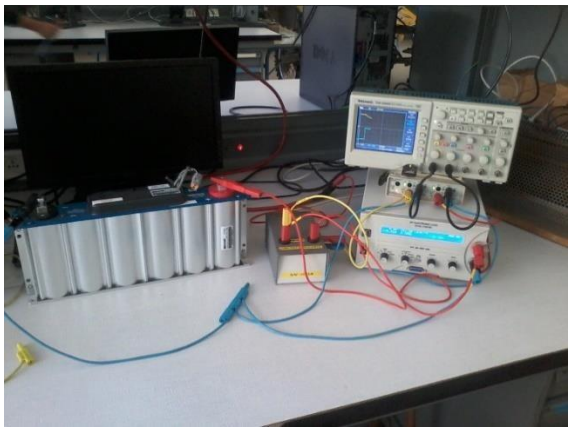

Fig. 10 Banque expérimentale de supercondensateurs Maxwell.

## 6. Simulation

La simulation numérique des performances de la PEMFC a été faite dans l'environnement Simulink en utilisant le modèle de pile à combustible de la bibliothèque de composants de SimPower Systems$^{TM}$. Afin de paramétrer le modèle de pile à combustible, des essais expérimentaux ont été effectués avec l'équipe BAHIA. L'enregistrement des réponses de tension a été fait à différentes largeurs d'impulsion de courant, plus précisément, des trains d'impulsions ont été demandés à différentes conditions de température et de stœchiométrie. Les paramètres du modèle de pile à combustible ont été ajustés afin de correspondre au comportement de la pile à combustible BAHIA. Le même processus a été suivi pour simuler les

performances de la banque de supercondensateurs en utilisant le modèle de de la bibliothèque de composants de SimPower Systems$^{TM}$. En autre, les unités de conditionnement de puissance ont été simulées avec des éléments des bibliothèques Simscape.

La consommation d'un véhicule électrique dépend de divers facteurs tels que la température, la vitesse, la charge, l'aérodynamique, les pneus et même les habitudes de conduite. Plusieurs études ont déjà démontré la difficulté à faire face à ces caractéristiques [11], [12]. Par conséquent, au cours des dernières années, plusieurs normes ont été définies pour décrire les performances typiques d'un véhicule électrique. Ces normes de conduite sont couramment utilisées dans les phases de conception, développement et essais de véhicules. Un cycle standard de conduite est un parcours fixe d'opération d'un véhicule qui permet de tester par exemple, les émissions provenant d'un véhicule dans des conditions reproductibles. Les cycles de conduite sont généralement définis en termes de vitesse du véhicule en fonction du temps. Il est également utile de noter que les cycles d'entraînement peuvent être utilisés pour une variété d'autres fins que la mesure des émissions, telles que les essais du moteur ou la durabilité des éléments du train de conduite [13].

Afin de valider la stratégie de gestion d'énergie, deux cycles de conduite normalisés ont été choisis : ECE-15 et UDDS. Le cycle de conduite ECE-15 est utilisé pour homologuer des véhicules lors de la commercialisation en Europe, il a été développé pour représenter les conditions de conduite typiques des villes européennes occupés et se caractérisent par une faible vitesse avec des arrêts fréquents. D'autre part, des programmes de conduite dynamométriques et de travail sont utilisés dans l'Environmental Protection Agency (EPA), National Vehicle & Fuel Emissions Laboratory (NVFEL) (Etats-Unis), pour mesurer les émissions des véhicules et faire des essais quantifiant l'économie du carburant. L'EPA Urban Dynamometer Driving Schedule (UDDS) est communément appelé le «LA4» ou «le test de la ville» et représente les conditions de conduite en ville.

Les cycles de conduite comportent de profils de vitesse. La vitesse du véhicule peut être traduite en puissance en tenant compte des caractéristiques mécaniques du véhicule, telles que la masse, le coefficient de friction, le coefficient de pénétration dans l'air, et la pente de la route, ainsi, le profil de courant de charge peut être estimé.

En supposant des caractéristiques typiques d'un petit véhicule, le profil de charge correspondant au cycle ECE-15 est présenté dans la Fig. 11, tandis que le profil de charge correspondant au cycle UDDS est présenté dans la Fig. 12. Puis, afin de les faire correspondre avec les capacités de la pile à combustible BAHIA FC, les profils de puissance ECE-15 et UDD ont été réduits à un maximum de 1 KW. Seulement 80 s ont été conservés du cycle ECE-15 et 1200 s du cycle UDDS.

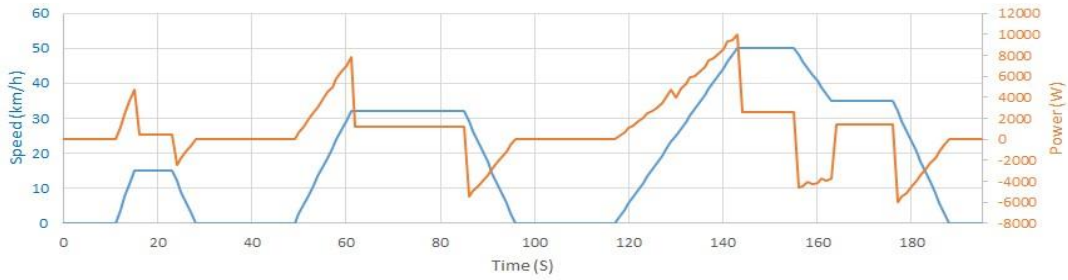


Fig. 11 Vélocité du véhicule et profile de puissance du cycle ECE-15.

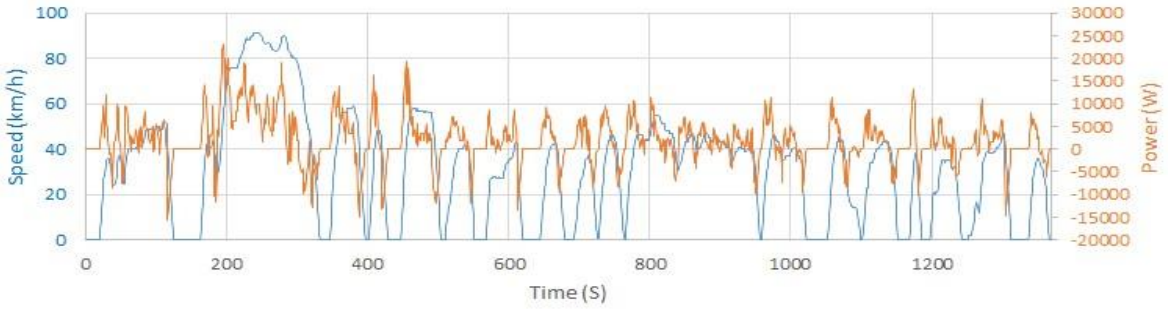


Fig. 12 Vélocité du véhicule et profile de puissance du cycle UDDS.

Dans le simulateur du générateur hybride, la pile à combustible est interfacée à la charge avec le convertisseur élévateur continu / continu et le supercondensateur avec le convertisseur continu / continu bidirectionnel, ils sont connectés en parallèle à un bus CC commun, qui est aussi interfacé à la charge. La Fig. 13 montre l'organisation fonctionnelle de la stratégie de contrôle.

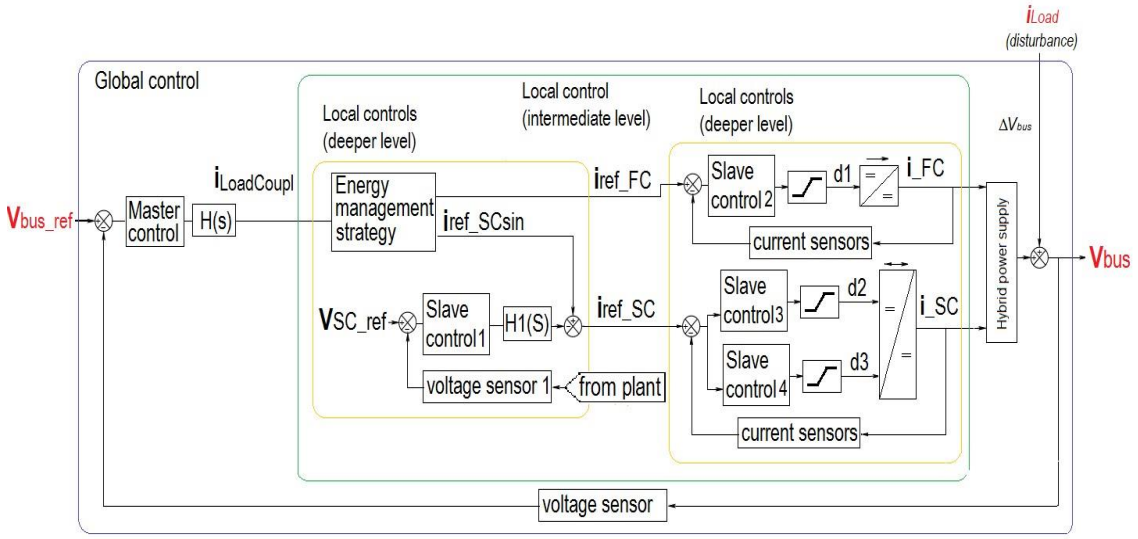


Fig. 13 Diagramme du contrôle fonctionnel de la stratégie.

Il s'avère important de remarquer que les cycles de mesures présentent des propriétés différentes de fréquence : par conséquent, différente répartition de la puissance entre les

sources peut être attendue par rapport à la mise en œuvre de la stratégie de gestion de l'énergie proposée.

Les valeurs négatives de la puissance résultent si la vitesse diminue, ce qui indique qu'une partie de l'énergie est dissipée en raison du freinage du véhicule. Le profil de puissance de la charge s'introduit comme l'entrée du système, y compris les valeurs de puissance négative ; ainsi, l'hypothèse idéale de freinage de régénératif a été faite, donc cette énergie est supposée être utilisée pour charger partiellement le supercondensateur.

Tout en considérant que les profils de puissance des cycles de conduite ont été requis au train électrique hybride, la simulation du système a démontré que les objectifs mis en jeu ont été atteints.

En ce qui concerne le contrôle global ou d'interprétation de la demande, la tension du bus est correctement régulée, car elle fluctue légèrement autour de la référence spécifiée à 48 V, en dépit des changements soudains dans la charge (Fig. 14 pour la CEE-15 et Fig. 15 pour UDDS).

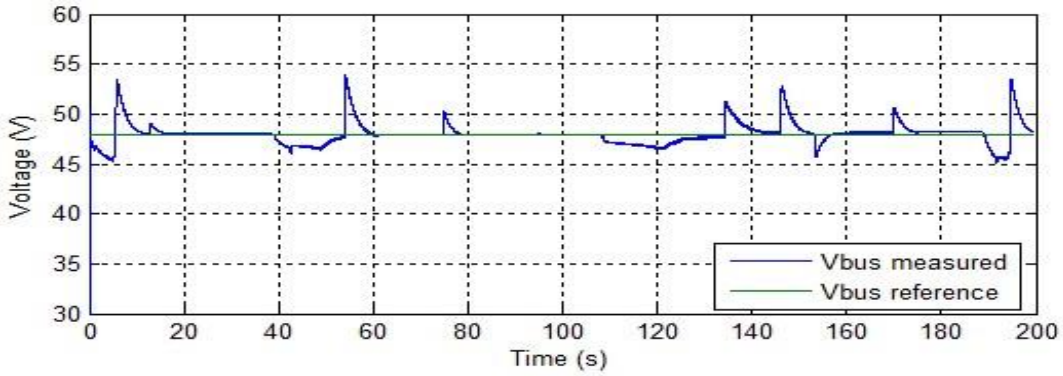


Fig. 14 Tension du bus ($Vbus$) avec le cycle ECE-15 en tant qu'entrée.

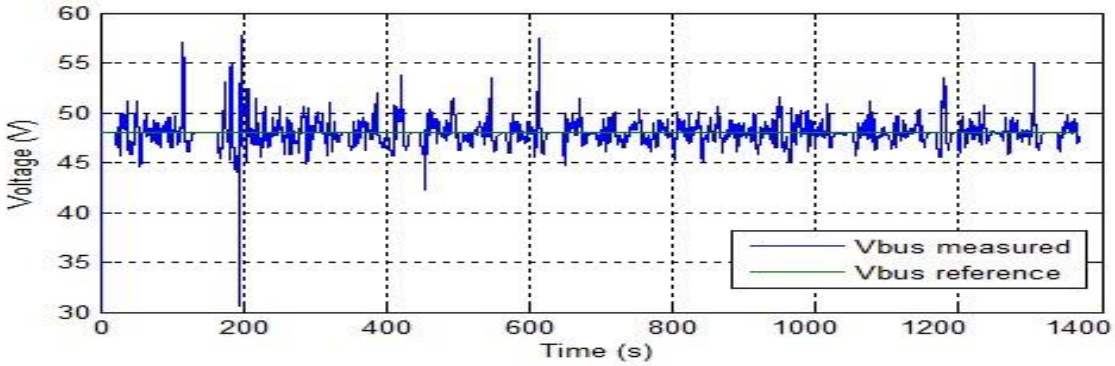


Fig. 15 Tension du bus ($V_{bus}$) avec le cycle UDDS en tant qu'entrée.

La vie de supercondensateur peut être considérablement réduite si l'état de charge ne reste pas dans certaines limites. En ce qui concerne la solution au problème de la régulation de l'état de charge de l'unité auxiliaire de puissance (deuxième niveau hiérarchique), le schéma suivant a été conçu : le fonctionnement du supercondensateur s'engage dans des conditions de pleine charge, l'objectif est donc de maintenir son état de charge entre 70% et 100% pendant que le générateur hybride est en opération. La sortie de tension n'est pas une mesure exacte de l'état de charge ; mais une approche simple consiste à contrôler la tension à un niveau correspondant à un état de charge de 90% avec la saturation du dispositif de commande, correspondant aux limites de fonctionnement du supercondensateur (SOC entre 70% et 100%). L'état de charge est continuellement enregistré au cours de la simulation et les résultats ont prouvé que le SOC de l'accumulateur reste dans les limites de sécurité, même si le cycle de conduite USD est exigée ; dans ce cas, on peut observer une utilisation plus forte du supercondensateur (Fig. 16 et Fig. 17).

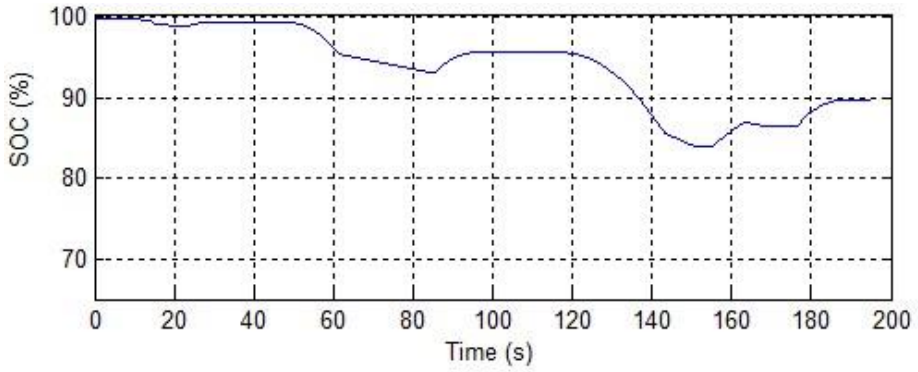


Fig. 16 État de charge du supercondensateur pour le cycle ECE-15.

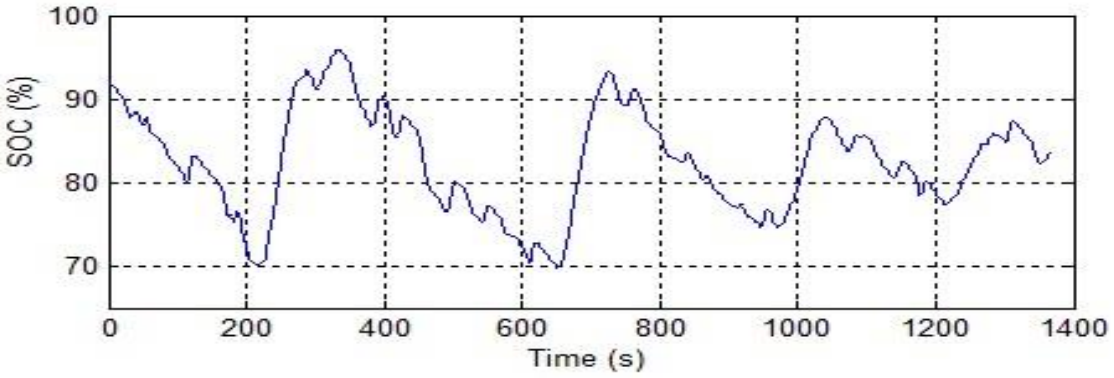


Fig. 17 État de charge du supercondensateur pour le cycle UDDS.

Il a également été vérifié que la puissance totale nécessaire pour satisfaire l'exigence de traction du véhicule face aux cycles de conduite est livrée sans problème. La demande totale de puissance dans le générateur correspond parfaitement à la puissance délivrée par les sources (Fig. 18). L'avantage de la stratégie proposée est vérifiée.

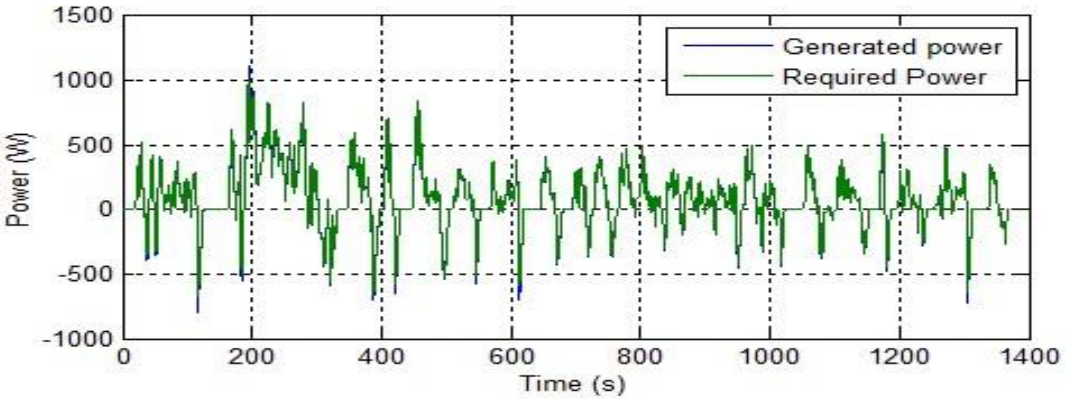


Fig. 18 Puissance délivrée et puissance requise par le véhicule en petite échelle de 1 kW.

La stratégie de répartition de la puissance proposée entre les sources (encore deuxième niveau hiérarchique) permet à la PEMFC de fonctionner seulement si nécessaire. En conséquence, la consommation de carburant est réduite et prévient des problèmes de manque d'oxygène, ce qui provoque des pertes de tension négatives ou « undershoot » due à des changements rapides de la demande en oxygène (Figure 5.11). On peut constater que le fonctionnement de la pile à combustible recouvre la région linéaire de puissance optimale du module BAHIA PEMFC, même si la pile à combustible ne fonctionne pas en permanence pendant la durée de la simulation, il fonctionne dans l'ensemble de la zone sûre (région ohmique) et une peut conclure que la pile à combustible ne pas surdimensionné ; à la place, elle est conduite en toute sécurité dans la limite maximum de ses capacités de réponse en fréquence. En autre, le démarrage et arrêt de la pile à combustible diminue par rapport à l'opération non-hybride.

En outre, dans les Fig. 19 et Fig. 20 on observe des périodes dans lesquels la PEMFC charge le supercondensateur, car la pile à combustible génère plus d'énergie qu'il est nécessaire pour alimenter le véhicule à ces instants. En résumant, la pile à combustible fait correctement les livraisons prévues à la charge, au supercondensateur. En plus, le convertisseur CC réussit à maintenir la tension du bus à la valeur de référence de 48 V.

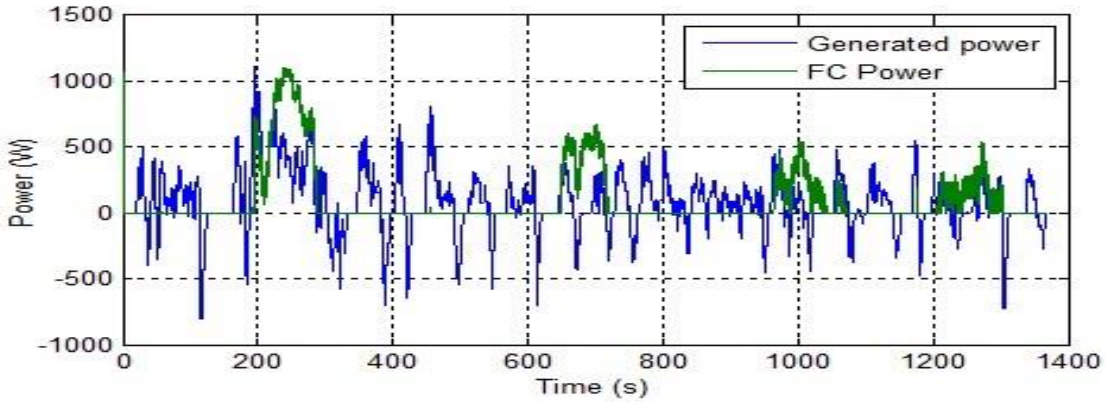


Fig. 19 Puissance délivrée au véhicule vs puissance générée par la pile a combustible (UDDS).

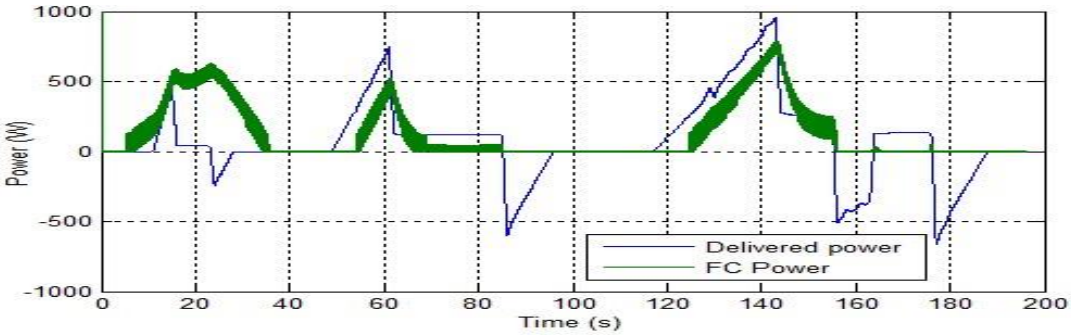


Fig. 20 Puissance délivrée au véhicule vs puissance générée par la pile à combustible (ECE-15)

La contribution supercapaciteur à la demande de puissance totale est représentée sur les Fig. 21 et Fig. 22. Étant donné que le UDDS est un cycle avec les exigences de puissance brusques et soudaines, le supercondensateur est actif presque tout le temps, opérant dans la livraison (valeurs positives) ou des périodes de récupération (valeurs négatives). La charge du supercondensateur s'effectue lorsque la demande de puissance du véhicule se caractérise par des signaux de basse fréquence (signaux verts dans la Fig. 21), et il est chargé de l'énergie récupérée du freinage (idéalement) lorsque la fréquence des signaux d'entrée, ainsi les capacités de la PEMFC ne sont pas dépassées.

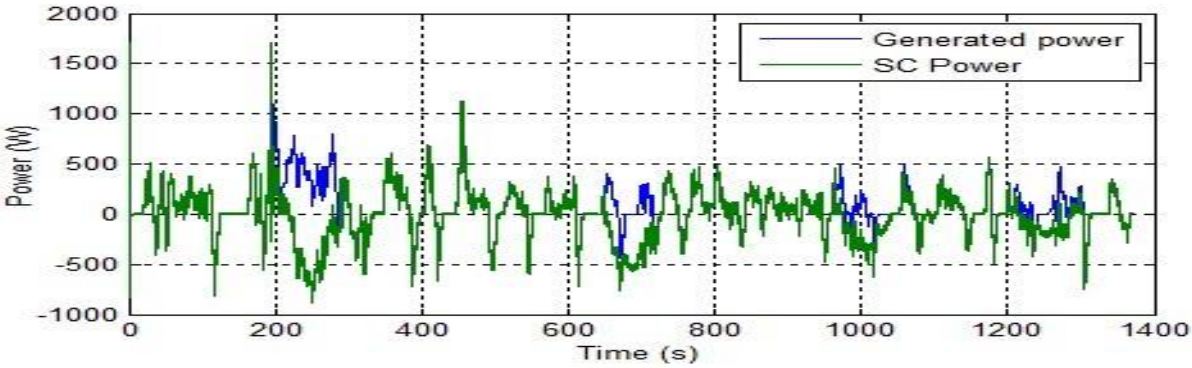


Fig. 21 Puissance délivrée au véhicule vs puissance délivrée par le supercondensateur (ECE-15)

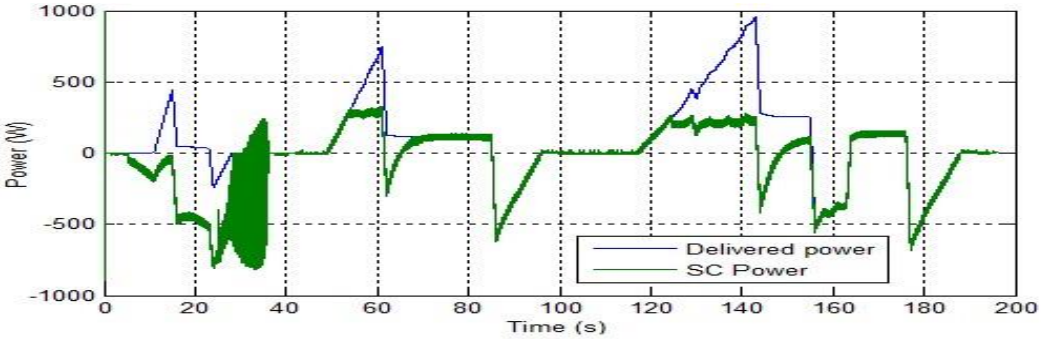


Fig. 22 Puissance délivrée au véhicule vs puissance délivrée/récuperée par le supercondensateur (UDDS)

Le supercondensateur ne dépasse la tension nominale (16 V) et, sous les cycle UDDS (également applicable à la CEE-15), la PEMFC ne fonctionne pas lorsque la demande est abrupte, l'économie de carburant d'hydrogène prévient la perte de tension, dit phénomène « d'undershot » ( Fig. 23).

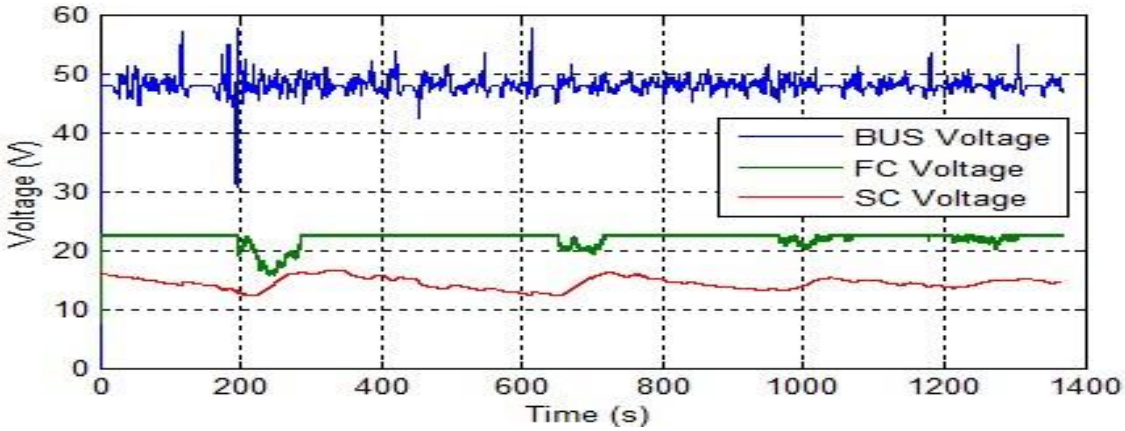


Fig. 23 Tension dans le bus $V_{bus}$ et dans les terminales des sources.

## 7. Conclusion

Dans cette étude, une stratégie de gestion de l'énergie conçue pour un générateur hybride a été proposée et évaluée dans un environnement de simulation. Le système hybride est composé par une PEMFC en tant que source d'énergie primaire et une banque de supercondensateurs en tant qu'unité de stockage d'énergie destinée à délivrer sollicitations de haute fréquence. Chaque source d'énergie comporte un convertisseur CC / CC, ce qui permet la connexion entre les sources et le bus à courant continu.

L'efficacité de cette stratégie contribue à distribuer dynamiquement l'énergie nécessaire entre la pile à combustible et le supercondensateur, ce qui permet d'exploiter chaque source dans sa région de fonctionnement plus effective et dans des conditions de sécurité, tout en réduisant le risque de dégradation. Cette stratégie est basée sur une approche de distribution fréquentielle, étant donné que la dynamique des sources d'énergie ne se tiennent pas dans la même gamme de fréquences (selon le tracé de Ragone).

Même lorsque la dynamique lente de la pile à combustible ne permet pas de répondre aux transitions rapides de demande de puissance, il n'y a que peu d'études qui tentent de résoudre le problème. En utilisant la méthodologie proposée, les phénomènes transitoires indésirables, tels que l'épuisement d'oxygène et l'utilisation de la pile à combustible dans la région de

concentration ayant an comportement non-linéaire, sont évités. La stratégie de gestion tire profit des caractéristiques dynamiques mesurées expérimentalement de la pile à combustible, tout en réduisant les cycles de charge du supercondensateur et en soutenant convenablement l'état de charge du supercondensateur.

Parmi les avantages de la stratégie de gestion de l'énergie proposée dans cette étude on cite les suivantes : l'utilisation de modèles commutés des convertisseurs de puissance améliorent la réponse des lois de contrôle face aux transitoires rapides. En plus, les délais habituellement présents dans des modèles simplifiés sont réduits. Les boucles de commande interne sont plus rapides que les boucles de commande externe ; ainsi, la structure imbriquée de la gestion de l'énergie permet la réaction rapide face aux perturbations ayant impacté fortement la sortie dans d'autres circonstances.

Les cycles standard UDD et CEE-15 de conduite en ville ont été sélectionnés avec le but d'évaluer la stratégie de gestion de l'énergie proposée parce que ces cycles ont plus d'accélérations et de décélérations que d'autres cycles de conduite. En outre, la vitesse et leurs signaux de puissance électrique associés montrent des mesures des comportement en fréquence très différents, ainsi, le cycle de conduite ECE-15 montre une dynamique plus lente, tandis que le cycle UDDS présente des changements rapides de la demande de puissance. Dans ce sens, l'exécution de la stratégie de gestion a été testée dans des scenarios différents, mais elle conduit, dans les deux cas, à la pile à combustible sur toute la zone de fonctionnement optimal et permet à cette source primaire de fournir l'énergie nécessaire afin de propulser le véhicule et charger le supercondensateur.

En outre, la tension du bus de CC est maintenue presque constante, à 48 V, tandis que l'état de charge du supercondensateur est toujours maintenu autour des valeurs souhaitées. Les objectifs de gestion sont atteints avec un degré différent de contribution des sources et en fonction des caractéristiques dynamiques de la charge ; mais, dans les deux cas étudiés, la pile à combustible fonctionne sur toute la zone sûre, en évitant la zone de concentration. Nous pouvons conclure que le générateur hybride n'est pas surdimensionné ou sous-dimensionné pour l'application sélectionnée. Définitivement, les résultats ont démontré l'efficacité de la stratégie de gestion de l'énergie dans une gamme de fréquences d'opération.

# 8. Bibliographie


[1] M. Winter and R. J. Brodd, “What are batteries, fuel cells, and supercapacitors?,” *Chem. Rev.*, vol. 104, no. 10, pp. 4245–69, Oct. 2004.

[2] D. B. Thounthong P, Chunkag V, Sethakul P, “Comparative study of fuel-cell vehicle hybridization with battery or supercapacitor storage device,” *IEEE Trans Veh. Technol*, 2009.

[3] X. Zhang, C. C. Mi, A. Masrur, and D. Daniszewski, “Wavelet-transform-based power management of hybrid vehicles with multiple on-board energy sources including fuel cell, battery and ultracapacitor,” *J. Power Sources*, vol. 185, no. 2, pp. 1533–1543, Dec. 2008.

[4] O. Erdinc, B. Vural, M. Uzunoglu, and Y. Ates, “Modeling and analysis of an FC / UC hybrid vehicular power system using a wavelet-fuzzy logic based load sharing and control algorithm,” *Int. J. Hydrogen Energy*, pp. 1–11, 2008.

[5] U. M. Erdinc O, Vural B, “A wavelet-fuzzy logic based energy management strategy for a fuel cell/battery/ultra-capacitor hybrid vehicular power system,” *J. Power Sources*, 2009.

[6] P. Thounthong, S. Raël, and B. Davat, “Energy management of fuel cell/battery/supercapacitor hybrid power source for vehicle applications,” *J. Power Sources*, vol. 193, no. 1, pp. 376–385, Aug. 2009.

[7] D. Feroldi, M. Serra, and J. Riera, “Energy Management Strategies based on efficiency map for Fuel Cell Hybrid Vehicles,” *J. Power Sources*, vol. 190, no. 2, pp. 387–401, May 2009.

[8] D. B. Thounthong P, Rael S, “Control algorithm of fuel cell and batteries for distributed generation system,” *IEEE Trans Energy Convers.*

[9] P. Thounthong, S. Raël, and B. Davat, “Control strategy of fuel cell/supercapacitors hybrid power sources for electric vehicle,” *J. Power Sources (J POWER SOURCES)*, vol. 158, no. 1, pp. 806–814, Jul. 2006.

[10] U. P. Xi, “Contribution à l ’ Etude d ’ Electro-générateurs à Pile à Combustible Conceptions d ’ Architectures et de Leurs Commandes,” 2010.

[11] Z. Dai, D. Niemeier, and D. Eisinger, “Driving Cycles : a New Cycle-Building Method That Better Represents Real-World Emissions,” *U.C. Davis-Caltrans Air Qual. Proj. 2008.*, no. 66, 2008.

[12] M. André, “The ARTEMIS European driving cycles for measuring car pollutant emissions,” *Sci. Total Environ. (SCI Total ENVIRON)*, vol. 334–335, no. Science of the total environment, pp. 73–84, 2004.

[13] T. Barlow, S. Latham, I. Mccrae, and P. Boulter, *A reference book of driving cycles for use in the measurement of road vehicle emissions*. 2009.

# *Table of contents*


**1. INTRODUCTION 1**

**1.1 BACKGROUND 1**
**1.2 PROBLEM STATEMENT 2**
**1.3 OBJECTIVES 3**
1.3.1 GENERAL OBJECTIVE 3
1.3.2 SPECIFIC OBJECTIVES 3
**1.4 PROJECT SCOPE 3**
**1.5 DOCUMENT ORGANIZATION 4**

**2. STATE OF THE ART 5**

**2.1 IMPORTANCE OF FUEL CELLS 5**
**2.2 FUEL CELL APPLICATIONS 6**
2.2.1 VEHICULAR APPLICATIONS. 6
2.2.2 DISTRIBUTED GENERATION 7
2.2.3 PORTABLE APPLICATIONS 7
**2.3 WHY FUEL CELL BASED SYSTEMS ARE NOT WIDELY USED TODAY 7**
**2.4 FC BASED, HYBRID POWER SUPPLY ARCHITECTURES 8**
**2.5 HYBRID SOURCES POWER CONDITIONING 10**
**2.6 ENERGY MANAGEMENT APPROACHES 11**

**3. THEORETICAL FRAMEWORK 14**

**3.1 FUEL CELLS 14**
3.1.1 PEMFC OPERATION 14
3.1.2 PEMFC STATIC AND DYNAMIC BEHAVIOR 16
**3.2 SUPERCAPACITORS 23**
3.2.1 OPERATING PRINCIPLE 24
3.2.2 THE DOUBLE-LAYER EFFECT 24
**3.3 POWER CONDITIONING CIRCUITS FOR FUEL CELL APPLICATIONS 27**

**4. THE HYBRID POWER SOURCE FC/SC** **29**

**4.1 THE PROPOSED ENERGY MANAGEMENT CONFIGURATION** **29**
4.1.1 GLOBAL CONTROL LOOP: **DEMAND INTERPRETATION** 31
4.1.2 SECOND HIERARCHY LEVEL: **ENERGY MANAGEMENT AND STATE OF CHARGE (SOC) BLOCKS** 32
4.1.3 THIRD HIERARCHY LEVEL: **POWER CONVERTERS CONTROL** 36
**4.2 DC/DC CONVERTERS: MODELING AND CONTROL** **39**
4.2.1 FUEL CELL CD/CD CONVERTER 42
**4.3 MODELS AT SIMULATOR** **50**
4.3.1 BAHIA® FUEL CELL 50
4.3.2 SUPERCAPACITOR MODEL AT SIMULINK 55

**5. TESTING AND RESULTS** **58**

**5.1 MATERIAL AND METHODS** **58**
**5.2 SIMULATION** **60**

**6. CONCLUSION** **67**

**BIBLIOGRAPHY** **69**

# *Table of figures*


*Figure 2.1 Direct integration topology* 8
*Figure 2.2 A single CD/CD converter connected to FC (one degree of freedom)* 9
*Figure 2.3 A single CD/CD converter connected to SC (one degree of freedom)* 9
*Figure 2.4 Two-converters structure* 10
*Figure 2.5. CD/CD Conversion topologies recommended for FC based systems.* 11
*Figure 2.6a Basic topology of a not isolated CD/CD boost converter* 11
*Figure 2.6b Basic topology of a not isolated CD/CD bidirectional converter* 11
*Figure 3.1 PEMFC operation scheme* 15
*Figure 3.2 Graph showing the voltage for a typical low temperature, air pressure, fuel cell* 17
*Figure 3.3 Fuel cell equivalent circuit* 18
*Figure 3.4 Pressure effect on FC efficiency* 20
*Figure 3.5 H2/O2 Fuel Cell ideal potential as a function of temperature* 21
*Figure 3.6 Double layer capacitance effect over the FC electrode surface* 21
*Figure 3.7 FC equivalent circuit including the double layer capacitance effect* 22
*Figure 3.8 Fuel cell voltage response due to capacitance of double-layer charge effect* 23
*Figure 3.9 Ragone plot displaying the energy and power properties of various technologies* 23
*Figure 3.10 Principles of operation for a supercapacito* 25
*Figure 3.11 Electric double layer capacitor* 26
*Figure 3.12 Buck and boost CD/CD converters* 28
*Figure 3.13 Reducer-elevator topology* 28
*Figure 4.1 Hybrid FC/SC power supply with energy administration* 31
*Figure 4.2 Overall control loop* 32
*Figure 4.3 Functional regulation scheme showing two levels* 33
*Figure 4.4 Measured FC current input and voltage output* 33
*Figure 4.5 Magnitude Bode plot of the BAHIA FC frequency response* 34
*Figure 4.6 Dynamic distribution of the required* $i_{Load}$ 35
*Figure 4.7 Functional regulation scheme showing the three levels* 36
*Figure 4.8 Graph showing the voltage for a typical low temperature, air pressure, FC. Bahia FC®* 37
*Figure 4.9 BAHIA stack voltage, system efficiency, and net power density varying with net current density* 38
*Figure 4.10 FC boost converter* 38
*Figure 4.11 Bahia FC polarization curve* 39
*Figure 4.12 Two-quadrant SC converter* 39
*Figure 4.13 Buck Converter* 40
*Figure 4.14 Boost Converter* 40
*Figure 4.15 Buck/Boost Converter* 40
*Figure 4.16 PWM Commutation signal from Vramp and Vref.* 41
*Figure 4.17 DC/DC converter control loop with PI controller example* 42
*Figure 4.18 DC/DC elevator converter* 43
*Figure 4.19 Elevator-reducer voltage and current waveforms at the inductor in CCM* 44
*Figure 4.20 Boost DC/DC converter with feedback voltage control.* 44
*Figure 4.21 Block diagram of the control loop for the boost DC/DC converter* 49
*Figure 4.22 Bahia Helion® polarization curve. Image by Helion® User Manual.* 50
*Figure 4.23 Fuel cell equivalent circuit at simulator* 51
*Figure 4.24 PEMFC parameters and response to a current step* 54
*Figure 4.25 PEMFC parameters and response to a current step (Simulation and experimental results)* 54
*Figure 4.26 Top: FC polarization curve. Bottom: Power ratio against current output* 55
*Figure 4.27 BMODO5OO Maxwell supercapacitor bank* 55

*Figure 4.28 Supercapacitor equivalent circuit at simulator* 55
*Figure 4.29 Voltage exchange rate at SC* 56
*Figure 5.1 Experimental Bahia system* 58
*Figure 5.2 Bahia system Diagram.* 59
*Figure 5.3 Experimental Maxwell supercapacitor bank* 59
*Figure 5.4 Vehicle speed and power profile for ECE-15 cycle* 61
*Figure 5.5 Vehicle speed and power profile for UDDS cycle* 61
*Figure 5.6 Functional control strategy diagram* 62
*Figure 5.7 Bus voltage ($V_{bus}$) with ECE-15 driving cycle* 63
*Figure 5.8 Bus voltage ($V_{bus}$) with UDDS driving cycle* 63
*Figure 5.9 Supercapacitor SOC during ECE-15 driving cycle* 64
*Figure 5.10 Supercapacitor SOC during UDDS driving cycle* 64
*Figure 5.11 Delivered power and required power by the vehicle (scaled to 1 kW).* 64
*Figure 5.12 Delivered power to the vehicle vs FC power generation (UDDS)* 65
*Figure 5.13 Delivered power to the vehicle vs FC power generation (ECE-15)* 65
*Figure 5.14 Delivered power to the vehicle vs FC power generation (ECE-15)* 66
*Figure 5.15 Delivered power to the vehicle vs SC power under delivery/recovery conditions (UDDS)* 66
*Figure 5.16 $V_{bus}$, FC and SC voltages.* 66

# Chapter 1

## Introduction

## 1. INTRODUCTION

### 1.1 Background

In our society, the availability of energy is strongly linked to the level of welfare, health and the life of the human being. However, most of the energy production comes from nonrenewable sources, generating pollution and global warming.

Production of clean and alternative energy is therefore not a culture or an attempt to improve the environment, but a necessity, moreover, it is also critical foreseeing the imminent exhaustion of non-renewable energy sources.

Fuel cells generate electricity without pollution because the only by-products are electricity, water and heat. Fuel cells represent then renewable and clean energy sources vis-à-vis the fossil derived energetics such as natural gas, carbon and petroleum.

Because its high specific energy and less environmental impact, fuel cells were originally intended to replace internal combustion engines. However, the state of development of this technology does not compete advantageously with internal combustion engines due to their cost and lower specific power [1].

Conversely, supercapacitors are high specific power and low specific energy systems, so they can deliver energy very quickly, but have inferior storage capacity. The combination of high specific energy and high specific power density can be obtained with the integration of a fuel cell-supercapacitor bank system.

This sources integration or hybridization extends the operating range and improves the dynamic response of the system, while reducing costs. This is possible because the power sources can be dimensioned based on their utilization rate, without overstating the design.

A proper energy management strategy leads to efficiently operated hybrid systems. Thus, the energy management strategy should propose an appropriate criterion for deciding when the fuel cell operates and when the batteries operate, that is, a suitable power split criterion.

The main purpose of this work is to conceive a power management strategy for a hybrid power source composed of a Proton Exchange Membrane (PEM) fuel cell (FC) module, a supercapacitor (SC) bank and their associated power conditioning units. The system architecture, the power conditioning topology and the appropriate models are chosen to ensure the power delivery required by the load, the system management strategy is designed to promote energy saving and less fatigue

to its elements. The proposed energy management strategy is validated in a simulation environment; the simulator is built with power sources modeling libraries and some formulated models, thus, it considers the dynamic behavior of the power train components, including the power conditioning units. The hybrid power source must be able to deliver the energy. The case study considered is scaled to provide 1.2 kW. Then, the hybrid management strategy is tested in the simulation environment using a scaled driving cycle.

## 1.2 Problem statement

Researches on hybrid power sources focus mainly on modeling, control, or power conditioning advances. Recent works deal also with the hybridization or integrated systems developments, but in general, the various aspects of modeling, design and system operation problems are treated at different levels of completeness and accuracy.

Frequently, there are works that focus on hybrid systems design or development, but these do not integrate always appropriately the behavior of the sources: fuel cell, supercapacitors or batteries. For example, researches in FC-SC hybrid power systems can be focused specifically on the design or performance analysis of power converters, whereas the FC and SC models are simplified. By the other side, when a research is focused on sources modeling, sometimes the power conditioning functionality is not considered properly. This can lead to undesirable effects on implementation, like supercapacitor overcharging, fuel cell starvation or delay in power delivery.

Therefore, the first challenge is to develop the hybrid power source simulator, incorporating the main phenomena and dynamic behaviors of the fuel cell and the supercapacitor. The simulation of hybrid systems is complex, since the integration of elements with different dynamic time responses and important interactions is necessary. A trade-off between simplicity and comprehensive phenomenological considerations is then required.

Hybridization offers the possibility to improve the generation system efficiency and to reduce the system cost. Then, hybrid systems become more flexible, but at the same time creates challenges concerning the control at different levels (regulation supervision, optimization or system administration), consequently the development of strategies for energy management is crucial. These challenges are the main problem addressed in this thesis. The defy is to devise a management strategy capable of supplying the continuous load demand and the abrupt changes of the load; handle the deficit or excess of energy production; improve the transient response of the system; reduce the size of the fuel cell; provide power in the ranges in which no degradation or damage occurs; guarantee the state of charge (SOC) of the SC and achieve a constant tension in the CD bus. With the goal to attain these administration requirements, local controllers and an overall control for the power distribution must be implemented, the design of the management strategy must take into account the static and dynamic performances of each source.

## 1.3 Objectives

### 1.3.1 General objective

To develop an energy management strategy for a 1.2 kW hybrid power train composed of a PEMFC and a Supercapacitor interfaced to the load by power-conditioning elements.

### 1.3.2 Specific objectives

- To define the hybrid system architecture and the power conditioning topology for providing a 48 V DC bus, considering mobile applications.
- To build a simulator of the hybrid power source scheme: PEMFC/SC, incorporating the prediction of the dynamic behavior of all the system components.
- To develop the criteria for load distribution between the power sources, in real time.
- To design the local control of the fuel cell-DC/DC converter arrangement.
- To design the local control of the SC-bidirectional DC/DC supercapacitor arrangement.
- To design the global control.
- To evaluate the complete simulator in the MatLab/Simulink environment for a standard driving cycle, scaled down to 1.2 kW.

## 1.4 Project scope

The proposed energy management control strategy is designed to calculate dynamically the power demand for each source. Due to the system complexity, cascade control loops are organized into blocks, in accordance with their functionality.

The simulation results demonstrate that the energy management strategy ensures the proper supercapacitor state of charge. Furthermore, it guarantees smooth and safe currents to the fuel cell while maintaining the elements on its operating point. In this conditions, the fuel utilization decrease in presence of abrupt changes and its efficiency is improved.

The project includes the energy management design, the system architecture definition, the power conditioning topology definition, the modeling justification and the control system design.

The fuel cell is simulated with SimPowerSystems, from Electric Drives, Simulink library. The fuel cell block is configured to reproduce the dynamic experimental behavior of a 1.2 kW Bahia PEMFC module, which is physically available at ENSAM Laboratory (Aix-Marseille, France).

The supercapacitor model is based on a Maxwell SC bank (500 F, 16 V) performance, it is also available at the ENSAM Laboratory.

The power conditioning units were designed and sized, according to the fuel cell requirements and dynamic models were formulated for different analysis purposes.

Finally, MatLab/Simulink simulations were carried out to demonstrate the effectiveness of the strategy.

## 1.5 Document organization

This document is organized into six chapters. The first chapter contains a brief background and the objectives are defined. The second chapter is a review of the technics and methodologies encountered in the literature, regarding the various aspects of this study. The third chapter is dedicated to explain the frequency-based distribution strategy, proposed for administrating scaled electrical vehicle solicitations, whereas chapter four is dedicated to describe the energy management strategy as a set of local and global nested controls, grouped in functional blocks and organized in hierarchical levels. The chapter five presents the strategy simulation and evaluation using scaled standardized driving cycles. Finally, the conclusions and future works are described in chapter 6.

# Chapter 2

State of the art.

## 2. STATE OF THE ART

Among the various sources of renewable energy, the technology of fuel cells (FC) has received considerable attention as an alternative to conventional energy sources due to its good efficiency, clean operation and cost-effective power supply. In particular, the technology of Proton Exchange Membrane Fuel Cell (PEMFC) prevails over other types of FCs technologies, due to the advantages in their operating characteristics and to the wide range of applicability. Hybrid power systems, integrating auxiliary power sources, can provide better results, considering the issues of performance and durability obtained from a number of possible sources configurations.

This chapter presents a review of recent trends in PEMFC powered hybrid systems including a detailed explanation of application areas and design architectures with different power electronics interfaces as well as energy management methods utilized in the daily life and proposed in scientific literature.

### 2.1 Importance of Fuel Cells

A Fuel Cell is an energy conversion device that converts the chemical energy of a reaction directly into electricity with water and heat by-products. There are several types of commercially available FCs, such as proton exchange membrane (PEM) FCs, solid oxide FCs, alkaline FCs, direct methanol FCs, etc. Among the various types of FCs, the PEMFC technology has found widespread use, especially in vehicular applications, distributed generation (DG) units and portable electronic equipment [2]. Some of the key advantages and some disadvantages of PEMFC systems over the other competitive types of FCs can be specified as follows [3]:

Advantages of PEMFC:

- They can operate at relatively low temperatures.
- They are tolerant to $CO_2$, so they can work with atmospheric air.
- They have high voltage, current and energy density.
- They can work at low pressure (1 or 2 bars), which adds security.
- They have a good tolerance to the difference of pressure of the reactants.
- They are compact and robust.
- They have a simple mechanical design.
- They use stable building materials.

Disadvantages:

- They have slow dynamics.
- They are very sensitive to impurities of hydrogen.
- They need humidification units of reactant gasses.
- They use very expensive catalyst (platinum) and electrolyte (solid polymeric membrane).

The slow dynamic behavior of the Fuel Cells, makes difficult to follow the fast load variations, typically from residential and vehicular applications. These fast energy demand periods frequently occurring in the operation of daily utilized systems produce high voltage drop in short time, typical causes are starvation and depletion phenomena.

In the case of the fuel or oxygen starvation, the FC performance degrades, and the cell voltage drops. Thus, to utilize an FC in dynamic applications, its current or power slope must be limited to prevent the fuel cell starvation problem. It is therefore recommended, when utilizing a PEMFC, to associate it with, at least, an auxiliary power source to improve the dynamic performances of the whole system. There are many types of auxiliary units for compensating the slow response characteristics of the PEMFC unit and increasing the efficiency of the overall system. Energy storage units such as batteries, supercapacitors (UCs), flywheels, etc. and secondary power units like micro-turbines, diesel generators, etc. can be classified as auxiliary power units to be used in hybrid systems based on PEMFCs. Specifically, energy storage units not only compensate the slow response phenomenon of PEMFC system, but also provide the advantage of recovering the re-usable energy. A well-known example is the kinetic energy recuperated from vehicles in motion during braking periods. The consumption of hydrogen for FC units can be significantly decreased if convenient energy recuperation is considered.

Because of different characteristics of multiple power sources in a PEMFC-based powered hybrid system, the efficiency and the fuel economy of these hybrid units mainly depend on a proper energy management strategy and well-designed power electronics architecture.

## 2.2 Fuel cell applications

Due to the fact that PEMFCs can generate power from a few Watts to hundred kilo-Watts and provide environmental friendly operation, they can be used in almost every application where local electricity generation is needed.

### 2.2.1 Vehicular applications.

FCs offer clearly advantages over the internal combustion engines (ICE) for vehicular applications because they are energy efficient, clean, and fuel flexible. Hydrogen FC systems have the potential to reach 60% peak efficiency on lower heating value (LHV) basis. Onboard the vehicle, conversion of hydrogen to traction power produces water only. Hydrogen can be produced from a variety of sources including fossil fuels such as natural gas, renewables such as solar and wind power, biomass, and nuclear energy [4].

Automobiles, buses, scooters, golf cars, utility vehicles (such as forklifts and airport vehicles), locomotives, tramways, boats, airplanes, underwater vehicles can be clarified as some of the applications of PEMFC systems in transportation area. Especially in automobile systems, almost all major car manufacturers have demonstrated prototypes of FC vehicles and announced future plans for production and commercialization in the near future [5].

### 2.2.2 Distributed generation

The term DG means any small-scale generation unit located near to the customers rather than central or remote locations. The major benefits of DG systems are saving in losses over the long transmission and distribution lines, installation cost, local voltage regulation, and ability to add a small unit instead of a larger one during peak load conditions [6].

PEMFC systems have been installed worldwide in many types of distributed centers such as hospitals, shelters, centers for elderly care, hotels, offices and schools. Moreover, PEMFC technology has found an application area in the field of telecommunications, where there is a need for a fully reliable electricity supply [7]. In these cases, the PEMFC system is connected to the grid to provide additional electrical power to the plant, or as an independent system of the grid to generate electricity in remote or isolated areas. The use of PEMFC in such systems may either be as a main power source or as a backup unit.

### 2.2.3 Portable applications

FCs can provide electrical power in places where the grid connection is not available and can be used as portable power units. Moreover, the use of PEMFCs for portable computers (laptops) and mobile phones initiated lately and this idea has found a widespread attention from manufacturers.

The researches of reputed companies such as Motorola, Toshiba, Samsung, Panasonic, Sanyo, and Sony have shown that mobile phones can be run for twice if compared to the one that uses a lithium battery with an equivalent size, moreover it needs only 10 min to recharge. As far as laptops are concerned, it has been shown that laptops with FCs may be working up to 5 h without refueling [8].

## 2.3 Why Fuel cell based systems are not widely used today

Many factors have limited the marketable development of FCs, including manufacturing cost, fuel generation and distribution, and system complexity and durability. The high manufacturing cost is caused by a number of factors: expensive raw materials used as catalysts, expensive membrane materials, and expensive fabrication processes for collector plates. In addition to manufacturing cost, fuel generation and distribution have also prevented widespread commercialization. Most FCs consume pure hydrogen or hydrogen-rich gas as the primary fuel. So far, experimental results and real-world applications of PEMFCs revealed that they perform best on pure hydrogen as anode input gas. However, for many applications, particularly mobile, due to the lack of availability of refuelling infrastructure and impractical storage techniques, pure hydrogen is not yet a viable option [9].

In summary, wider use of PEMFCs can only be expected in a near future, when important and rather complex problems will be solved. The necessary actions to increase the fuel cell technology growth are summarized as follows [10]:

- Longer the lifetime of the power plants, finding better stability of the catalysts and membranes.
- Lower the cost of production of the PEMFC, which can be achieved by the promoting the development of catalysts without platinum by using alternative structures, such as carbon nanotubes and cheaper membranes.
- Developing new plants for hydrogen production admitting a wider selection of primary fuels or new production technologies.
- Providing refueling stations, especially for vehicular applications.

## 2.4 FC based, hybrid power supply architectures

The selection of the power-conditioning unit for hybrid systems including PEMFC is based on some significant factors including lower cost, higher efficiency, electrical isolation, ripple free and reliable operation. Considering the above-mentioned factors as well as the load requirements characteristics of the application area, various topologies may be used for interfacing the PEMFC hybrid systems. One of the simplest structures for parallel operation of PEMFC hybrid systems includes the direct integration of PEMFC system with the auxiliary power unit as shown in Figure 2.1.

The direct integration topology interconnects each power source directly to the load via the CD bus. Some advantages of this configuration can be obtained: a simple structure, energy reversibility (due to supercapacitor), natural energy management, favorable FC behavior in case of failure and low cost.

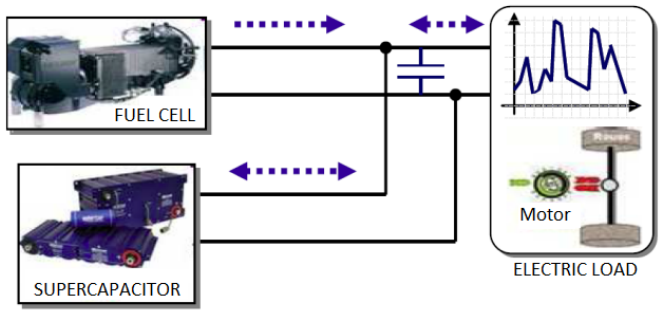


Figure 2.1 Direct integration topology

The direct integration topology is attractive because it does not require a high-power DC/DC converter, thus the complexity, cost, weight, and volume of the system are significantly reduced. This topology is proposed by Honda [11] , for a combined PEMFC/Ultracapacitor (UC) powered vehicular system. Uzunoglu and Alam [12] utilized this topology for a stand-alone system, while Yalcinoz and Alam, applied the same topology for portable applications. The same topology is also utilized by Onar [13] as a part of his study and analysis of the combination of FC and UC in a Wind Turbine/PEMFC/ UC hybrid system for stand-alone applications.

However, when using this topology, special attention to the system power is required. Furthermore, it is necessary to design a special supercapacitor with a lower impedance than the FC, which usually oversize the capacitance value and increments the system costs.

Different designs of a topologies with only one DC/DC converter unit are shown in Figures 2.2 and 2.3. The topology in Figure 2.2 regulates the output power of the FC system while the rest of the energy between the load demand and the FC output power is naturally supplied by the auxiliary unit. The topology in Figure 2.3 is based on the regulation of the auxiliary system output power or the regulation of the DC bus voltage. There are many studies in the literature using both topologies. Topology in Figure 2.2 is utilized by Jiang [14] for PEMFC/Battery hybridization, by Xu.[15] for PEMFC/Battery powered city bus, and by Fontela [16] for an airport vehicle powered by PEMFC. Moreover, the second topology in Figure 2.3 is applied by Payman [17] for PEMFC/UC hybridization while the same hybridization structure is also employed by Chen [18].

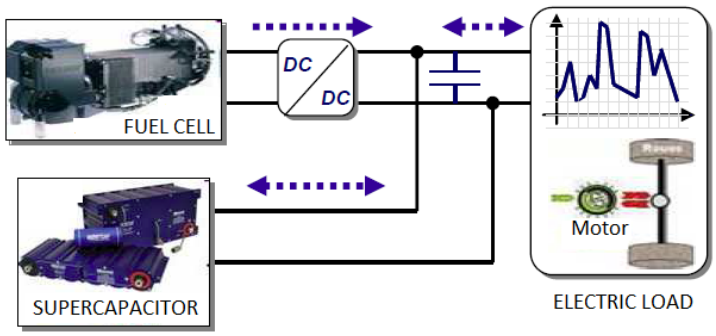


Figure 2.2 A single CD/CD converter connected to FC (one degree of freedom)

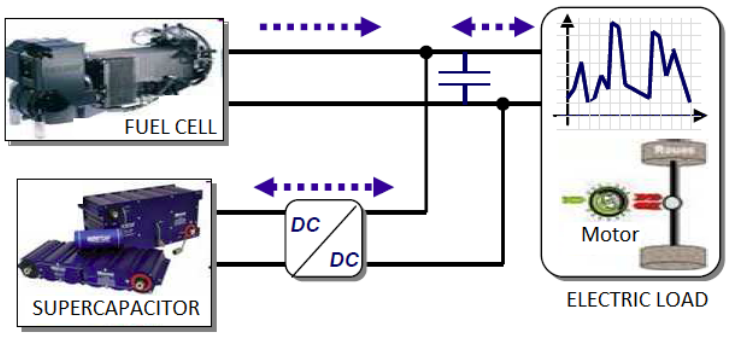


Figure 2.3 A single CD/CD converter connected to SC (one degree of freedom)

Although this structure is simple (it has a single CD/CD converter), the DC Bus voltage is limited to the voltage encountered at the element directly connected to the DC bus. This has the effect of reducing the system flexibility, but voltage variations are supported by the load.

On the other hand, the topology more recurrently reported in the literature for hybrid systems is composed of multiple DC/DC converters as seen in Figure 2.4. In this topology, the DC/DC converter of one of the available power sources is employed for the DC bus voltage regulation which is called ‘‘voltage-oriented-control’’. The rest of the converters are controlled for power tracking by a

‘‘power-oriented-control’’ methodology. Thus, the proposed power-conditioning unit provides the capability of delivering the desired power value from the hybrid power sources while keeping the bus voltage at the desired level. This topology has been applied in different areas. The studies of Zhang [19], Erdinc [20], [21], Thounthong [9], [22], and Feroldi [23] are some examples of the usage of multiple converter topologies for transportation areas. Other studies of Thounthong [24] and [25] are examples of DG systems application for this hybrid structure. Similarly, Stewart [26] utilized this topology for a DG hybrid unit, where the system consists of a PEMFC, a photo-voltaic collector, and a battery, linked to a metal hydride and high pressure gas storage system. Furthermore, an electrolyzer produces the hydrogen consumed by the FC.

This structure, although more complex, implies more flexibility to design the power management strategy. It has two converters that can regulate the voltage of each source while adequately protects the fuel cell.

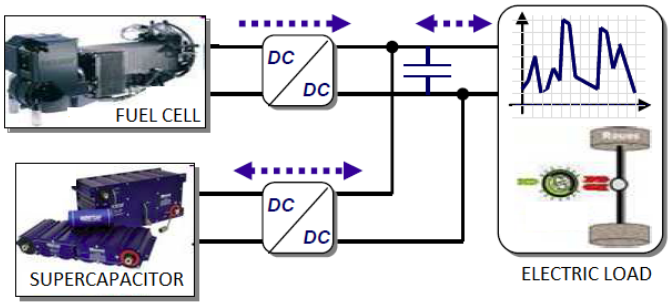


Figure 2.4 Two-converters structure

The topologies reported above have been generally used for applications with a PEMFC as the main power source. However, a specific classification can be made for distributed systems, where the principal power sources are renewable energy sources (wind or solar), with an FC as a backup source.

## 2.5 Hybrid sources power conditioning

The design of the DC / DC converters must take into account a variety of factors, e.g., the system functionality, the power dimensioning, the components technology, the associated control needs, and the number of inputs and outputs required. Many researchers focuses on improving the performance or reducing the number of elements in the design of the converter. Other researches focus on the extention of the components lifecycle. Other authors propose the use of DC/DC converters in applications with fuel cells according to the power level, isolation or system architecture (Figure 2.5).

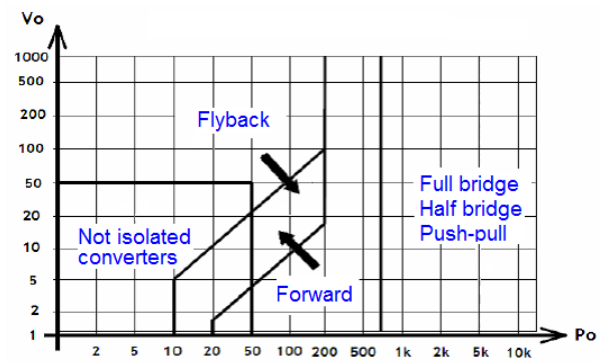


Figure 2.5. CD/CD Conversion topologies recommended for FC based systems. Image by [27].

The basic topologies for a nonisolated unidirectional converter and a bidirectional nonisolated converter are shown in Figure 2.6a and 2.6b, respectively.

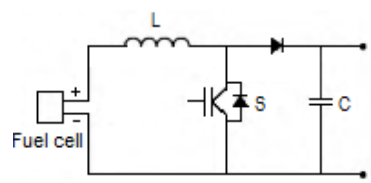


Figure 2.6a Basic topology of a not isolated CD/CD boost converter

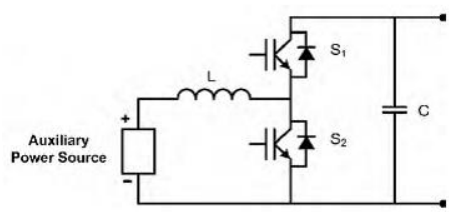


Figure 2.6b Basic topology of a not isolated CD/CD bidirectional converter

There are more complex CD/CD converter topologies and they are usually designed for specific objectives. Some examples for hybrid sources are found in [28], Thounthong [29], Khan and Tolbert [30], Farzanehfard [31] and Solero [32].

## 2.6 Energy management approaches

Due to the multidisciplinary character of the power trains with multiple-sources, the efficiency and the fuel economy of these hybrid systems depend essentially on the efficiency of the energy management strategy (EMS). It is widely accepted that the uninterrupted operation and transient behavior of the FC stack increases the mechanical stresses inside the FC, and consequently

decreases the stack lifetime. On the other hand, the continuous regulation of state variables (such as reactant flow, stack temperature, humidity, flow and pressure) directly leads to more constraining requirements of the dynamic responses of actuators (valves, motors, etc.) and sensors (pressure, flow rates, temperatures, humidity, etc.), and potentially increase the cost of the overall system.

Nowadays, there are many studies using intelligent-based algorithms for developing energy management strategies for use in PEMFC powered systems, such as fuzzy logic and neural networks. Gao [33] provided the power distribution in a ‘‘hydrogen’’ powered hybrid bus composed of PEMFC as the main power source and battery/UC combination as the auxiliary unit. The fuzzy logic controller applied in [34] utilized the SOC values of auxiliary units and the required power demand of the bus as inputs for determining the output power values of FC and UC systems. Erdnic [20] regulated the energy management in PEMFC/ UC and PEMFC/Battery/UC powered hybrid vehicular systems using fuzzy logic. Fuzzy structures of Erdinc utilized the SOC values of battery and/or UC units and a transient-free form of the vehicular power demand (provided by a load sharing algorithm) based on standard driving cycles as inputs and gave the requested power value from PEMFC system as the output.

Li and Liu [35] proposed an fuzzy logic controller design for a PEMFC/Battery hybrid system with a similar structure to that presented by [21], [20], [36], [37], with optimized parameters of their FLC for maximal efficiency of the energy control.

Another intelligent method used for controlling hybrid systems is the neural network approach. Neural network models are computer programs, designed to emulate human information processing capabilities such as knowledge processing, speech, prediction, classifications, and control. The ability of neural network systems to spontaneously learn from examples and to provide adequate and quick responses to new information which are not previously stored in memory has generated increasing acceptance for this technology in various engineering fields.

Another management energy strategies are optimization based. That means that the optimal reference power signals for the on-board power sources are calculated by minimizing a cost function. The cost function usually represents the fuel consumption or emissions, especially for vehicular applications. If this optimization is performed over a fixed driving cycle, a global optimum solution can be found. Many approaches such as optimal control theory, linear programming, dynamic or stochastic programming, genetic algorithm, simulated annealing, linear and nonlinear model predictive, and game theory are utilized for solving the aforementioned global optimization problem.

Rodatz [38] presented an experimentally implemented “equivalent fuel consumption minimization strategy’’ aiming at minimizing the hydrogen consumption while maintaining drivability in a PEMFC/UC hybrid vehicular system. Xu [39] performed a similar optimization approach for an FC/Battery hybrid bus. Similar fuel consumption minimization-based approaches were also utilized by Paladini [40] for FC/Battery/UC hybridization in a vehicle simulation environment.

On the other hand, the Frequency decoupling based energy management strategies consider that, during the daily operation of a system, load transitions may occur frequently. This is particularly true for vehicular systems applications. The transient changes of the load demand may occur repeatedly

and cause dynamic stress onto the FC membrane due to pressure oscillations and possible oxygen starvation, and subsequently, reduce the lifetime of the FC system. Thus, to ensure FC lifetime prolongation by preventing the FC system from load changes with high frequencies, researchers have applied different frequency decoupling techniques. The basic approach for this issue is inserting a first-order low-pass filter (transfer function of a delay with a suitable time constant) to stablish a cutoff value, limiting the FC operation.

Liu [41] proposed a first-order filter for distributing the power in a PEMFC system. In general, the most conventional filtering techniques like Butterworth high and low-frequency filters, etc. have been utilized.

Uzunoglu and Alam [42] applied a wavelet-based energy management strategy for a PEMFC/UC hybrid vehicular system. A similar wavelet-based approach was utilized by Zhang [43] for a PEMFC/Battery/UC hybrid system. Erdinc [44] and Ates [45] also utilized the wavelet transform as a part of their energy management approaches.

Becherif and Henni [46] proposed to connect, at the output of the FC, a boost converter in series with a bidirectional converter. The load is considered as a DC machine.

There are many energy management approaches. Use of one architecture or another depends on the researcher interest, but as it has been described in this chapter, depending on the hybrid system conformation, current proposals for improving energy administration concern the design of supply configurations, dictating the interactions between the sources and the load along with the connections between the sources and their power conversion units. In the next chapters, the frequency-based energy management strategy that we propose is explained.

On the other hand, based on control strategies at different levels, the administration of hybrid systems entails a variety of objectives, however, the focus is on the power splitting approaches [47], [48],[49]. Other important features that management strategies incorporate increasingly are the dynamics modeling of the fuel cell and the estimation of the accumulators SOC[50], [51], [52], [53], [54],[55].

After analyzing the state of the art, it was observed that even if numerous researches have reported on the subject, few studies have taken into account the proper dynamics of each source in order to optimize the global performance of the hybrid power supply. Consequently, the goal of this work is to implement a complete simulator integrating dynamical models of the sources and power conditioning units.
The control strategy consists of nested loops, arranged in three functional levels of hierarchy. The central idea is to find the optimal set point for each energy source, according to their own physical properties. Contrary to the existing control strategies, this strategy dynamically calculates the appropriate power demand for each energy source. Due to the complexity of the system, cascade control loops are proposed, organized in blocks, according to the system functionality and dynamics.

# Chapter 3

## Theoretical framework

## 3. Theoretical framework

Designing an FC-based power source requires a basic component operation knowledge. Using the FC itself as a power source is not viable due to some disadvantages as mentioned in chapter 2. In the same regard, FC power systems incorporate energy backups, including but not limited to batteries, supercapacitors, photovoltaic cells, wind generators, etc.

Power conditioning is a relevant aspect, given the dependency that the integration of power sources and storage represents. Further aspects of the power conditioning units that influence the entire system are the efficiency, security and costs.

The theoretical framework for all the subsystems that integrates the hybrid system, along with local and global control strategies are presented in this chapter. Finally, the FC/SC simulation model for the hybrid energy source is described.

### 3.1 Fuel Cells

The fuel cell is an electrochemical device where the chemical energy obtained from the fuel is transformed into direct current electrical energy. Fuel cells are conformed by an electrolytic layer in contact directly with an anode and a cathode of porous nature. To operate a FC, the anode is fed with a fuel (composed by hydrogen, natural gas or methanol) and, with an oxidant in the cathode (normally oxygen, air or hydrogen peroxide). The resulting chemical reaction produces water, heat and an electrical current.

There are five basic fuel cell structures, all of them working under the same electrochemical and thermodynamic principles, nevertheless, the structural and mechanical design is completely different. At present, existing FCs are: PAFC or phosphoric acid, MCFC or molten carbon, SOFC or solid oxygen, AFC or Alkalines and finally, the PEMFC or protonic exchange membrane. The selection of the type of FC depends on the required power level and cogeneration necessities; the application goes from small portable applications, up to vehicular applications, microcogeneration, co-generation and heat generation, or distributed generation. The FC are normally classified in function of the electrolyte but, classification can also be done considering the operating temperature, the power level, the efficiency and the application field. The operating temperature determines the heat production capabilities, FCs operate in a truly wide range, from 23 °C (AFC) to 1000 °C (SOFC).

#### 3.1.1 PEMFC operation

Like every other electrolytic FCs, the PEMFC is conformed by an anode, a cathode and an electrolyte. In a PEMFCs these elements are called the membrane-electrode assembly. Within this assembly, the polymeric membrane works as the electrolyte and is contained between two metallic plates

called bipolar plates, this structure is referred as a mono-cell. The bipolar plates serves for supplying the gasses and provide an electrical connection between mono-cells [56].

The PEM operation principle is shown in Figure 3.1 [56]. The process starts when the hydrogen and oxygen are fed at the defined pressure. The fuel then spreads uniformly across the bipolar plates channels, until the anode of the cell is reached (A). In a similar way, the pure oxygen stored in a tank under pressure or the air from a compressor follows the same path but through the cathode (B).

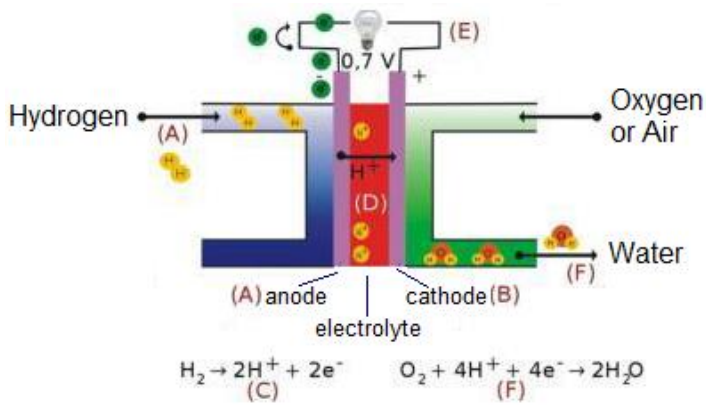


Figure 3.1 PEMFC operation scheme. Image by [56].

At the anode, the $H_2$ molecules spread through the pores in the diffusion plates. Afterward, these molecules arrive at the catalytic plate, where they get linked with the catalyst, causing the reduction in the ionization potential and the molecule dissociation (or breakdown) into atoms. In other words, the molecular hydrogen ($H_2$) is transformed into ($H^+$) protons and ($e^-$) electrons through the anode reaction (C). H+ ions migrate through the electrolyte by means of leaps (D). Resulting ions adhere to the negatively loaded radicals up to the cathode, due to the existing water in the cell. The cell gets its name from this operation mode, due to the proton exchange between the electrodes, referred to the $H^+$ transport through the membrane.

The electrons cannot pass through the membrane because it is built with an isolating material then, it conducts through the metallic plates conforming an external electrical circuit. An external load (E) can be fed with the electrons current, the main product of this device.

At the same time, the ions in the cathode ($H^+$) migrate through the membrane, the electrons, transported by the external circuit and the oxygen molecules moving to the surface links in the catalyzer producing water through the cathode reaction (F). The water and exothermic reactions are the secondary products.

In this way, a mono-cell generates a voltage around 0.7V . In order to get a higher voltage, a number of mono-cells are electrically connected in series for supplying the demanded voltage and power, this is called FC stack.

Combining the cell stacking with auxiliary elements enables the cell to operate at the right pressure, temperature and humidity parameters. The resulting system is a FC plant balance.

*Auxiliar parts*

Depending on its power capability, a fuel can or cannot include auxiliary subsystems. These subsystems provide support to the cell for different operational requirements, including a battery for the starting energy. Subsystems can be (48):

- The reactant supply subsystem,
- The heat spread subsystem, for cooling up the cell and assert the right temperature for the incoming gasses
- The power conversion subsystem that allows a useful voltage delivery. (Output voltage varies significantly through the time, what is not suitable for traction motors or vehicle electronics)
- The water handling subsystem including:
    a) A de-ionized water supply device to humidify gasses
    b) A water separator for the humidifier water recycling.

### 3.1.2 PEMFC static and dynamic behavior

Just like in the non-ideal real electrical sources, the voltage at the FC terminals varies depending on multiple factors, e.g. external load, operation zone, temperature and pressure.

The way to understand the steady state behavior of a FC is the polarization curve. The characteristic profile of a typical FC is shown in Figure 3.2. There are three main operation zones and, for any of these, there are associated voltage losses. The characteristic voltage losses are due to non ideal behavior and resistances to transport of materials and electric energy. The operating regions are explained below [57].

**Activation losses.** Is referred to the voltage losses due to the electrodes reactions slowness. A portion of the generated voltage is consumed in driving the electron transfer to the electrodes. This is a nonlinear kind of overpotential.

**Ohmic losses.** Resistive losses in this region relate to the electron flow through the electrodes material and the interconnections, as well as per the resistance to the electrons flow through the electrolyte. It is considered the optimal operating zone, where the FC must be conducted all the time.

**Concentration losses.** Problems related to the diffusion of the reactants through porous material in the electrodes surfaces causes the characteristic behavior of this region. Operation in this region is not recommended since it combines high voltage drops with very high current densities.

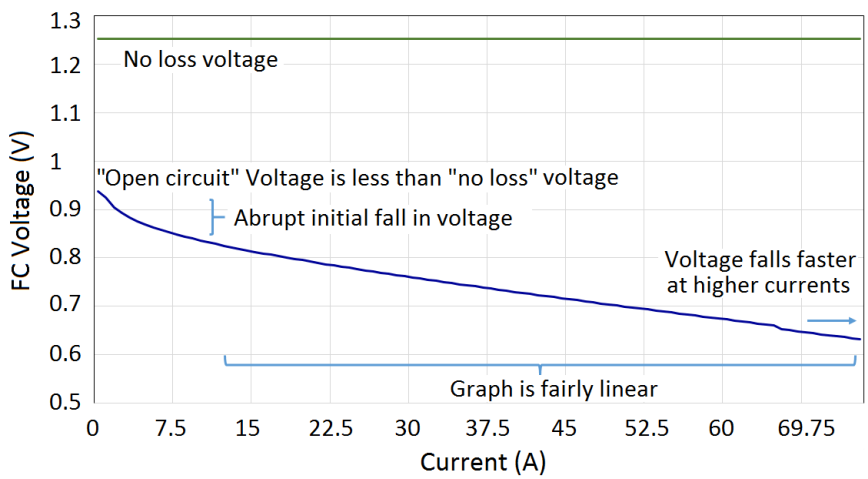


Figure 3.2 Graph showing the voltage for a typical low temperature, air pressure, fuel cell

Considering the current density values in the previous graph, it can be seen that [57]:

- At the starting point (to the extreme left of the curve), open circuit voltage is lower than the expected theoretical value. Beside this, a fast nonlinear drop is happening at the beginning.
- The presence of an operation zone, where the voltage drop is constant and slow and can be approximated to a linear drop.
- Finally, in the operation limit zone (at the extreme right of the curve), the high current density leads to a faster voltage drop.

#### *3.1.2.1 Fuel cell equivalent circuit*

In general, the voltage at the FC terminals is different than the voltage developed inside the fuel cells, obtained from Nernst equation (3.1). This is due to the activation, ohmic, and concentration voltage drops inside fuel cells, as shown in Figure 3.2. These voltage drops are functions of load current and fuel cell temperature and/or pressure. The ohmic voltage drop is a linear function of fuel cell load current, but the ohmic resistance is normally a function of fuel cell temperature. The activation and concentration voltage drops are nonlinear functions of load current as well as pressure and/or temperature inside the fuel cell [6].

From Figure 3.2, the output voltage of a fuel cell can be written as:

$$V_{FC} = E_{FC} - V_{act} - V_{ohm} - V_{con} \tag{3.0}$$

Where:

$\boldsymbol{V_{FC}}$ *Fuel cell output voltage*

$\boldsymbol{E_{FC}}$ *Fuel cell internal voltage*

$\boldsymbol{V_{act}}$ *Voltage drop by activation*

$\boldsymbol{V_{ohm}}$ *Ohmic voltage drop*

$\boldsymbol{V_{con}}$ *Voltage drop by concentration losses*

Figure 3.3 shows the FC equivalent circuit with the static elements described in this section.

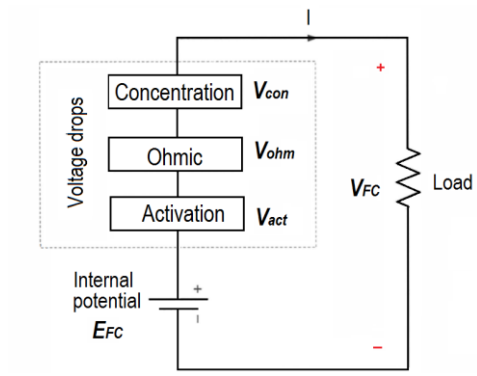


Figure 3.3 Fuel cell equivalent circuit. Image by [6].

Along with the load current, pressure and temperature, the FC double layer capacitance impacts the dynamic response. Description of this effect and the voltage overpotentials ($V_{act} - V_{ohm} - V_{con}$) is shown below.

### Reversible voltage (Nerst potential)

The cell reversible voltage ($\boldsymbol{E_{FC}}$) is the open circuit potential in thermodynamic equilibrium. This potential expression, considering pressure and temperature changes is:

$$E_{FC} = \frac{\Delta G}{2F} + \frac{\Delta S}{2F}(T - T_{ref}) + \frac{RT}{2F}\left[ln(P_{H_2}) + \frac{1}{2}ln(P_{O_2})\right]$$

$$= E^0 + \frac{\Delta S}{2F}(T - T_{ref}) + \frac{RT}{2F}\left[ln(P_{H_2}) + \frac{1}{2}ln(P_{O_2})\right] \tag{3.1}$$

where:

| | |
|---|---|
| $E^0$ | *The electromotive force at standard pressure.* |
| *ΔG* | *Free Gibbs energy delta, J/mol.* |
| *F* | *Faraday's Constant, 96.487 C mol$^{-1}$.* |
| *ΔS* | *Entropy delta, J/K mol.* |
| *R* | *Universal gas constant, 8.314 J/mol K.* |
| $(P_{H_2})(P_{O_2})$ | *Hydrogen and Oxygen partial pressures (atm).* |
| *T* | *Cell operation temperature, K* |
| $T_{ref}$ | *Reference temperature, K.* |

Using PEMFC electrochemical model associated values, it is possible to simplify the Nerst potential expression as described in the equation 3.2.

$$E_{NERST} = 1.229 - 0.85 * 10^{-3}(T - 298.15) + 4.31 * 10^{-5}T\left[ln(P_{H_2}) + \frac{1}{2}ln(P_{O_2})\right] \tag{3.2}$$

The Nerst voltage relates the electric response of the FC to the Gibbs free energy, the entropy and the measured variables as the reaction temperature and the electrode-electrolyte interface partial pressure, as it can be noticed in the equation (3.1). Equation (3.2) defines de Nerst voltage only in terms of measurable variables [57].

### Activation overpotential

The activation over potential usually happens in the cathode, causing the most relevant cell voltage drop in the low to mid temperature cells.

The electrodes overpotential needs to be considered seriously, however, in high temperature fuel cells, its relevance is lower. The activation potentials produced in the anode and cathode are calculated through equation (3.3) in both cases:

$$V_{ACT} = -\left[\xi_1 + \xi_2 * T + \xi_3 * T * \ln\left(C_{O_2}\right) + \xi_4 * T * \ln(i)\right] \tag{3.3}$$

Where:

*I* *Cell operation current, (A).*

$\left(C_{O_2}\right)$ *Cathod catalytic interface oxygen concentration, (mol/cm$^3$)*

$\xi'$ *Specific cell model parametric coefficients.*

### Ohmic overpotential

The losses due to the electrical resistance of the electrodes, and the resistance to the flow of ions in the electrolyte, are the simplest to understand and to model. The size of the voltage drop is simply proportional to the current. Equation (3.4):

$$V = IR \tag{3.4}$$

In most fuel cells the resistance is mainly caused by the electrolyte, though the cell interconnects or bipolar plates can also be important.

### Overpotential by concentration or mass transport

If the oxygen present in the cathode is fed through the atmospheric air, over the fuel cell operation, the oxygen concentration in the electrode region will be slightly reduced. This reduction is associated with a change in the oxygen partial pressure, and it depends on the required electrical current and the system characteristics. In a similar way, depending on the load requests, the hydrogen concentration at the anode could be reduced.

The effect on this pressure reduction or the partial pressure, results in a change on the open circuit voltage due to the reactants pressure change. The voltage change due to hydrogen consumption is represented with equation (3.5):

$$\Delta V = \frac{RT}{2F} ln\left(\frac{P_2}{P_1}\right) \tag{3.5}$$

The fuel gas pressure change is obtained as follows: a limit *i* is considered in the current density, where the maximum fuel flow to the cell takes place; current density cannot exceed this value because the cell cannot be fed at a higher flow speed. At this current density, pressure will be barely zero. If $P_1$ is the zero-pressure current density and, a linear pressure drop is assumed in a corrent density of $i_1$ then, $P_2$ for every current density is given by equation (3.6):

$$P_2 = P_1\left(1 - \frac{i}{i_1}\right) \tag{3.6}$$

Replacing (3.6) in (3.5):

$$\Delta V = \frac{RT}{2F} ln\left(1 - \frac{i}{i_1}\right) \tag{3.7}$$

Equation 3.7 serves to compute the voltage change due to the masses transport in the electrodes. This equation can be also represented as indicated in (3.8):

$$\Delta V = -B * ln\left(1 - \frac{i}{i_1}\right) \tag{3.8}$$

Where $B$ constant depends on the characteristic behavior of the mono-cell. For hydrogen fuel it becomes as indicated in equation (3.7).

### *3.1.2.2 The pressure impact on the efficiency*

The electrochemical reaction speed is proportional to the hydrogen and oxygen partial pressures. Given this, if the delivered air pressure increases, the performance of the FC will also be enhanced. Nonetheless, this behavior is not linear (Figure 3.4).

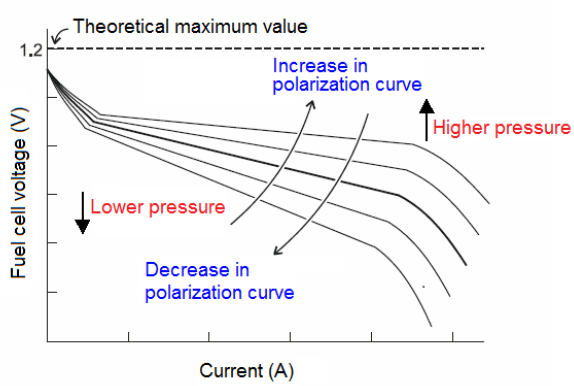


Figure 3.4 Pressure effect on FC efficiency. Image by [27].

It is worth to mention that, operating the FC at very high or very low pressure, requires the assessment of the system efficiency impact.

### *3.1.2.3 The temperature impact on the efficiency*

Temperature changes produce similar effects. The FC performance improves when the operation temperature is increased. This is because, at higher temperatures, the masses transfer within the cell is better and lower transport resistances are produced. When temperature increases, the electrical conductivity in metals decreases, while the electrolytic ionic conductivity increases. This combined behavior increases the reaction speed. The voltage classical response to the operating temperature variation in the FC is shown in Figure 3.5.

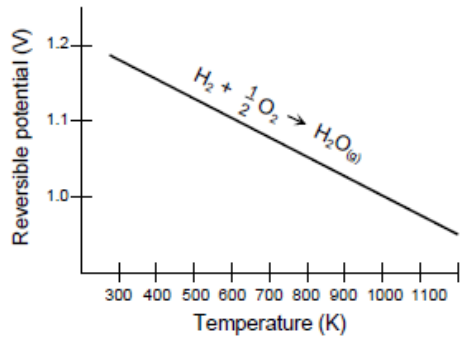


Figure 3.5 H2/O2 Fuel Cell ideal potential as a function of temperature. Image by [27].

Figure 3.4 shows the relation of voltage to cell temperature. Because the figure shows the potential of higher temperature cells, the ideal potential corresponds to a reaction where the water product is in a gaseous state (i.e., $E^o$ is 1.18 volts).

The impact of temperature on the ideal voltage, E, for the oxidation of hydrogen is also shown in Table 3.1 for the various types of fuel cells. Each case assumes gaseous products as its basis [27].

| **Temperature** | 25°C | 80°C | 100°C | 205°C | 650°C | 800°C | 1100°C |
|---|---|---|---|---|---|---|---|
| **Cell type** | PEMFC | PEMFC | AFC | PAFC | MCFC | ITSOFC | TSOFC |
| **Ideal Voltage** | 1.18 | 1.17 | 1.16 | 1.14 | 1.03 | 0.99 | 0.91 |

Table 3.1 Ideal Voltage as a Function of Cell Temperature [27]

### 3.1.2.4 Double-layer capacitance

In a fuel cell, the electrodes are separated by the electrolyte (Figure 3.5), creating two thin layers in the boundaries, namely, the anode-electrolyte and the electrolyte-cathode layers, where a small amount of electrical charge is stored. This accumulation of charge within the boundary layers is known as the "Electric double layer capacitance" and the energy storing can be seen as a capacitive effect dictating the electric dynamic behavior of the FC. The positive and negative ions gathering in the porous electrode surface, creates a capacitor behavior is appreciated in Figure 3.6.

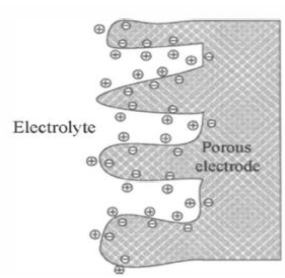


Figure 3.6 Double layer capacitance effect over the FC electrode surface. Image by [27].

The following expression is used for representing the equivalent capacitance:

$$C = \varepsilon \frac{A}{l} \tag{3.9}$$

*Where:*

| | |
|---|---|
| $\varepsilon$ | *Electrolytic electric permittivity.* |
| $A$ | *Electrolytic-electrode gap effective surface.* |
| $l$ | *Gap thickness.* |

In a real FC, if the area $A$ is larger and the distance $l$ is smaller due to the porous electrode structure (in the order of nanometers), higher capacitance values result (from hundreds of $\mu$F to a few F).

The FC equivalent circuit of Figure 3.3 can be modified to include the double layer capacitance effect, as shown in Figure 3.7, as a result, the new equivalent circuit is suitable for modeling the electric dynamic performance of the FC [6].

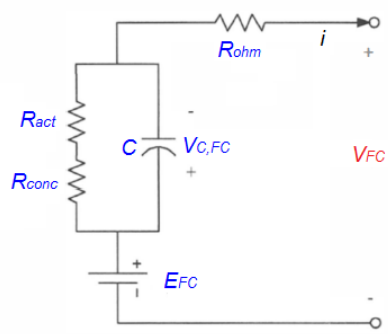


Figure 3.7 FC equivalent circuit including the double layer capacitance effect. Image by [6].

$R_{ohm}, R_{act}\ y\ R_{conc}$ in Figure 3.7 correspond to the ohmic, activation and concentration resistances (defining the related overpotentials), respectively. The voltage through the capacitor is defined by:

$$V_{C,FC} = \left(i - C\frac{dV_{C,FC}}{dt}\right)(R_{act} + R_{con}) \tag{3.10}$$

Only the activation and the concentration resistances affect the circuit time constant $\tau = (R_{act} + R_{con})C$ (the voltage through the double layer capacitance $V_{C,FC}$). This is because only the changes to these two resistances are related to the electrochemical reactions inside the FC. The ohmic resistance is just the resistance originated by the voltage ohmic losses.

Output FC voltage is then expressed with:

$$V_{FC} = E_{FC} - V_{C,FC} - V_{ohm} \tag{3.11}$$

$V_{C,FC}$ is time dependent, and the time constant is $\tau$.

Figure 3.8 shows the FC voltage response to different $C$ values ($V_{FC}$). Using some typical FC parameters, the $\tau$ constant is in the order of miliseconds.

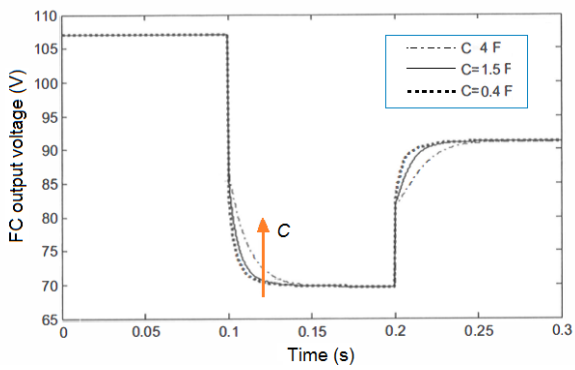


Figure 3.8 Fuel cell voltage response due to capacitance of double-layer charge effect. Image by [6].

## 3.2 Supercapacitors

The supercapacitor (also known as ultracondenser, ultracapacitor, supercondenser or dual layer condenser) is an electrochemical capacitor with a nonusually high energetic density. These devices do not require dielectric, so they can be built in almost any size, from a stamp size, ideal for cell phones, up to the largest sizes used in hybrid vehicles.

These devices have an electrolytic solution that allows the static electric energy storage. Regardless its electrochemical nature, no chemical reactions are produced inside these devices.

With high power density, the supercapacitors are suitable for handling fast or sudden energy demand changes. Compared with batteries, the SCs main difference lies in the specific energy and specific power. SCs, compared with the batteries, have significantly lower energy density, but also higher power density.

The Ragone plot in Figure 3.9 compares the specific energy and specific power for different energy generation or energy storage systems [1].

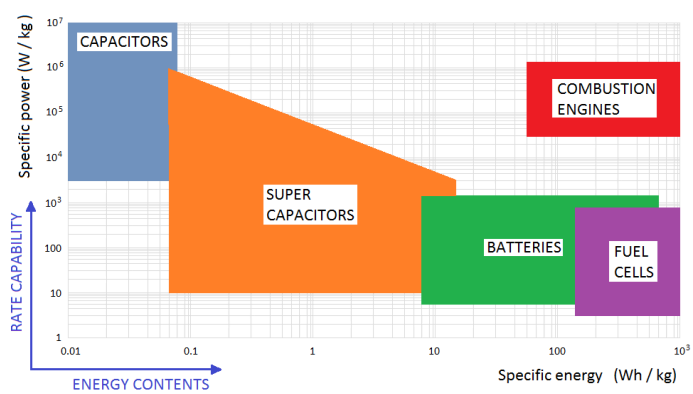


Figure 3.9 Ragone plot displaying the energy and power properties of various technologies

### 3.2.1 Operating principle

The physics behind the electrolytic capacitors were first described by Hermann von Helmholtz back in 1853. He concluded that the interaction between a conductor and the electrolyte inside a capacitor is determined by electrostatic relations and that there are no chemical reactions involved in the process [58]. The supercapacitor is based on this theory and it is an improved version of the original capacitor design.

Compared to a normal capacitor, when highly concentrated solutions are used, the distance between opposite sign electrical charges through the electrode-electrolyte interface can lie in the Angstroms range. Given this, if the proper material is used to construct the electrode, it is possible to have a supercapacitor.

**The Electrode.** For traditional capacitors, the electrodes are built with thin surfaces, where the electrical charges gather. In the supercapacitor, the electrodes are a kind of micro-porous structure, sometimes made of carbon, where the electrolyte deposits around them. The result of using this kind of structure is a significant larger area of the electrostatic condensers. By isolating the anode and the cathode, a very thin membrane is used between the SC electrodes. Despite of the membrane isolation from the electrodes surface, ions transportation is still allowed freely.

**The Electrolyte.** The main difference between the supercapacitor and the ordinary electrostatic capacitor is that the electrolyte of supercapacitors contains free charges in the form of ions. The ordinary capacitor does not have this type of free charges. There are two main electrolytes today on the market, mixtures of salts with acetonitrile (CAN) or propylene carbonate (PC). The properties of the electrolyte set the rated voltage for the capacitors. The rated voltage must be lower than the oxidation voltage for the electrolyte. If the oxidation voltage is reached, a chemical process is started in the electrolyte that creates gases from the electrolyte. Today, electrolytes that give a rated voltage of up to 2.8 V are available. One important property of the electrolyte is that it must enable the dissolution of some types of salt which promote the existence of free ions in the capacitor. Another desired property is that the ions have a high mobility within the electrolyte. This is because the mobility mostly determines the series resistance of the supercapacitor. High mobility gives low series resistance and vice versa. The other contribution to the series resistance comes from the resistance in the conductors but that is relatively low compared to the contribution from the electrolyte. In some applications, a third important property can be added to the electrolyte, it is the temperature stability for attaining the ion mobility. This property differs between the two electrolytes that are used today. The ACN electrolyte gives a more stable series resistance during temperature changes compared to PC, especially at low temperatures. The drawback of using ACN is that this substance has an environmental disadvantage. If the capacitor is over charged to the oxidation voltage, the resulting gases contain cyanide which is a toxic substance and for this reason it is not allowed to be used in some nations [59].

### 3.2.2 The double-layer effect

In order to define the supercapacitor and to characterize its properties and fundamental parameters, its principles of operation are given in figure 3.10.

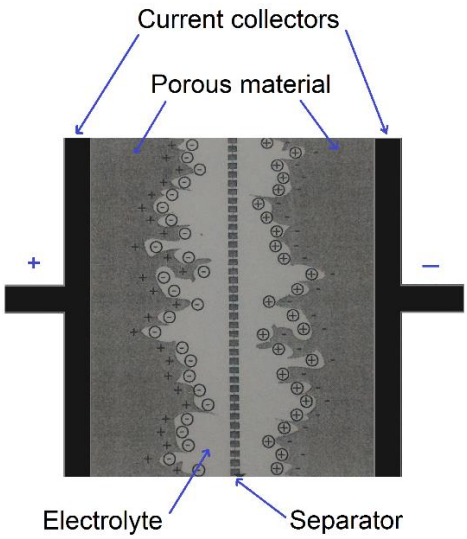

Figure 3.10 Principles of operation for a supercapacitor. Image by [60].

A supercapacitor consist of two electrodes that are galvanically isolated by a separator, which is soaked in an electrolyte. The two electrodes are created by deposition of a porous material on a metal film. The metallic film is generally aluminum, whereas charcoal (activated charcoal) is chosen as the porous material. When the component is charged, the charges stored at the interface between the porous material and the electrolyte. The used activated charcoal enables charge to be stored on a significant active surface while offering a good electric conductivity.
The function of the electrolyte is to ensure the mobility of the ions it contains towards the electrodes. The anions should be able to progress freely towards positive electrode, whereas the cations should be able to progress freely towards negative electrode. The electrolyte may be solid, but is generally liquid. The choice of the electrolyte is the result of a compromise between the voltage performance and the ionic conductivity. Minimization of the latter leads to a choice of electrolytes that have low dissociation voltages (1V). In order to avoid oxido-reduction mechanism, which would lead irreversible mechanism during the charge and discharge phases, the operating voltages of the supercapacitor must be limited (from 2.5 to 3 V).

The separator is generally a sheet of paper. Its role is that of an insulator, which should prevent any galvanic contact between the electrodes. However, it must be able to be soaked in electrolyte without reducing the electrolyte's ionic conductivity. Two principal parameters lead to the energy density of a current supercapacitor: the maximum voltage that can be applied and its capacitance.
As a previously introduced, the maximum voltage is defined by the choice of electrolyte. Currently, the choice is based on electrolytes offering operating voltages between 2.5 and 3 V, the latter at the detriment of the ionic conductivity, which will be reduced [60].

The capacitance values for a supercapacitor go from a farad to a kilofarad. Such capacitances are obtained using the principle on which the operation of the supercapacitor is based: the electric double-layer introduced by Helmholtz in 1879 and shown in Figure 3.11.

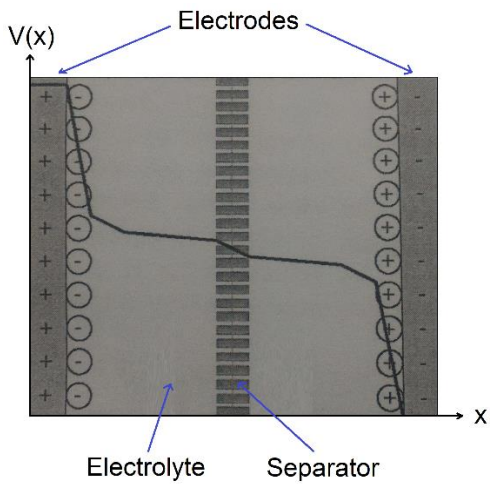


Figure 3.11 Electric double layer capacitor. Image by [60].

During charging, anions contained in the electrolyte are attracted towards the positive electrode, whereas cations converge towards the negatively charge electrode. At the interface between each of the two electrodes and the electro two double-layers are formed. These two double-layers lead to capacitances defined by Equation 3.12.

$$C = \frac{\varepsilon A}{d} \tag{3.12}$$

where:

| | |
|---|---|
| *A* | *Surface* |
| *d* | *Electric charges gap* |
| *ε* | *Dielectric constant* |

The SC stored energy is defined as:

$$E = \frac{CV^2}{2} \tag{3.13}$$

where:

| | |
|---|---|
| *Q* | *Stored energy* |
| *C* | *Capacitance* |
| *V* | *Voltage* |

Therefore, we can regard the supercapacitor as two capacitors in series with other, representing the two double layers of the two electrodes. The equivalent capacitance obtained is due to the effective surface of the two electrodes, as well as the dimension of the anions and cations. This leads to significant capacitances, of up to a kilofarad. Finally, we must remember that the maximum voltage admissible is determined by the choice of electrolyte. This voltage is between 2 and 3 V [60].

## 3.3 Power conditioning circuits for fuel cell applications

Characteristic phenomena in the hybrid feeding systems, such the slow dynamics, output voltage variability, physical equipment damage risk or sensibility to inner current sudden changes can be better addressed where an adequate power conditioning topology and the right controllers are chosen. Some of these phenomena are described below.

**Slow cell dynamics.** Slow dynamics occurs due to the electrodes electrochemical reaction kinetics, the fuel (hydrogen) flow pressure variability and the oxidant agent (oxygen). At the starting point, the cell capability for supplying energy is not optimal, due to the slow reaction speed, increasing gradually until the optimal operation point is reached. The voltage response is slow then, some applications consider the use of battery banks for providing the optimal voltage level during the startup.

**Fuel Cell output voltage variability.** The FC delivers a no regulated CD voltage, that represents a disadvantage compared to other power sources; this is the main reason why the cell is not adequate for direct feed applications, requiring additional conversion stages (CD/CD, CA/CA) for delivering a regulated output voltage.

**Inner current sudden changes sensibility.** Considering the type of load and its behaviors, sudden current changes must be absorbed or driven by the system in order to avoid FC damage due to the starvation effect.

**Galvanic Isolation.** For power levels beyond 1 kW [61], it is highly desirable to protect the FC against feedback currents, commonly present in certain topologies. The galvanic isolation (high and low frequency transformers) are considered for such systems.

**DC/DC Converters classification.**

For the feeding system, either based on FC or hybrid systems, it is necessary to maintain a constant voltage at the output terminals, regardless of the inner voltage and load variations. A DC/DC converter performs this task, working under two basic principles: reducer or elevator and many other topologies can be derived out of these two.

In general, DC/DC converters are also classified in isolated and non-isolated. Topology examples for non-isolated converter are the reducer (buck), the elevator (boost), reducer-elevator, half bridge and full bridge converters. On the other side, the isolated converters use an electric isolation device, normally a high frequency transformer, between the input and output; being the flyback, forward, push-pull and the isolated half and full bridge converters examples of the isolated topologies.

It is desirable for studying any electronic circuit the use of linear techniques. Nevertheless, switched mode power converters are nonlinear and discontinuous circuits. For characterizing these circuits, it is necessary to split into linear sub-circuits and, thereafter, use state average modeling techniques to linearize and analyze the small signal behavior [6]. Figures 3.12 and 3.13 show the basic DC/DC conversion topologies and summarize the behavior of each converter type.

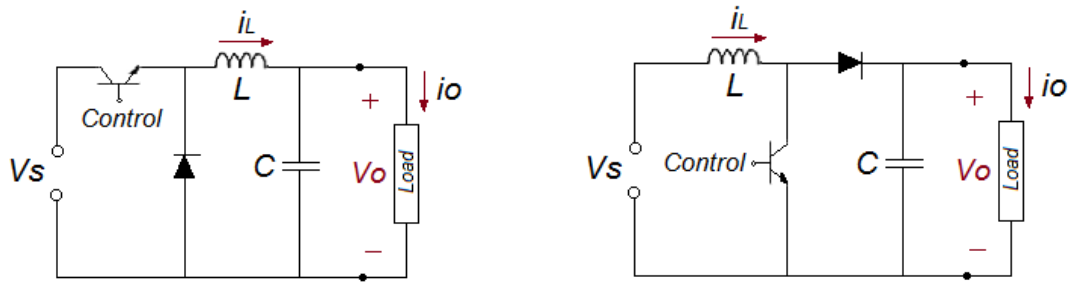


a) Buck topology b) Boost topology

Figure 3.12 Buck and boost CD/CD converters

**Reducer converter (Buck).** The main feature of this converter is the lower voltage at the output compared with the input, another features of this converter are the design simplicity, simple control, short circuit and overcurrent protection, easy implementation and the small-required cap for voltage ripple minimization at the output (Figure 3.12a).

**Elevator converter (Boost).** Presents a higher voltage at the output, compared with the input (Figure 3.12b). The main drawback of this converter is the lack of short circuit protection at the output, because the diode provides a direct short between the input and output. Along with this, it presents a bad transient response, which is hard to stabilize, thus, and additional series active device for short circuit protection is recommended. Other features of this converter are the high efficiency, its simplicity and a great power factor, since the input current is not switching and high RMS current is present in the switching element.

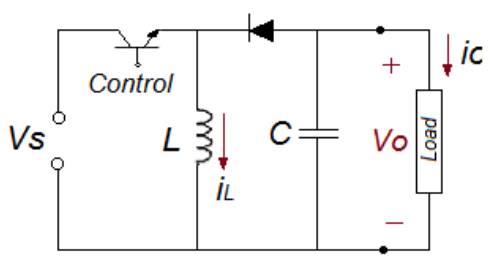


Figure 3.13 Reducer-elevator topology

**Reducer-elevator topology (Buck-boost).** It is used for inverting the output polarity (Figure 3.13). The output voltage can be either higher or lower than the input, depending that on the duty cycle. This converter is derived from the cascade connection of a buck and boost converters. The features of this converter are high efficiency, inverted polarity output voltage without using transformer, its simplicity, the possibility for either elevate or reduce the voltage and allows discontinuous input and output currents.

Besides these topologies, there are several more complex topologies that have been proposed for FC based feeding systems but, for the sake of simplicity, only the most commonly used topologies for these systems were mentioned.

# Chapter 4

## The hybrid power source FC/SC

## 4. THE HYBRID POWER SOURCE FC/SC

This chapter is dedicated to present the regulation architecture developed to coordinate the hybrid renewable source for typical solicitations of electric vehicles in a scaled operating range of 1 kW. The hybrid system is composed of a Polymer Electrolyte Membrane Fuel Cell (PEMFC) module, a supercapacitor bank and their respective power conditioning units. In order to optimize the overall operation, the proposed strategy is organized in three hierarchical levels, and the power demand for each energy source is determined in real time with a basis on a frequency distribution and a cutoff frequency, defined in accordance with the dynamical capabilities of the sources.

### 4.1 The proposed energy management configuration

The system builds on the typical constant DC bus voltage for hybrid vehicle structures. The hybrid system is composed of a fuel cell, a supercapacitor bank and their respective power conditioning units. The fuel cell is the principal source and the supercapacitor bank operates as the backup source. The energy management strategy coordinate all the elements in the system to provide continuously the necessary traction, and at the same time, to keep constant the bus voltage ($V_{bus}$) and maintain the SC SOC.

The proposed hybrid source comprises a small-scale 48 V dc bus supplied by a PEM FC Bahía® module (400 W - 1100 W, 0 A - 70 A nominal), coupled with a Maxwell supercapacitor bank (400 F, 16 V), which operates as the auxiliary source. A boost DC/DC converter does the power conditioning for the FC, while a bidirectional DC/DC converter manages the delivery and recovery cycles of the SC Bank. Such converters are connected in parallel and regulate the DC bus, where the load is powered.

Thus, the emphasis of the proposed rule-based strategy for administrating a hybrid system is on the consideration of the PEMFC and SC performances through experimental measurements, and basic behavioral and dynamic capacities estimations, with improvements regarding:

1. The fulfillment of the complete energy demand in the hybrid system: we recalculate the instantaneous energy demand by accounting the power deficit and excess, e.g. the load demand, the SC charge requirements and the extra energy supply, such as regenerative

vehicle braking for the conduction cycles scaled tests. The strategy includes simple conditions statements for accounting the global demand.

2. A straightforward method for assuring the SC SOC: the strategy implies a simple SC voltage control to indirectly regulate the SC SOC, but also infers this state. From the previously described methods, we consider the *book-keeping* estimation for supervising on-line the SC SOC, as a tool serving to verify the effectiveness of the SC SOC regulation [62].

3. The power split strategy based on the PEMFC performance measurements: experiments were registered with the aim to analyze the response of the PEMFC module at different operating conditions. These signals aided to determine the real PEMFC frequency operating domain and its limits for subsequently, determining the cutoff frequency useful to restrict the PEMFC operation. Then, we used model block libraries for simulating the sources dynamics, these were configured in accordance with the real behavior of the experimental module to take on-line decisions.

(i) The PEMFC operation remains in the safety region: the strategy also includes simple conditions statements for preventing the PEMFC to operate in the concentration region.

The design of the energy management strategy is organized in three hierarchical levels [63]. The first level is the global control loop, defined as the demand interpretation block, which has the main objective of regulating the voltage on the DC bus. Here, the load enters as the disturbance signal. The output of this global control block represents the input of the following control loops with lower hierarchical levels. The second level involves internal control loops, responsible for the SC SOC regulation and the definition of the adequate power split between the FC and the SC bank. The third level has internal control loops coordinating the interaction between power conditioning units and the sources (Figure 4.1). The simulator is built in the MatLab/Simulink environment and uses power systems libraries. The PEMFC output voltage electric dynamic response is determined by the double layer capacitance effect.

The following sections provide a detailed description of the energy management strategy as well as the assumptions necessary for its development. The evaluation of the proposed strategy is described in chapter 5, using scaled driving cycles.

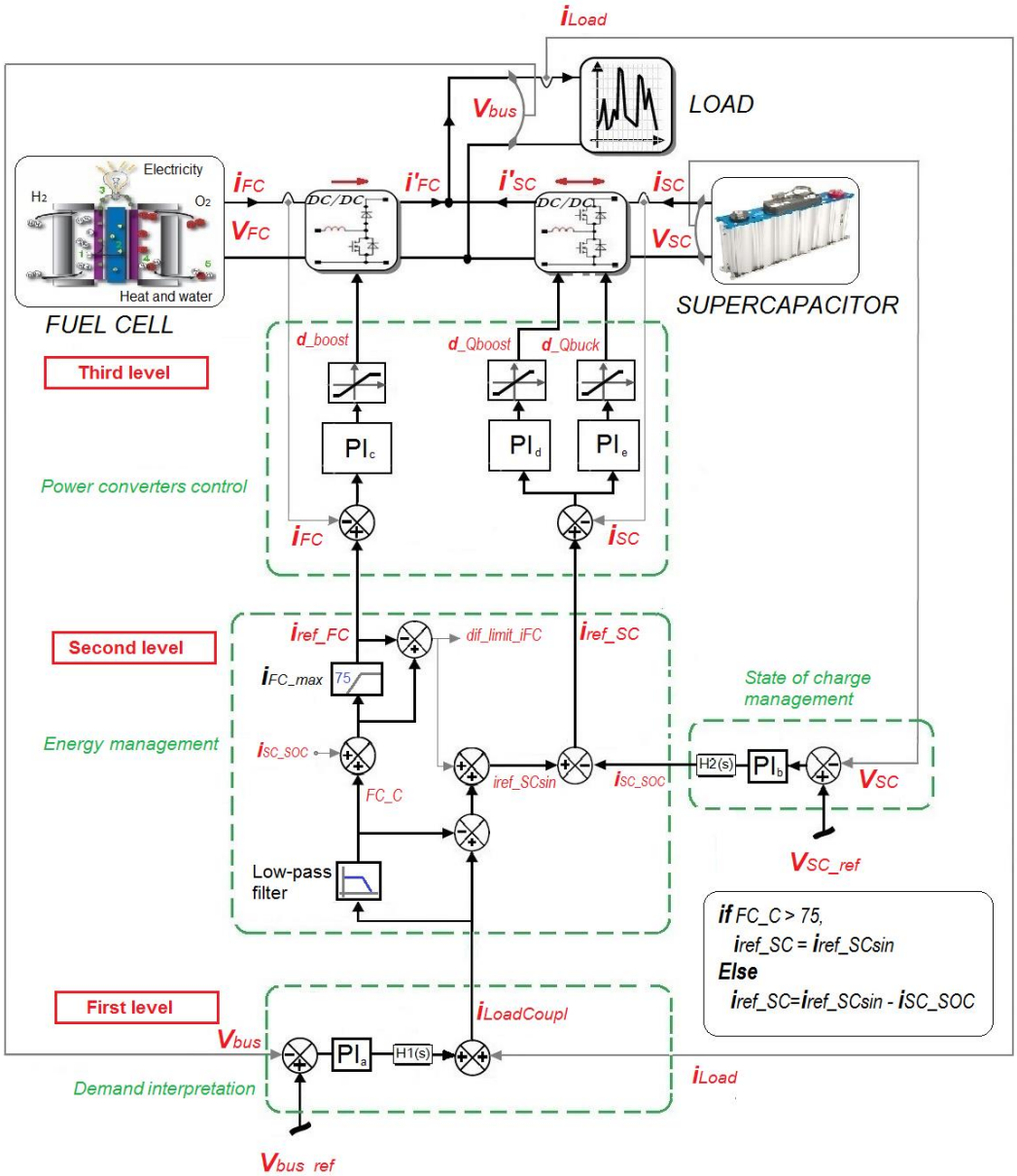


Figure 4.1 Hybrid FC/SC power supply with energy administration

### 4.1.1 Global Control Loop: Demand interpretation

The global control loop has two objectives. The first objective is to regulate the bus voltage ($V_{bus}$) to 48 V DC. The second is to obtain the current reference ($I_{ref}$) for the fuel cell and the supercapacitor, which determines the energy demand for each source.

The load demand does not represent the total energy demanded to the system. The global demand must be calculated at every moment considering the deficit and extra energy within the complete system.

The global control loop is depicted in Figure 4.1 The block receives two inputs: the measured ($V_{bus}$) and the current requirement of the load ($i_{load}$). The block output is the current reference for the "Energy Management" block.

This block has an inner voltage PI controller (master control). The variable $i_{Load}$ is treated as a disturbance and is added to the output of the $V_{bus}$ controller. Local control loops (grey boxes in Figure 4.2) are part of the lower hierarchy blocks, explained in sections *4.1.2 and 4.1.3*.

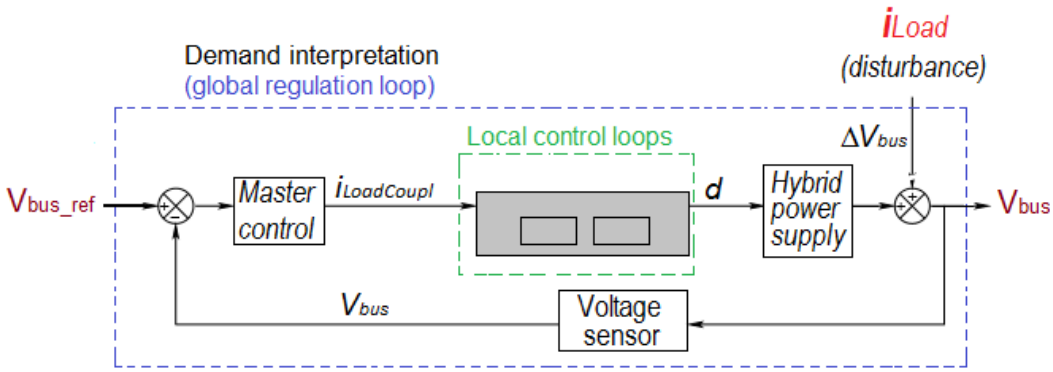


Figure 4.2 Overall control loop

The advantage of developing a nested structure of the energy management is that it can react to disturbance before affecting the output. Therefore, local drivers (or internal control loops) should be faster than external control loops.

### 4.1.2 Second hierarchy level: Energy management and State of charge (SOC) blocks

This level is the foremost step of the proposed energy management strategy and is composed of two functional blocks: the energy power distribution block and the SC SOC regulation block (Figure 4.3).

The objective of the energy management block is to determine the power split between the sources in order to define the FC and SC current references. The design of the energy management strategy takes into consideration that the dynamical behavior of the sources does not stand into the same range of frequency, i.e., FCs are high-density devices, but they have lower power capabilities than SC, and consequently have slower responses than SC. This is a classical result [63], but here the split rule is improved to operate the system efficiently under important current variations, by taking into account the SC SOC and the FC capabilities. More precisely, to enhance the FC performance, it is fundamental to determine appropriately the bandwidth corresponding to the characteristic FC power-density.

Therefore, the fuel cell cutoff frequency is calculated from experimental voltage-current signal measurements for a step trains load profiles.

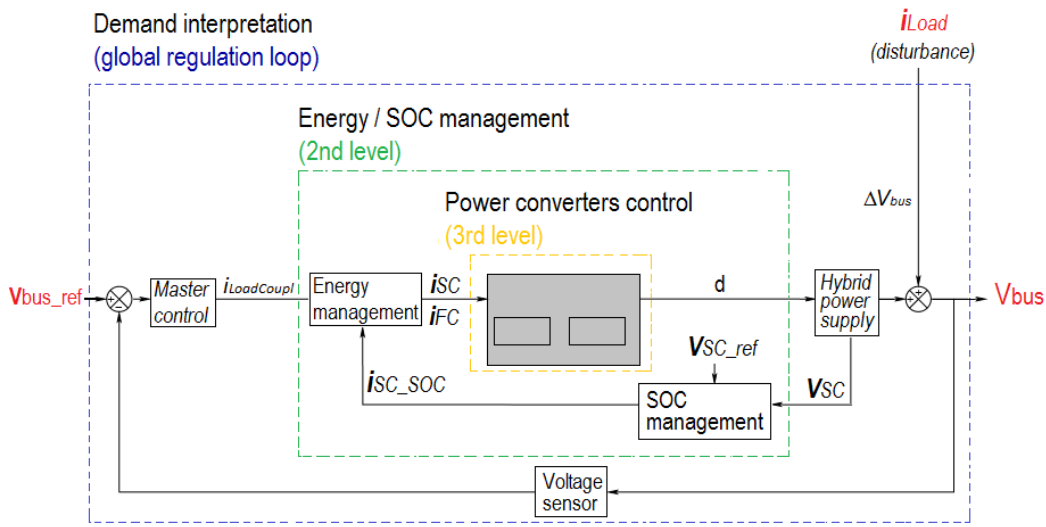


Figure 4.3 Functional regulation scheme showing two levels

From experimental data, it was possible to interpret the behavior of the system. As input, a current pulse with modulation was applied to de Bahia FC. As output, the FC voltage was measured. Figure 4.4 a) shows one of the current train pulses applied to the FC Bahia (at nominal conditions) and Figure 4.4 b) shows the FC voltage response.

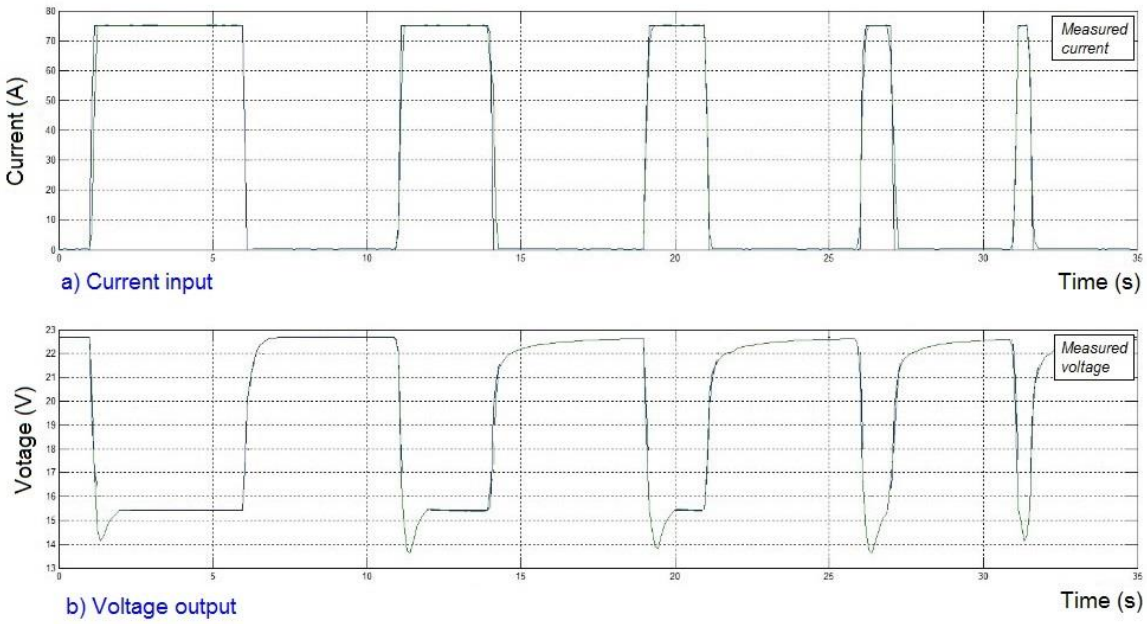


Figure 4.4 Measured FC current input and voltage output

The cut-off frequency ($f_{limit}$) of the low-pass filter depends on the FC characteristics (it is specially linked to the FC compressor performance and its control).

Low frequencies components are obtained by a first order low-pass filter, RC circuit. The difference between the original signal and the low frequencies components is used to

determine the high frequency SC demand. The value of $f_{limit}$ is the maximal frequency selected to operate the fuel cell, then it was determined from the experimental behavior at different operating conditions. A series of pulsed current with variable width inputs were demanded to the BAHIA FC at three different temperatures: 50°C, 55°C and 60°C, and three different stoichiometric oxygen excess ratios: 1.5, 2 or 2.5. The criterion to choose the cut-off frequency was to guarantee operation in the high electric efficiency and within the linear region, regardless of temperature and stoichiometry variations. Hence, the experimental temperature and stoichiometric conditions cover a wide electrical performance, always in the desired region, i.e., currents between 0.194 and 75.18 A, and output voltage in the range of 13.159 to 22.832 V. The voltage measured at the PEMFC terminals were registered as the corresponding outputs. With the measured input-output experimental data, the frequency response of the BAHIA FC was estimated via a spectral analysis (Blackman-Tukey spectral analysis) with frequency-dependent resolution. Figure 6 displays the Bode magnitude plot of the frequency response. It was observed that the frequencies that lie within the bandwidth characterizing the BAHIA FC are between 10 mHz and 50 mHz. (Figure 4.5). The fuel cell response is faster when the stoichiometric excess ratio increases, but for values higher than 2 the response becomes slower, this fact correlates well with theory because the optimal operation of a fuel cell is typically close to 2. On the other hand, it is well accepted that the increase of temperature has a direct proportional influence on the voltage output, nevertheless, the fuel cell data shows a bigger influence of the stoichiometry. From the frequency fuel cell data obtained, one can observe that the frequency beyond which the fuel cell is not able to respond is 50 mHz. Thus, the cut-off frequency $f_{limit}$ at which the low pass filter will not pass signals is set to this highest value obtained (50 mHz).

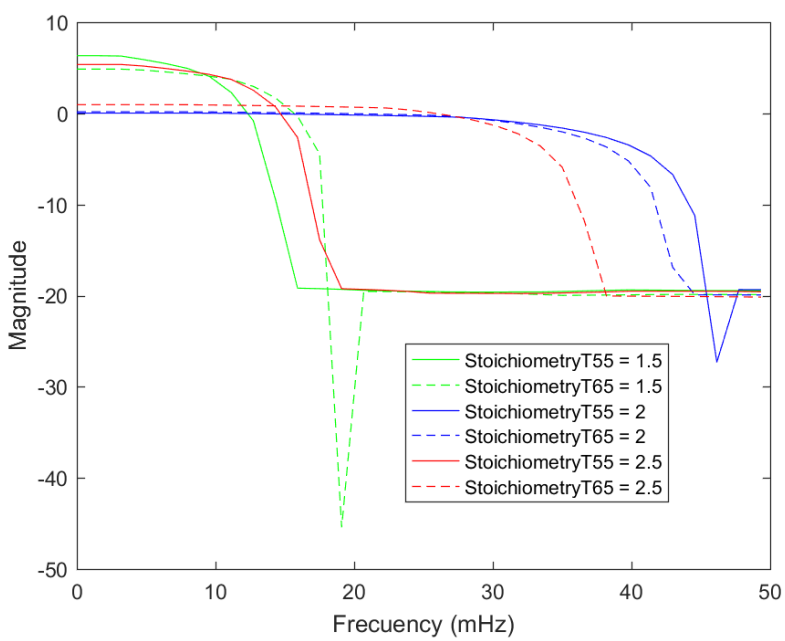


Figure 4.5 Magnitude Bode plot of the BAHIA FC frequency response

Then, by filtering technics, the contribution of the load current provided by the FC can be calculated safely and efficiently (Figure 4.6). The high frequencies are supplied by the Supercapacitor and low frequencies are provided by the fuel cell. That is to say, the proposed strategy is intended to improve the operating conditions of both sources.

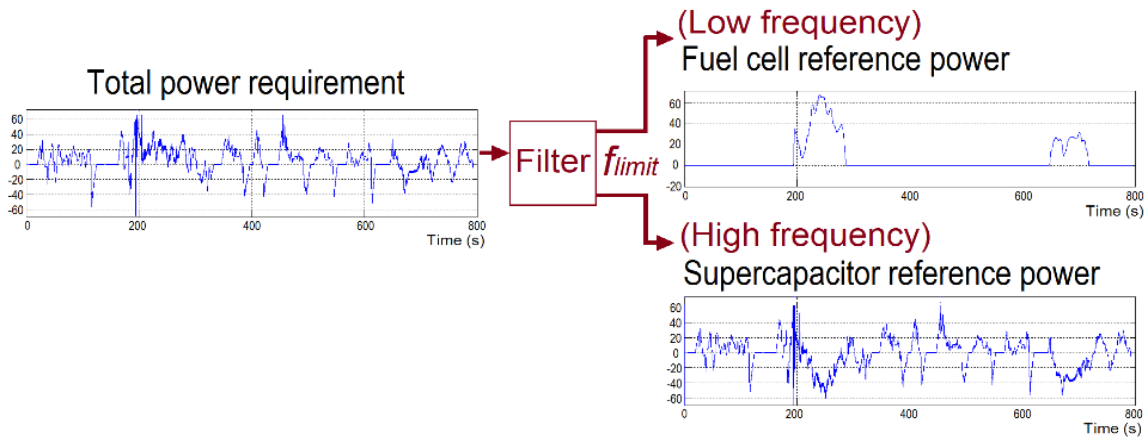


Figure 4.6 Dynamic distribution of the required $i_{Load}$

The energy management block receives the total reference current ($i_{LoadCoupl}$), which is equivalent to the total current needed for satisfying the two main objectives of the system (to provide the traction power while maintaining $V_{bus}$ at a constant value). Firstly, the current reference ($i_{ref_FC}$) for the fuel cell is determined as follows (Figure 4.0): the total load $i_{LoadCoupl}$ passes through a low-pass filter, then the $i_{sc_soc}$ signal is added and the resulted current is limited to a maximum of 75 A (the maximum current supported by de Bahia FC to stay in the optimal operating region). The addition of the $i_{sc_soc}$ signal is needed for balancing the total load ($i_{sc_soc}$ is the output of SOC block and is subtracted from the total SC current reference $i_{ref_sc}$). Then, to prevent losses and errors when the total current reference signal is determined, the difference that overflows the limit of 75 A ($dif_limit_if_c$), is added to the SC. Afterwards, to determine the current reference for the supercapacitor ($i_{ref_SC}$), the total load $i_{LoadCoupl}$ passes through a high-pass filter and the *dif_limit_ifc* signal (previously calculated from the excess of the maximum current supported by de FC) is added. Subsequently, the subtraction of the $i_{sc_soc}$ signal represents the SC charge ensuring the SOC regulation.

Regarding the SC SOC, accurate estimation of the accumulators (batteries or supercapacitors) SOC remains a challenge. Chang [64] summarizes the various methods of estimation as:

*Direct measurement*: This method consists in using physical accumulator properties, such as the voltage and impedance; *book-keeping* estimation, which consist in integrating the discharging current over time to calculate the SOC.

*Adaptive systems:* This method consists in adjusting on line the SOC for different discharging conditions.

*Hybrid methods*: These are combinations of the described methods.

As mentioned before, we used the *book-keeping* estimation method for on-line supervision of the SC SOC. The goal is to verify the effectiveness of the SC SOC regulation.

At the same level, the SOC block is used to determine the current reference ($i_{SC\ soc}$) for conserving the SC SOC on a proper range. The regulation of the SC SOC is made indirectly with a voltage PI controller whose reference corresponds to 90% of the nominal voltage. Then, the current reference from the SOC block goes to the energy management block.
The SOC is calculated as follows:

$$SOC = 100\left(\frac{Q_{init} - \int_0^t i(\tau)d\tau}{Q_T}\right) \tag{4.0}$$

*Donde:*

$Q_{init} = Initial\ charge\ (C)$
$Q_T \quad = Total\ charge\ (C)$
$i(\tau) \quad = Current\ (A)$

For the SC sizing, the energy storage and the delivery/recovery rates were determined using known techniques [65].

### 4.1.3 Third hierarchy level: Power converters control

This block interacts directly with the SC and the fuel cell (Figure 4.7) to adapt the FC and the SC output voltages to the desired $V_{bus}$ voltage, using two different power conditioning units.

A number of topologies for DC/DC converters exist. For the FC, a simple and classic design of boost converter was chosen because it is usually efficient and low cost. For the SC, a half-bridge bidirectional is used to conduct the delivery and recovery cycles, it also has the characteristics of low cost and simple design.

The power converter control block is fed with the FC and the SC reference currents, which are compared with the measured inductors currents from each power converter. Then, a current control algorithm provides the corresponding duty cycle (d) signals for both dc/dc converters.

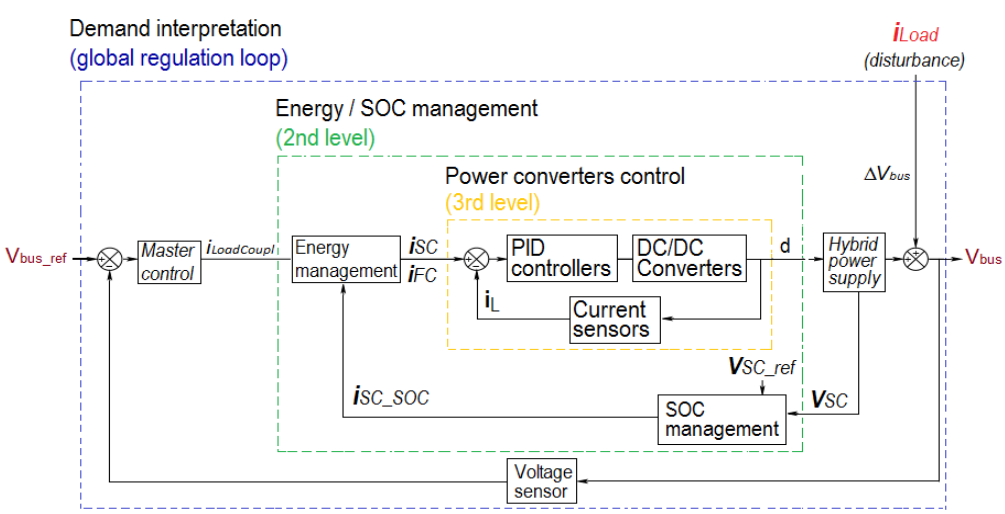


Figure 4.7 Functional regulation scheme showing the three levels

For designing the controllers, it is important to consider that the real FC power delivery is lower than the ideal or theoretical voltage (Figure 8). Remembering that the theoretical value of the FC open circuit voltage (EOC) is given in the expression:

$$E_{OC} = K_C E_n \tag{4.1}$$

Kc is the voltage constant at nominal condition of operation. $E_n$ is the Nernst voltage, which is the thermodynamics voltage of the cells and depends on the temperatures and partial pressures of reactants and products inside the stack (V).

$$E_n = 1.229 + (T - 298)\left(\frac{-44.43}{zF}\right) + \left(\frac{RT}{zF}\right)\ln(P_{H2}P_{O2}) \tag{4.2}$$

Where:

*R = 8.3145 J/(mol K)*
*F = 96485 A s/mol*
*z = Number of mobile electrons*
*$P_{H2}$ = Partial pressure of hydrogen inside the stack (atm)*
*$P_{O2}$ = Partial pressure hydrogen inside the stack (atm)*
*k = Boltzmann constant (1.38064852 x $10^{23}$ J/K)*
*T = Operation temperature (K)*

The voltage for a cell operation below 100°C is 1.2 V. However, in the real FC voltage is often considerably less. Figure 4.8 shows the performance of a typical single cell operating at normal air pressure. The polarization curve shows a rapid initial voltage drop (activation region); then, the voltage diminishes linearly (is the ohmic region). Sometimes, at higher current densities, the voltage tends to fall faster (concentration or diffusion region) [57]. Especially when air is used as oxidant the voltage dropping is faster and non-linear. Conversely, when pure oxygen is fed, the voltage drop is slighter.

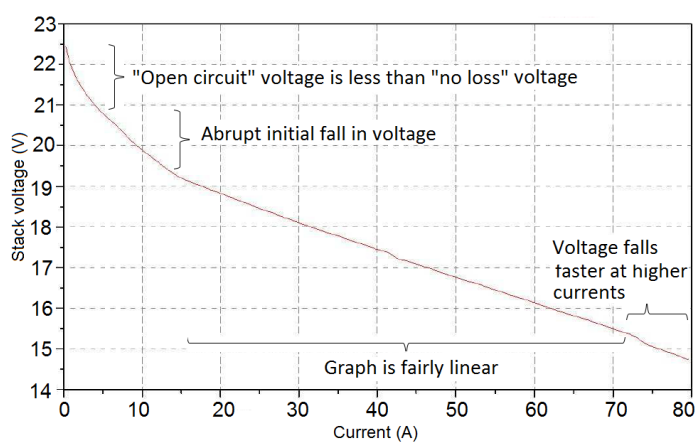


Figure 4.8 Graph showing the voltage for a typical low temperature, air pressure, FC. Bahia FC®

The efficiency curve in FCs is strictly homothetic to the voltage curve. However, fuel cells need auxiliary elements to assure the design operating conditions of temperature, pressure, flow and humidity. For calculating the power consumed by the air or oxygen supply system, the energy losses in this equipment and the motor drive consumption must be taken into account.

Figure 4.9 shows the FC voltage, system efficiency, and the net power density varying with net current density of a hydrogen–air PEMFC. The optimal operating region of the FC system is in the middle region of the current range. A large current leads to low efficiency due to the large voltage drop in the FC stack and, conversely, a very small current leads to diminish the efficiency due to the increased percentage contribution of the auxiliary equipment in the total energy consumption [66].

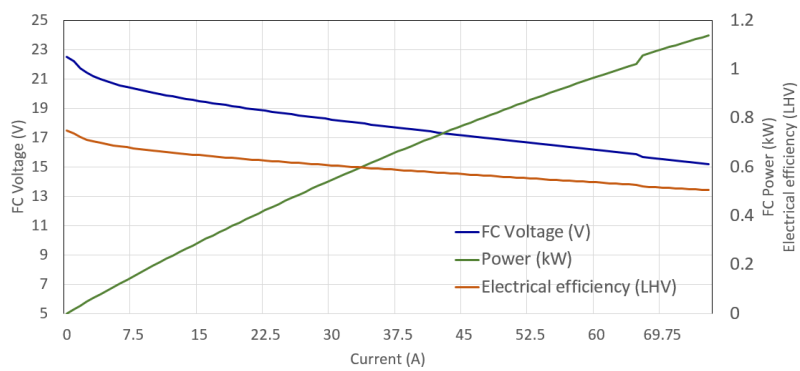


Figure 4.9 BAHIA stack voltage, system efficiency, and net power density varying with net current density

Hence, by using the boost converter, the FC is forced to work in the current density that corresponds to the best tradeoff between efficiency and power region; the operation in the ohmic region is generally adequate.

Figure 4.10 shows the boost converter used to adapt the FC voltage (which is between 15.7 V – 22.5 V at rated power), to the standard automotive 48 V dc bus. It is composed of a high frequency inductor *L*, an output filtering capacitor *C*, a diode *D* and a main switch *IGBT/Diode1*. The switch *IGBT/Diode2* is a shutdown device for test bench security to prevent the FC stack from short circuit in case of accidental *IGBT/Switch1* destruction or a faulty regulator operation.

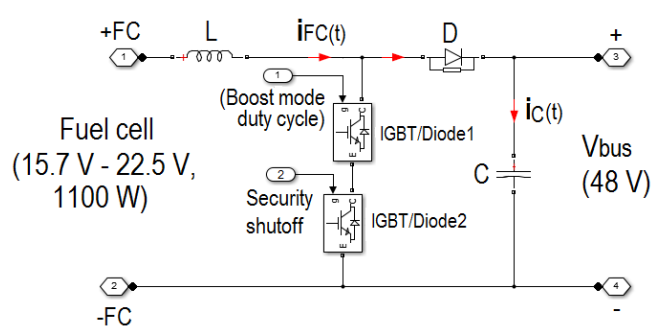


Figure 4.10 FC boost converter

For a boost converter, the higher the duty ratio (or the larger the voltage difference between the input and output), the lower is its efficiency. On the contrary, the output voltage of the converter will not be boosted to a distinctly higher voltage if the duty ratio is too low. A duty ratio around 55% can be used for the dc/dc converters at the fuel cells rated operating point [67].

The FC boost converter is current controlled. Using the average state space method [68], the converter model is obtained. Then, for tuning the controller, Ziegler-Nichols method is used.

Figure 4.11 shows the BAHIA FC module polarization curve [69]. As mentioned above, the optimal operating region of the FC system is in the middle of the curve. Limits to the Boost dc/dc converter were fixed to ensure operating in FC linear region (ohmic region – in a range between 15.7 and 19 V and 15 to 75 A, or equivalently from 0.285 to 1.178 kW). Therefore, DC bus voltage is regulated ensuring the maximum efficiency without falling into degradation zone.

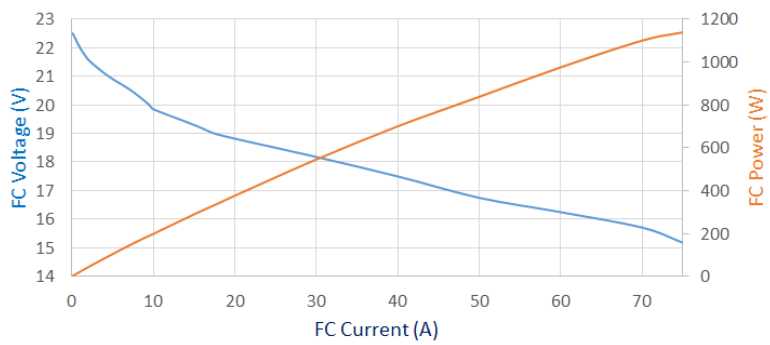


Figure 4.11 Bahia FC polarization curve

The supercapacitor bank is connected to the DC bus through a 2-quadrant dc/dc converter, as shown in Figure 4.12. *RL1* represents the inductor used for energy transfer and filtering. The inductor size is usually defined by switching frequency and current ripple. The current $i_{SC}$ across the storage device can be positive or negative, allowing energy transference in both directions. This is a current controlled converter, driven by pulses applied to both IGBT gates.

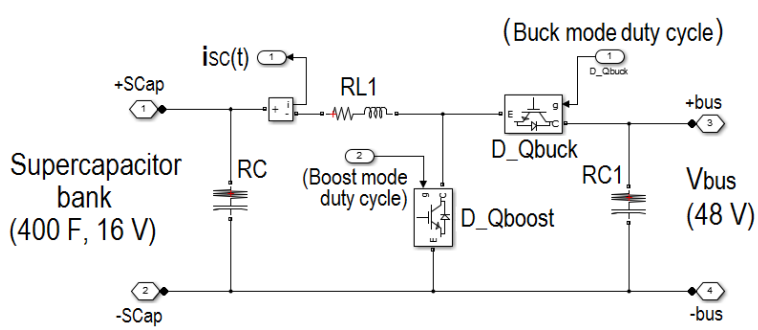


Figure 4.12 Two-quadrant SC converter

## 4.2 DC/DC converters: modeling and control

A fuel cell-based power source requires a power conditioning system to deliver properly the electric energy, DC/DC converters are power electronics topologies that allows, from a constant or variable

DC input, to control the DC voltage at the converter output. There are multiple applications for these converters: computer power supplies, power distributed systems, electric vehicles power systems, etc. The three power converters basic configurations are: Buck (reducer), Boost (elevator) and Buck-Boost (reducer-elevator). Both, experimental operation and numerical simulation of the integrated system are cumbersome tasks due to a number of challenges, e.g. the dissimilar response times of the fuel cell and the power conversion unit produce impedance-coupling difficulties and impose effort and time demanding numerical simulations [70].

The conventional cited configurations allows elevating, reducing or reducing/elevating the sourced voltage ($v_s$) at the converter output ($v_o$). There are four basic elements in these configurations: the inductor (L), the capacitor (C), the diode and a controller switch (Q); the properties for each topology depends on how these four elements are connected as shown in Figures 4.13, 4.14 and 4.15.

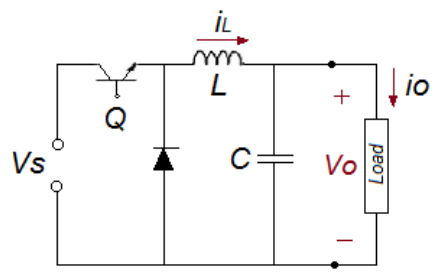


Figure 4.13 Buck Converter

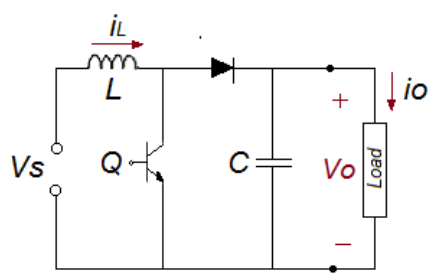


Figure 4.14 Boost Converter

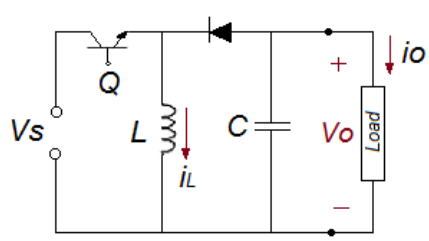


Figure 4.15 Buck/Boost Converter

For controlling the output voltage, the variable to control is the switching pattern for the controlled switch. The simplest strategy is to commute the switch at a fixed frequency, changing only the

activation time, what is called Pulse Width Modulation or PWM. For implementing this strategy, the common way is to compare a sawtooth wave ($v_{ramp}$) at fixed frequency and $V_{max}$ voltage peak with a ($v_{ref}$) reference voltage for getting a ($v_{PWM}$) enabling voltage as shown in (Figure 4.16).

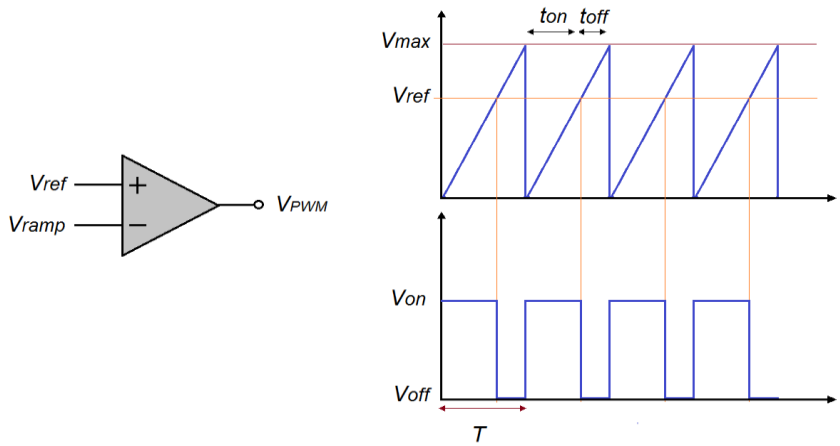


Figure 4.16 PWM Commutation signal from V*ramp* and V*ref.*

As noticed in Figure 4.16, $0 \leq v_{ref} \leq V_{max}$ constrains for $v_{ref}$ must be always stated, so, if $t_{on}$ is the switch ON time and *T=1/f* is the switching period, the *U* or duty cycle is defined as:

$$U = \frac{t_{on}}{T}, \quad where\ 0 \leq U \leq 1 \tag{4.3}$$

The DC/DC converters are usually designed for working under specified operating conditions, commonly the specifications must include the desired output voltage (*Vo*), the nominal input voltage (*Vs*) and the loading conditions. Given this information, it is possible to calculate the suitable average duty cycle for the converter. Nonetheless, the converter is exposed to external factors as:

- Input voltage disturbances
- Loading conditions variability
- Parasitic resistances and voltage drops in the circuit reactive elements.

The influence of to these external factors dictates the necessity of a control loop in order to regulate the desired output voltage. Then, the control problem statement is proposed assuming that the interest variables (defined in Figure 4.16) have both, a constant and a fluctuating part:

$$v_S = V_S + \hat{v}_S(t) \tag{4.4}$$

$$v_o = V_0 + \hat{v}_O(t) \tag{4.5}$$

$$u = U + \hat{u}(t) \tag{4.6}$$

The target is to reduce the output voltage variations, given the impact of the different disturbances at the input voltage and the loading resistance, by adding a correction factor in the duty cycle *û(t).* A proportional-integral based (PI) control in the feedback loop is sufficient for achieving the control objectives. The control loop is described in Figure 4.17.

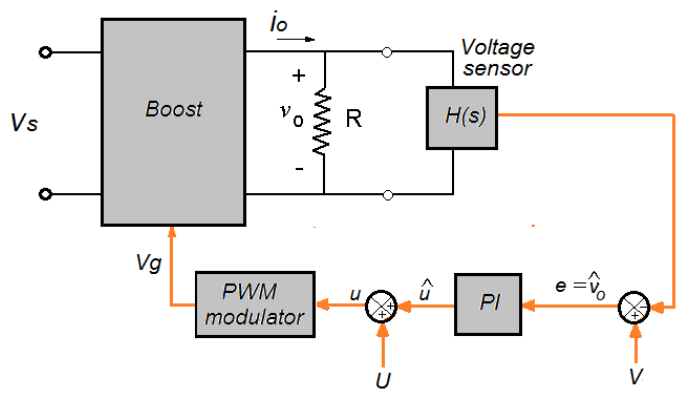


Figure 4.17 DC/DC converter control loop with PI controller example

The control system actuator (PWM modulator) uses the structure shown in Figure 4.16. The output voltage of this actuator is the polarization voltage for the active switch gate ($v_g$). Highlighting that the error signal ($e$) processed by the PI controller is also representing the output voltage variation $\hat{v}_O$ over the desired average value, it is emphasized that the control target is to minimize this variable.

The following section introduces the mathematical model predicting the PEMFC and the SC converters performances.

### 4.2.1 Fuel cell CD/CD converter

The converters mathematical model is formulated assuming a continuous conduction mode (CCM). For this mode, the inductor absolute current is always greater than zero $\left(\left|i_{dd_in}\right| > 0\right)$, the inductor current and the capacitor voltage have a constant value and a fluctuating part around the average value. This fluctuating operation condition is linked to the inductance value, the converter load resistance and the switching frequency.

For the continuous conduction mode (CCM) in the elevator converter, it must be true that:

$$\frac{2Lf}{R} > U(1-U)^2 \tag{4.7}$$

In the same way, to keep the elevator-reducer converter in the CCM, the next constraint must apply:

$$\frac{2Lf}{R} > (1-U)^2 \tag{4.8}$$

The common technique for getting the converters models is based on the state space method, defining the twofold operating states of the active switch Q: ON (μ=1) and OFF (μ=0).

Thereafter, two states of the system are considered: the inductor current $i_L$ and the output voltage $v_o$ (which is also representing the capacitor voltage)

Figure 4.18 show the DC/DC elevator converter diagram to analyze.

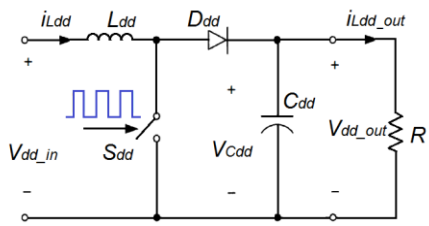


Figure 4.18 DC/DC elevator converter

The steady state voltage and current inductor $L_{dd}$ waveforms are shown in Figure 4.18. For the ON state, the $S_{dd}$ switch in Figure 4.17 is ON and the diode $D_{dd}$ is OFF. The voltage through the inductor is the input voltage or $i_{dd_in}$. At the same time, the inductor current increase with a $V_{dd_in}/L_{dd}$ slope. When the $S_{dd}$ switch is OFF, the $D_{dd}$ diode is ON and the voltage through the inductor change to $V_{dd_in} - V_{dd_out}$. During this time $(t_{off})$, the inductor current will decrease with in a ratio defined by $(V_{dd_out} - V_{dd_in})/L_{dd}$ . For the steady state, the inductor average current value $i_{L_{dd}}$ is constant over the switching period $T_S$, while $v_{L_{dd}} = L_{dd}(di_{L_{dd}}/dt)$, the inductor voltage integral $v_{L_{dd}}$ is zero over a switching period when the circuit is in steady state. Then, the elevator-reducer converter integral is:

$$\int_{T_s} V_{L_{dd}}(t)dt = V_{dd_{in}} * t_{on}(V_{dd_{in}} - V_{dd_{out}})t_{off} = 0 \tag{4.9}$$

From the previous equation, it is possible to obtain the steady state output voltage as:

$$V_{dd_out} = \frac{1}{1-d} V_{dd_in} \tag{4.10}$$

Where, $d = t_{on}/T_s$ is the switching pulse duty cycle.

The duty cycle *d* is always lower than 1 for the DC/DC elevator converters. The duty cycle cannot be equal to 1 because in that case, the $S_{dd}$ switch in Figure 4.17 will be always on, shorting to ground the input all the time, what is obviously not a normal operation condition. For $0 \leq d < 1$, the converter output voltage is bigger than the input voltage. For the DC/DC elevator converters, the duty cycle *d* is normally below 0.85 [71].

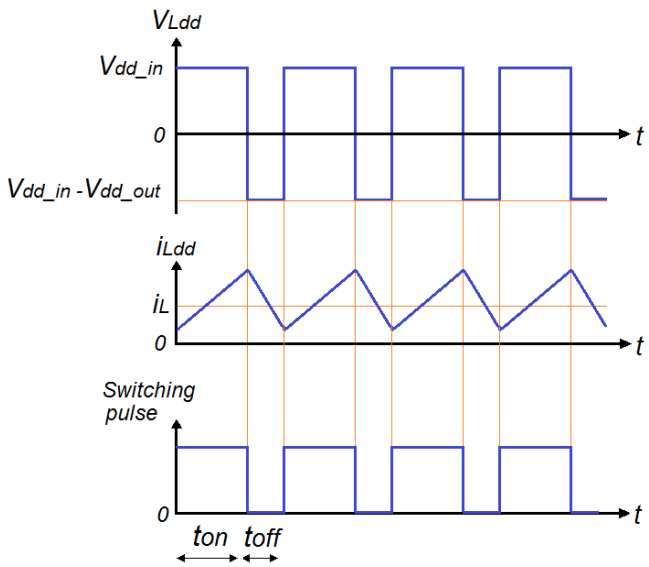


Figure 4.19 Elevator-reducer voltage and current waveforms at the inductor in CCM

Figure 4.20 shows a boost DC/DC converter with an output voltage regulation feedback control. The controller for the converter regulates the DC bus voltage within a desirable range. The output voltage is measured and compared with a reference value, and the error signal is processed through the PWM controller, which can be a simple proportional-integral (PI) controller. The output of the controller is used to control the pulse-with modulator to generate a PWM pulse series with the right duty cycles so that the output voltage follows the reference value.

In order to apply classical control analysis and design methods (such as Nyquist criterion, Bode plots, and root locus analyses) in converter controls, small-signal state-space models for the above boost and buck converters are needed, which are discussed in this section. These models are based on the state-space averaging technique developed by Middlebrook [68].

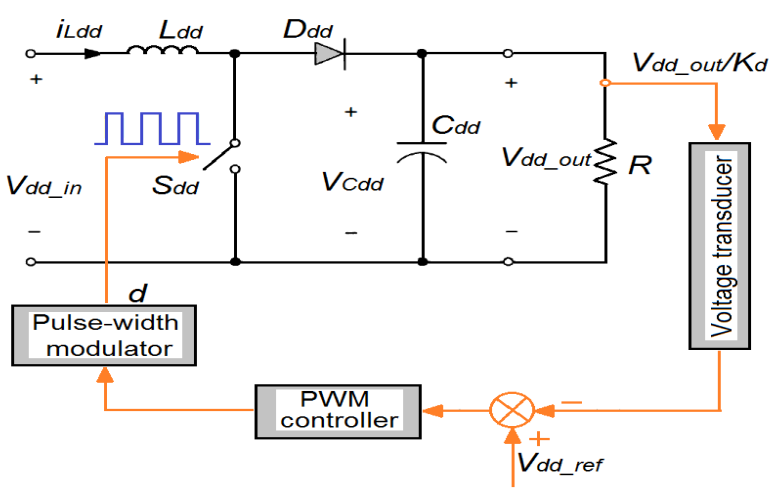


Figure 4.20 Boost DC/DC converter with feedback voltage control.

In Figure 4.20, take $x_1 = i_{L_{dd}}$ and $x_2 = v_{C_{dd}}$ as state variables:

$$x = X + \tilde{x}$$

$$d = D + \tilde{d}$$

$$v_{dd_in} = V_{dd_in} + \tilde{v}_{dd_in}$$

$$v_{dd_out} = V_{dd_out} + \tilde{v}_{dd_out} \tag{4.11}$$

The symbol ~ is used to denote small perturbation signals, and state variable $X$ denotes the system operating point. When the switch $S_{dd}$ is on and diode $D_{dd}$ is off, the state-space representation of the main circuit is derived from the Kirchhoff laws and is written as:

$$\dot{x} = A_1 x + B_1 v_{dd_in}$$

$$v_E = C_1^T x \tag{4.12}$$

where:

$$x = [x_1 \; x_2]^T$$

$$A_1 = \begin{bmatrix} 0 & 0 \\ 0 & -1/RC_{dd} \end{bmatrix}$$

$$B_1 = \begin{bmatrix} 1/L_{dd} \\ 0 \end{bmatrix}$$

$$C_1^T = [0 \quad 1] \tag{4.13}$$

Symbol $T$ represents the transpose operation of a matrix. When switch $S_{dd}$ is off and diode $D_{dd}$ is on, the state-space equation of the circuit turns out to be:

$$\dot{x} = A_2 x + B_2 v_{dd_in}$$

$$v_{dd_out} = C_2^T x \tag{4.14}$$

Where:

$$A_2 = \begin{bmatrix} 0 & -1/L_{dd} \\ 1/C_{dd} & -1/RC_{dd} \end{bmatrix}$$

$$B_2 = \begin{bmatrix} 1/L_{dd} \\ 0 \end{bmatrix}$$

$$C_2^T = [0 \quad 1] \tag{4.15}$$

Therefore, the average state-space model of the main circuit at the operating point is:

$$\dot{x} = Ax + Bv_{dd_in}$$

$$v_{dd_out} = C^T x \tag{4.16}$$

Where:

$$A = [A_1 d + A_2(1-d)] = \begin{bmatrix} 0 & -(1-d)/L_{dd} \\ 1-d/C_{dd} & -1/RC_{dd} \end{bmatrix}$$

$$B = [B_1 d + B_2(1-d)] = \begin{bmatrix} 1/L_{dd} \\ 0 \end{bmatrix}$$

$$C^T = [C_1 d + C_2(1-d)]^T = [0 \quad 1] \tag{4.17}$$

Then, the small signal model for the boost DC/DC converter can be written as:

$$\dot{\tilde{x}} = A_d \tilde{x} + B_d \tilde{x} + B_v \tilde{v}_{dd_in}$$

$$\tilde{x} = [\tilde{x}_1 \quad \tilde{x}_2]^T,\ A_d = \begin{bmatrix} 0 & -(1-d)/L_{dd} \\ 1-D/C_{dd} & -1/RC_{dd} \end{bmatrix}$$

$$B_d = \begin{bmatrix} X_2/L_{dd} \\ -X_1/C_{dd} \end{bmatrix}, B_v = \begin{bmatrix} 1/L_{dd} \\ 0 \end{bmatrix} \tag{4.18}$$

$X_1$ y $X_2$ are the steady-state values of $x_1$ y $x_2$, respectively.

From the state-space model (time domain) to transfer function, we used Laplace domain:

$$\dot{x}(t) = Ax(t) + Bu(t)$$

$$y(t) = Cx(t) + Du(t) \tag{4.19}$$

Considering the system described by previous equations, and expressing in Laplace domain:

$$\mathcal{L}\{\dot{x}(t) = Ax(t) + Bu(t)\}$$

$$sX(s) - x(0) = AX(s) + BU(s) \tag{4.20}$$

and

$$\mathcal{L}\{y(t) = Cx(t) + Du(t)\}$$

$$Y(s) = CX(s) + DU(s) \tag{4.21}$$

It is obtained:

$$(sI - A)X(s) = BU(s) + x(0)$$

$$X(s) = (sI - A)^{-1}BU(s) + (sI - A)^{-1}x(0)$$

$$Y(s) = [C(sI - A)^{-1}B + D]U(s) + C(sI - A)^{-1}x(0) \tag{4.22}$$

Therefore, the first equation term represents the transfer function.

$$G(s) = \frac{Y(s)}{U(s)} = C(sI - A)^{-1}B + D \tag{4.23}$$

The second term $C(sI - A)^{-1}x(0)$ is the response at the initial condition.

The transfer function has a dimension $G(s) \in \mathbb{R}^{p\,X\,m}$, according to the number of inputs ($p$) and outputs ($m$) of the original system. (Expressed in equations 4.19)

Following this process, we obtain:

$$\frac{\tilde{\imath}_L(s)}{\tilde{d}(s)} = \frac{(CRs + 1)X_2 + (R - DR)X_1}{CLRs^2 + LS + (R + D^2R - 2DR)}$$

$$\frac{\tilde{v}_C(s)}{\tilde{d}(s)} = \frac{-R(DX_2 - X_2 + LX_1s)}{CLRs^2 + LS + (R + D^2R - 2DR)}$$

(4.24)

Those functions were used for designing the boost converter.

The main components of a DC/DC converter can be determined by its technical specifications, such as rated and peak voltages and currents, and tolerable input current and output voltage ripples [72]. Based on the FC/SC system described in previous sections, technical specifications are summarized in the Table 5.1:

| **Specification** | **Value** |
|---|---|
| Input voltage, Vi | 15 V |
| Ouput voltage, Vo | 48 V |
| Rated power | 1300 W |
| Input current ripple, $\Delta i_L/i_L$ | $\leq 20\%$ |
| Ouput voltaje ripple, $\Delta V_O/V_O$ | $\leq 5\%$ |

Table 4.1 Specifications of the Boost CD/CD converter

The input voltage is determined as 15 V. So the converter will have a little wider input voltage range than the designed input voltage (15. V fuel cell output).

The reason for choosing a slightly lower converter-rated voltage is because of degradation effect of a fuel cell stack over its operating time. The output voltage of a fuel cell will drop slightly over the time due to its performance degradation [57]. In order to draw a relatively smooth current from each fuel cell array, the ripple of the inductance current at the rated operating point is set to be less than 5%. The output voltage ripple is set to a typical value, less than 5% [6]. A boost dc/dc converter with the topology shown in Figure 4.17 is designed to meet these specifications.

**Switching Frequency.**
Since the rated power of the boost converter will be 1300 W, IGBT (Insulated Gate Bipolar is a good choice for the switching device in the circuit [72]. The switching frequency of IGBTs is normally less than 50 kHz. In this design, the switching frequency ($f_s$) is chosen as 10 kHz.

Equivalent resistive load at the rated operating point is:

$$R = \frac{V_{dd_out}^2}{P_{dd,N}} = \frac{48^2}{1300} = 1.77\Omega$$

(4.25)

The duty cycle $D$ is:

$$D = 1 - \frac{V_{dd_{in}}}{V_{dd_{out}}} = 1 - \frac{15}{48} = 0.6875$$

(4.26)

Then, the rated input (inductor) current can be obtained as:

$$\bar{I}_{L_{dd},N} = \frac{V_{dd_{in}}}{(1-D)^2 R} = \frac{15}{(1-0.6875)^2(1.77)} \approx 86.8\ A$$

(4.27)

**Inductance $L_{dd}$.** Based on the requirement specified for the input current ripple (to be less than 20%), we get:

$$\frac{\Delta i_{Ldd}}{\bar{I}_{L_{dd},N}} = \frac{D(1-D)^2 R}{f_s L_{dd}} < 20\% \rightarrow L_{dd} > \frac{5D(1-D)^2 R}{f_s}$$

That is:

$$L_{dd} \geq \frac{5(0.6875)(1-0.6875)^2(1.77)}{10000} = 59.41\mu H$$

(4.28)

$L_{dd}$ is chosen as 1.2 mH for the design.

**Capacitance $C_{dd}$.** The output voltage ripple percentage can be calculated as:

$$\frac{\Delta V_O}{V_O} = \frac{D}{RC_{dd}} \leq 5\% \rightarrow C_{dd} \geq \frac{D}{0.05Rf_S} = \frac{0.6875}{(0.05)(1.77)(10000)} = 776.8\mu F$$

(4.29)

$C_{dd}$ is chosen as 1000 $\mu F$.

**Switch S**. According to the selected component parameters, the maximum current through the switch at the rated operating point is Interruptor S.

$$I_{S_{dd,max}} = I_{L_{dd,max}} = (86.779)(1.1) = 95.457\ A$$

The peak switch voltage at the rated operating point is:

$$V_{S_{dd,max}} = V_{dd_out} = 48\ V$$

**Power Diode D.** The peak forward current through diode D at the rated operating point is:

$$I_{D_{dd,max}} = 95.457\ A$$

The peak inverse voltage across the diode at the rated operating point is:

$$V_{D_{dd,max}} = V_{dd_out} = 48\ V$$

A summary of the boost converter component values is contained in Table 4.2:

| Component | Value |
|---|---|
| $L_{dd}$ | 1.2 mH |
| $C_{dd}$ | 1000 $\mu F$ |
| $D$ | 0.6875 |
| $R$ | 1.77Ω |
| $I_{D_{dd,N}}(X_1)$ | 86.8 A |
| $V_{dd_out}(X_2)$ | 48 V |

Table 4.2 Parameters

Figure 4.20 shows the circuit of a boost DC/DC converter with an output voltage regulation loop. Figure 4.21 shows a transfer-function block diagram for that circuit, when it is linearized around its operating point [68].

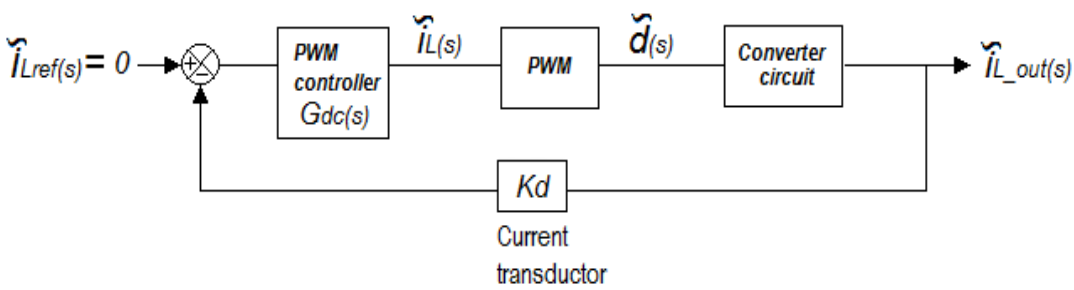


Figure 4.21 Block diagram of the control loop for the boost DC/DC converter

Where $T_{PWM(s)} = \frac{\tilde{d}(s)}{\tilde{\imath}_L(s)}$ and $T_P = \frac{\tilde{\imath}_{L_out}(s)}{\tilde{d}(s)}$.

For the boost dc/dc converter shown, its transfer function (output voltage over duty ratio) $T_{p(s)}$ was obtained in previous section:

$$T_p = \frac{\tilde{\imath}_L(s)}{\tilde{d}(s)} = \frac{(CRs+1)X_2 + (R-DR)X_1}{CLRs^2 + LS + (R + D^2R - 2DR)} \tag{4.30}$$

Where:

*D Switch duty cycle*
*$X_1$ Average current through L inductor*
*$X_2$ Output voltage at rated operating point*
*$K_d$ Current transductor constant. It is stablished at 1/48, being $V_{bus}$ the desired DC voltage*.

For the PWM controller, it was chosen a PI controller. The transfer function is:

$$G_{dc}(s) = \frac{k_{dp}s + k_{di}}{s} - k_{dp}\left(1 + \frac{k_{di}}{k_{dp}}\frac{1}{s}\right) \tag{4.31}$$

## 4.3 Models at simulator

### 4.3.1 BAHIA® fuel cell

BAHIA fuel cell is a PEMFC, 400 W – 1000 W, 70 A at rated power. Figure 4.22 shows the polarization curve provided by the manufacturer.

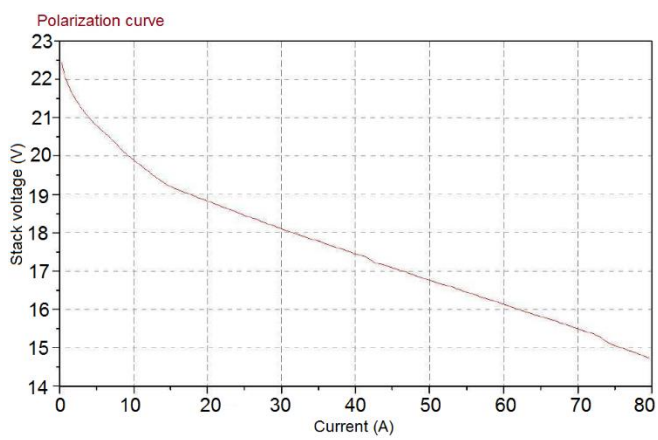


Figure 4.22 Bahia Helion® polarization curve. Image by Helion® User Manual.

The model is based on the equivalent circuit of a fuel cell stack shown below:

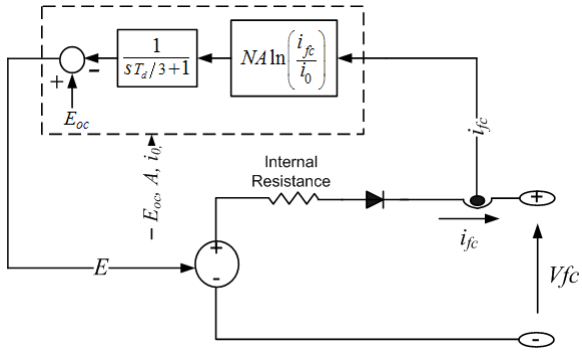


Figure 4.23 Fuel cell equivalent circuit at simulator. Image by [73].

The model represents a particular fuel cell stack operating at nominal conditions of temperature and pressure. The parameters of the equivalent circuit are based on the polarization curve obtained from the manufacturer datasheet. Table 1 displays the steady state performance configuration.

| **PEM fuel cell parameters** | Value |
|---|---|
| Voltage at 0A and 1 A $[V_0(\text{V}), V_1(\text{V})]$ | [22.5 22] |
| Nominal operating point $[I_{nom}(\text{A}), V_{nom}(\text{V})]$ | [70 15.71] |
| Maximum operating point $[I_{end}(\text{A}),\ V_{end}(\text{V})]$ | [75 15.18] |
| Number of cells | 12 |
| Nominal stack efficiency (%) | 46 |
| Operating temperature (Celsius) | 70 |
| Nominal air flow rate (lpm) | 300 |
| Nominal supply pressure [Fuel (bar), Air (bar)] | [1.3 1.1] |
| Nominal composition (%) [H2 O2 H2O (Air)] | [99.99 21 1] |
| Fuel cell response time (sec) | 0.4 |

Table 4.3. Parameters characterizing the Bahia PEMFC using the fuel cell stack model library

The detailed model represents a particular fuel cell stack when the parameters such as pressures, temperature, compositions and flow rates of fuel and air vary. These variations affect the open circuit voltage ($E_{OC}$), the exchange current ($i_0$) and the Tafel slope ($A$). $E_{OC}$, $i_0$ and $A$ are modified as follows:

$$E_{OC} = K_C E_n$$

$$i_o = \frac{zFK\left(P_{H_2}P_{O_2}\right)}{Rh} e^{\frac{-\Delta G}{RT}}$$

$$A = \frac{RT}{Z \propto F} \tag{4.32}$$

where:

*R =* *8.3145 J/(mol K)*
*F =* *96485 A s/mol*
*z =* *Number of moving electrons*
$E_n$ = *Nernst voltage, which is the thermodynamics voltage of the cells and depends on the temperatures and partial pressures of reactants and products inside the stack (V)*
*α =* *Charge transfer coefficient, which depends on the type of electrodes and catalysts used.*
$P_{H2}$ = *Partial pressure of hydrogen inside the stack (atm).*
$P_{O2}$ = *Partial pressure of oxygen inside the stack (atm).*
*k =* *Boltzmann's constant* $= 1.38 \times 10^{-23}$ *J/K*
*h =* *Boltzmann's constant* $= 6.626 \times 10^{-34}$ *J s*
*ΔG =* *Size of the activation barrier which depends on the type of electrode and catalyst used.*
*T =* *Temperature of operation (K).*
$K_c$ = *Voltage constant at nominal condition of operation.*

Nominal conversion rates are calculated with:

$$U_{f_{H_2}} = \frac{n_{nom}\Delta h^0(H_20(gas))N}{zFV_{nom}}$$

$$U_{f_{O_2}} = \frac{60000RT_{nom}NI_{nom}}{2zFP_{air_{nom}}V_{lpm_{nom}}{}^{-0.21}}$$

(4.33)

Donde:

$\eta_{nom}$= Nominal LVH efficiency of the stack (%)
$\Delta h^0(H_2O(gas))$= $241.83 \times 10^3$ J/mol
$V_{nom}$ = Nominal voltage (V)
$I_{nom}$= Nominal current (A)
$V_{lpm(air)nom}$= Nominal air flow rate (l/min)
$P_{airnom}$= Nominal absolute air supply pressure (Pa)
$T_{nom}$= Nominal operation temperature (K)

From these rates of conversion, the nominal partial pressures of gases and the Nernst voltage can be derived. With $E_{OC}$, $i_0$ and $\mathrm{A}$ known and assuming that the stack operates at constant rates of conversion or utilizations at nominal condition, $\alpha$, $\Delta\mathrm{G}$ and $K_C$ can be determined. If there is no fuel or air at the stack input, it is assumed that the stack is operating at a fixed rate of conversion (nominal rate of conversion), that is, the supply of gases is adjusted according to the current demand, so that they are always supplied with just a bit more than the required quantity to the stack by the load, at every moment.

The 60000 constant comes from the conversion from the flow rate expressed in liter/min units to $m^3/s$ (1 liter/min = 1/60000 $m^3/s$).

The partial pressures and the Nernst voltage are determined as follows:

$$\begin{cases} P_{H_2} = \left(1 - U_{f_{H_2}}\right) x\% P_{fuel} \\ P_{H_2O} = \left(w + 2y\% U_{f_{O_2}}\right) P_{air} \\ P_{O_2} = \left(1 - U_{f_{O_2}}\right) y\% P_{air} \end{cases} \tag{4.34}$$

and

$$E_n = \begin{cases} 1.229 + (T - 298)\dfrac{-44.43}{zF} + \dfrac{RT}{zF}\ln\left(P_{H_2} P_{0_2}^{1/2}\right) & when\ T \leq 100°C \\ 1.229 + (T - 298)\dfrac{-44.43}{zF} + \dfrac{RT}{zF}\ln\left(\dfrac{P_{H_2} P_{0_2}^{1/2}}{P_{H_2O}}\right) & when\ T \leq 100°C \end{cases} \tag{4.35}$$

where:

$P_{H_2O}$ = *Partial pressure of water vapor inside the stack (atm)*
$w$ = *Percentage of water vapor in the oxidant (%)*

From the partial pressures of gases and the Nernst voltage, the new values of the open circuit voltage ($E_{OC}$) and the exchange current ($i_0$) can be calculated.

The parameters $\alpha$, $\Delta G$ and $K_C$ are calculated based on the polarization curve at nominal conditions of operation along with some additional parameters, such as the low heating value (LHV) efficiency of the stack, composition of fuel and air, supply pressures and temperatures. They can be obtained from the manufacturer datasheet.

The maximum current that the stack can deliver is limited by the maximum flow rates of fuel and air. Beyond that maximum current, the voltage output of the stack decreases abruptly as more current is drawn. The response time and the dynamics due to the flowing conditions (peak utilization and corresponding voltage undershoot values) obtained from the measurements, can be considered in the model, ensuring the dynamic representation of the FC caused by temperature and flow variations.

The response time ($T_d$) @ 95% is used to model the double layer capacitance phenomenon due to the build up of charges at the electrode/electrolyte interface. This phenomenon influences only the activation voltage. The peak utilization *($UfO2_{(peak)}$)* and the corresponding voltage undershoot ($V_u$) are used to model the effect of oxygen depletion (due to the air compressor delay) on the cell output voltage produced by abrupt current changes.

Current step and interrupt test were made on the BAHIA Fuel cell to represent its dynamics. The Figure 4.24 shows the typical stack response from these tests and shows the parameters characterizing the dynamic behaviors explained above ($T_d$, $Uf_{O2(peak)}$ and $V_u$).

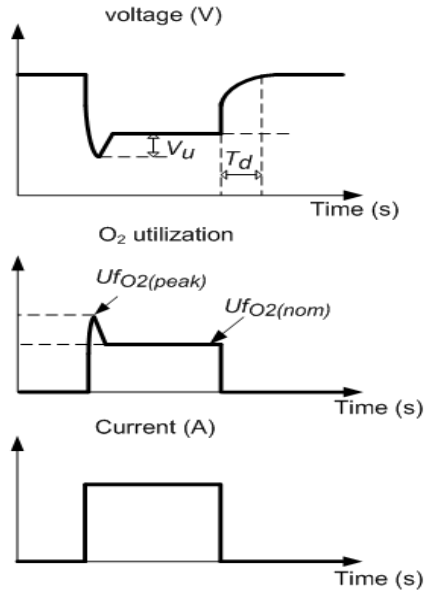


Figure 4.24 PEMFC parameters and response to a current step. Image by [73].

The response time ($T_d$) depends on the fuel cell stack itself and is usually given on the datasheet. The parameters for flow dynamics ($U_{fO2(peak)}$ and $V_u$) depend on the dynamics of external equipments (compressor, regulator and loads) and they are not provided by manufacturers as their values depends on the FC characteristics and the load variation. For simulation, the user may assume values of $U_{fO2(peak)}$ between 60% to 70% and $V_u$ between 2-5% of the stack nominal voltage.

Figure 4.25 shows experimental measurements (in green), along with the simulation results (in purple). The current step input can be seen in the graphic at the top.

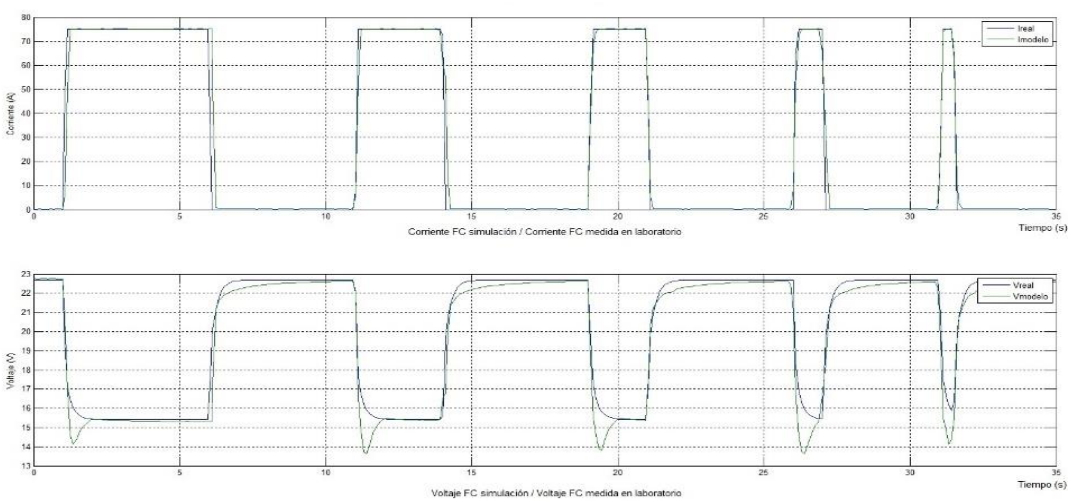


Figure 4.25 PEMFC parameters and response to a current step (Simulation and experimental results)

Figure 4.26 shows the FC polarization curve, as well as the power ratio against current output.

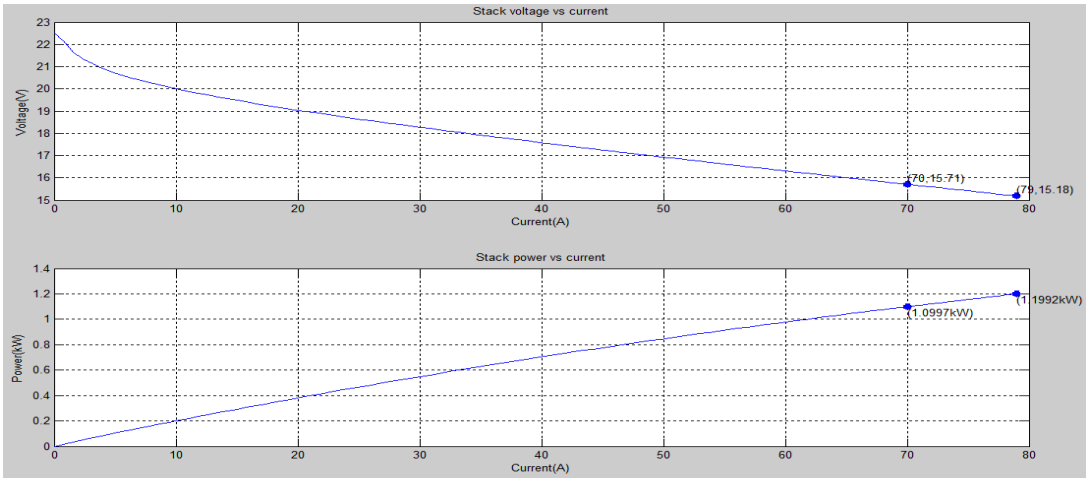


*Figure 4.26 Top:* FC polarization curve. Bottom: Power ratio against current output

## 4.3.2 Supercapacitor model at Simulink

The double layer and self-discharge effects at supercapacitor can be explained with the Tafel and the Stern equations. The model used for simulation has two 500 Farads, 16 Volts Maxwell supercapacitors (Figure 4.27).

Figure 4.27 BMODO5OO Maxwell supercapacitor bank

The Supercapacitor block implements a generic model parameterized, based on Tafel and stern equations as shown below in Figure 4.28:

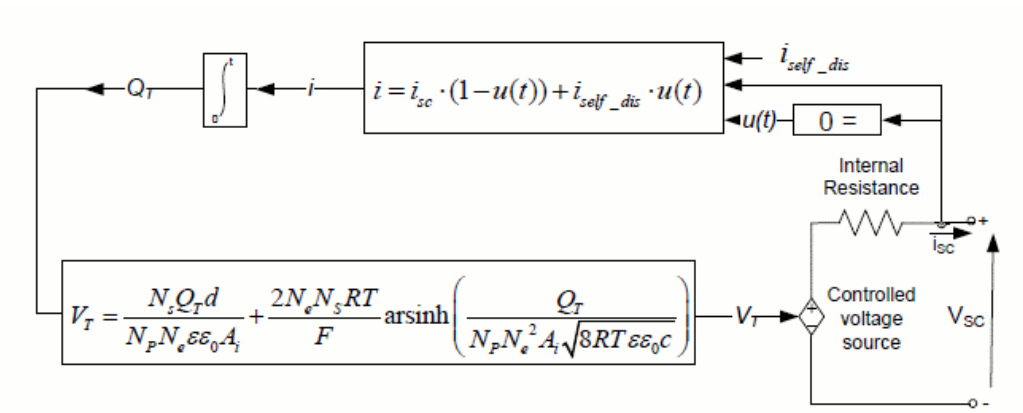


Figure 4.28 Supercapacitor equivalent circuit at simulator. Image by [73].

The SC output voltage can be expressed by Stern equation:

$$V_{SC} = \frac{N_s Q_T d}{N_p N_e \varepsilon \varepsilon_0 A_i} + \frac{2N_e N_s RT}{F} sinh^{-1}\left(\frac{Q_T}{N_p N_e^2 A_i \sqrt{8RT\varepsilon\varepsilon_0 c}}\right) - R_{SC} i_{SC}$$

(4.37)

Were:

$$Q_T = \int i_{SC} dt$$

(4.38)

Supercapacitor self-discharge is represented when $i_{SC}$ = 0 as:

$$Q_T = \int i_{self_dis} dt$$

(4.39)

where:

$$i_{self_dis} = \begin{cases} \dfrac{C_T \propto_1}{1 + sR_{SC}C_T} & si\ t - t_{oc} \leq t_3 \\ \dfrac{C_T \propto_2}{1 + sR_{SC}C_T} & si\ t_3 < t - t_{oc} \leq t_4 \\ \dfrac{C_T \propto_3}{1 + sR_{SC}C_T} & si\ t - t_{oc} \geq t_4 \end{cases}$$

(4.40)

Constants $\alpha_1$, $\alpha_2$, and $\alpha_3$ are the SC voltage exchange rate during the time intervals ($t_{OC}$, $t_3$), ($t_3$, $t_4$) y (*t4*, *t5*) respectively as shown below in Figure 4.29:

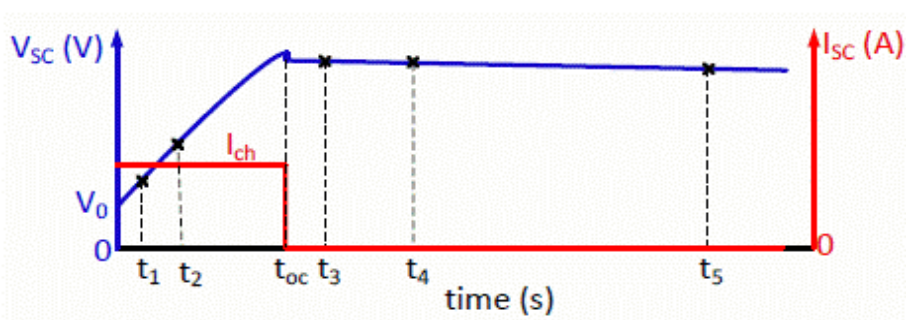


Figure 4.29 Voltage exchange rate at SC. Image by [73].

| Variable | Description |
|---|---|
| $A_i$ | Interfacial area between electrodes and electrolyte ($m^2$) |
| $c$ | Molar concentration ($mol/m^3$), $c = 1/(8N_A r^3)$ |
| $r$ | Molecular radius (m) |
| $F$ | Faraday constant |
| $i_{sc}$ | Supercapacitor current (A) |
| $V_{sc}$ | Supercapacitor voltage (V) |
| $C_T$ | Total capacitance(F) |
| $R_{sc}$ | Total resistance (ohms) |
| $N_e$ | Number of electron layers |
| $N_A$ | Avogadro constant |
| $N_p$ | Number of capacitors in parallel |
| $N_s$ | Number of capacitors in series |
| $Q_T$ | Electric charge (C) |
| $R$ | Ideal gas constant |
| $d$ | Molecular radius (m) |
| $T$ | Operation temperature (K) |
| $\varepsilon$ | Material permittivity |
| $\varepsilon_0$ | Permittivity of free space |

Table 4.3 Constant description

The SOC of a fully charged supercapacitor is 100% and the SOC of an empty supercapacitor is 0%. The SOC is calculated with equation (4.41). As explained in chapter 2, this estimation of the SOC is utilized to monitor the SC SOC within the hybrid generator simulator:

$$SOC = \frac{Q_{init} - \int_0^t i(\tau)d\tau}{Q_T} 100 \tag{4.41}$$

Supercapacitor model assumptions:

- Internal resistance and capacitance are assumed constant during the charge and the discharge cycles.
- The model does not take into account temperature effect.
- No aging effect is taken into account.
- Charge redistribution is the same for all values of voltage.
- The block does not model cell balancing.
- Current through the supercapacitor is assumed to be continuous.

# Chapter 5

## Testing and results

## 5. Testing and results

### 5.1 Material and methods

The experimental data used in this work is obtained from two systems: A Bahia PEMFC power module and a Maxwell supercapacitor bank. The Bahia power module is an industrial didactic bench composed of a stack of 24 PEM mono-cells, generates a voltage from 14 to 22 V and provides a maximum current of 75 A, the module incorporates reactants supply manifolds with an air humidifier and a water circuit to control the operating stack temperature (Figure 5.1). The module has three circuits: the hydrogen circuit, the oxygen circuit and the cooling water circuit (Figure 5.2).

Figure 5.1 Experimental Bahia system

In the first circuit, the hydrogen enters in dead-end mode on the anode side, from a storage tank with pressure regulation and furnished with a pressure sensor PT400.

The air enters in circulating mode on the cathode side. The stoichiometry of oxygen can be selected in a range of 1.5 to 2.5. All the experiments were done with stoichiometric oxygen excess ratio equal to 1.5. In the second circuit, the oxygen is obtained from the air provided by a lateral channel blower; the air passes through a membrane humidifier before being fed to the fuel cell stack. The non-reacted humidified air leaving the fuel cell stack is reutilized in the humidifier and then it is released to the atmosphere. The experiments were carried out at a relative humidity of 80%.

In the third circuit, the water is utilized in a cooling circuit to mitigate the heat of the exothermic reactions. The cooling circuit has a temperature controller always in operation. The temperature was then regulated at a value reference of 65_C.

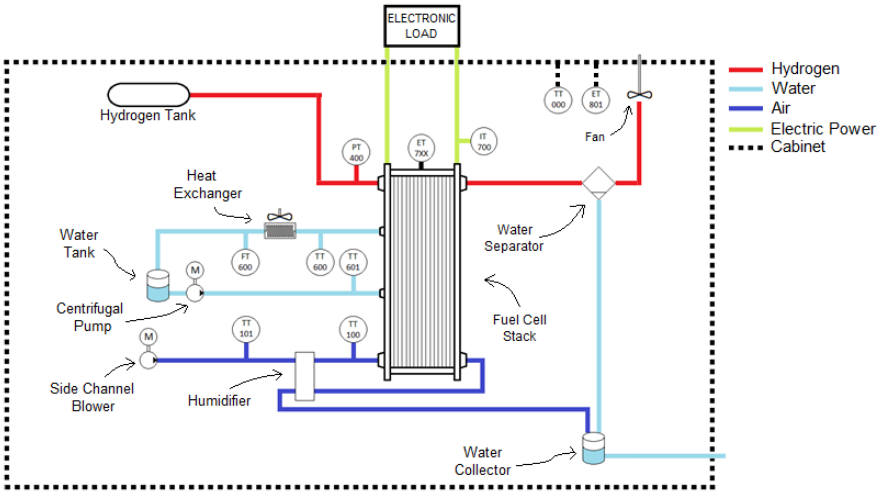


Figure 5.2 Bahia system Diagram. Image by [74].

The Maxwell supercapacitor bank MOD0500 P016 B01 is composed of six supercapacitors connected in series (Figure 5.3); the module specifications are summarized in Table 5.1 Experiments were carried out in order to register the supercapacitor behavior in delivery and recovery cycles. The data was enregistered at constant current values in a range of 5 to 40 A, with increments of 5 A. The current was measured with a hall e_ect sensor providing 5 V / 50 A. The measurements were treated with a data acquisition system of National Instruments, model USB-9211A.00000. An elektro-automatik DC source, model EA-PS 8080-120, supplies energy to charge the supercapacitor and an EA elektro-automatik electronic load, model EA-EL 9080-200, recovers energy from the supercapacitor to emulate the discharge cycle.

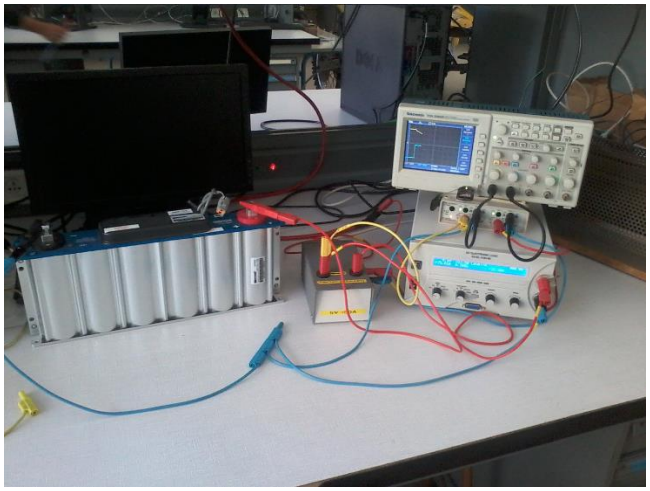

Figure 5.3 Experimental Maxwell supercapacitor bank

| | |
|---|---|
| Rated Capacitance 500 F | 500 F |
| Minimum Capacitance, initial | 500 F |
| Maximum Capacitance, initial | 600 F |
| Maximum $ESR_{DC}$, initial | 2.1 mΩ |
| Test Current for Capacitance and $ESR_{DC}$ | 100 A |
| Rated Voltage | 16 V |
| Operating Temperature Minimum | -40 °C |
| Operating Temperature Maximum | 65 °C |

Table 5.1 Supercapacitor Parameters

## 5.2 Simulation

The simulation of the PEMFC was done in the Simulink/MatLab/Simulink environment using the generic hydrogen fuel cell stack model from the Electric Drives/Extra Sources component libraries of SimPowerSystems™. In order to parametrize the FC model, experimental tests were performed with the BAHIA power module, registering the voltage responses at different current pulse widths (each pulse train at different temperature and stoichiometry conditions). Parameters in the FC model were adjusted to match the BAHIA FC behavior. The same process was done to simulate the SC bank with the supercapacitor block included in the abovementioned libraries of Simulink. The SC block implements a generic model parameterized to represent the most popular types of supercapacitors. The power conditioning units were simulated with elements of Simscape Libraries.

The consumption of an electric vehicle depends on various factors such as temperature, speed, load, aerodynamics, tires and even the driver habits. Several studies have already demonstrated the difficulty to deal with these features [75], [76]. Therefore, in recent years, several drive standards have been defined to describe typical drive performances. These driving standards are commonly used in the phases of design, development and testing of vehicles. A driving cycle is a fixed schedule of the vehicle operation which allows an emission test to be conducted under reproducible conditions. Driving cycles are usually defined in terms of vehicle speed and gear selection as a function of time. It is also useful to note that driving cycles may be used for a variety of purposes other than emissions measurement, such as engine testing or drive train durability [77].

In order to validate this work, two normalized driving cycles were chosen: ECE-15 and UDDS. The ECE-15 driving cycle is used to approve vehicles for marketing in Europe, it was developed to represent typical driving conditions of busy European cities and is characterized by a low speed with frequent stops. On the other hand, chassis dynamometer driving schedules and shift schedules are used in the Environmental Protection Agency (EPA), National Vehicle & Fuel Emissions Laboratory (NVFEL) (USA), for vehicle emissions and fuel economy testing. The EPA Urban Dynamometer Driving Schedule (UDDS) is commonly called the "LA4" or "the city test" and represents city driving conditions.

The driving cycles consists of velocity profiles. The vehicle velocity can be translated into power, taking into account some mechanical characteristics of the vehicle, such as the mass, the friction,

the air penetration coefficient, and the slope of the road (equation 5.3), then, the current load profile can be calculated from the power profile.

$$P_{Motor} = \left[C_r M g cos(\propto) + M g sin(\propto) + M\frac{dV}{dt} + \frac{1}{2}\rho S C_x V^2\right] \quad (5.0)$$

Where:

| | |
|---|---|
| *V* | *Vehicle speed (m/s)* |
| *M* | *Vehicle mass (1000 kg)* |
| *G* | *Gravitational constant (9.81 m/s$^2$)* |
| *a* | *Road gradient (0°)* |
| $C_r$ | *Vehicle friction coefficient (0.01)* |
| $C_X$ | *Aerodynamic coefficient (0.3)* |
| *ρ* | *Air density (1.225 kg/m$^3$)* |
| *S* | *Front surface (2.5 m$^2$)* |

Assuming typical values for a small vehicle, the load profile is obtained for ECE-15 driving cycle (Figure 5.4) and for UDDS driving cycle (Figure 5.5). Then, in order to match with the BAHIA FC capacities, the ECE-15 and UDDS power profiles were scaled to a maximum of 1 KW. Only 80 s were kept from the ECE-15 cycle and 1200 s from the UDDS cycle.

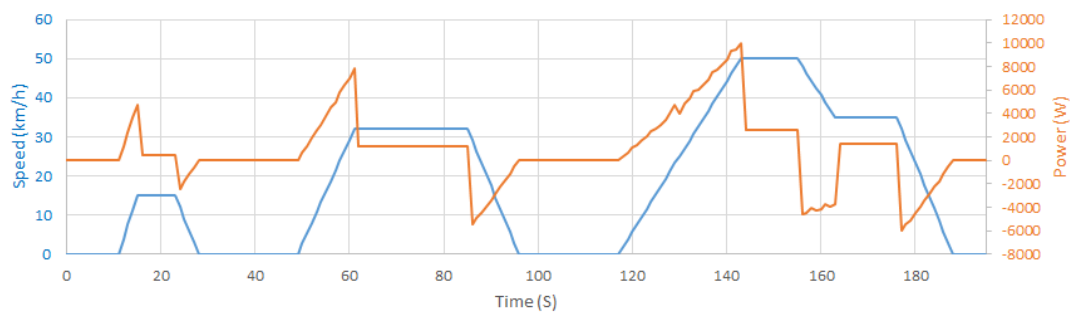


Figure 5.4 Vehicle speed and power profile for ECE-15 cycle.

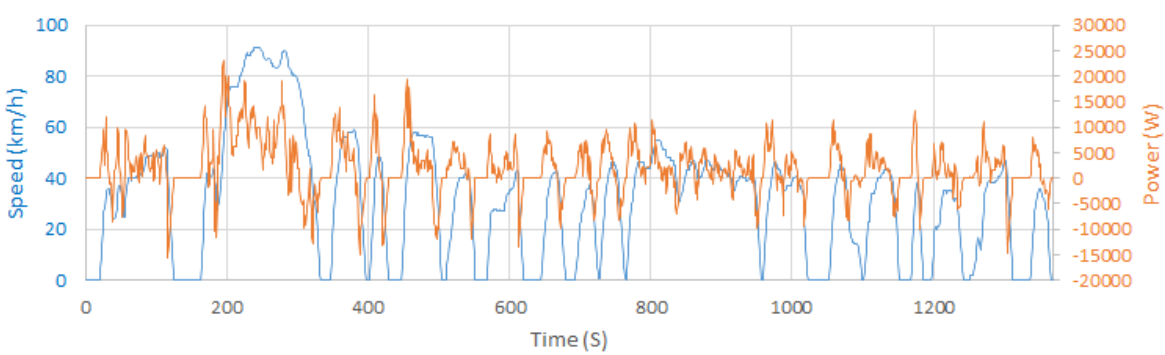


Figure 5.5 Vehicle speed and power profile for UDDS cycle.

The simulation includes a PEMFC, a SC bank, one boost and one bidirectional dc/dc converter. The FC is interfaced to the load with the boost dc/dc converter, and the SC with the bidirectional dc/dc converter are placed in parallel, connected to a common DC bus, interfaced to the load. Figure 5.6 shows the functional control strategy organization.

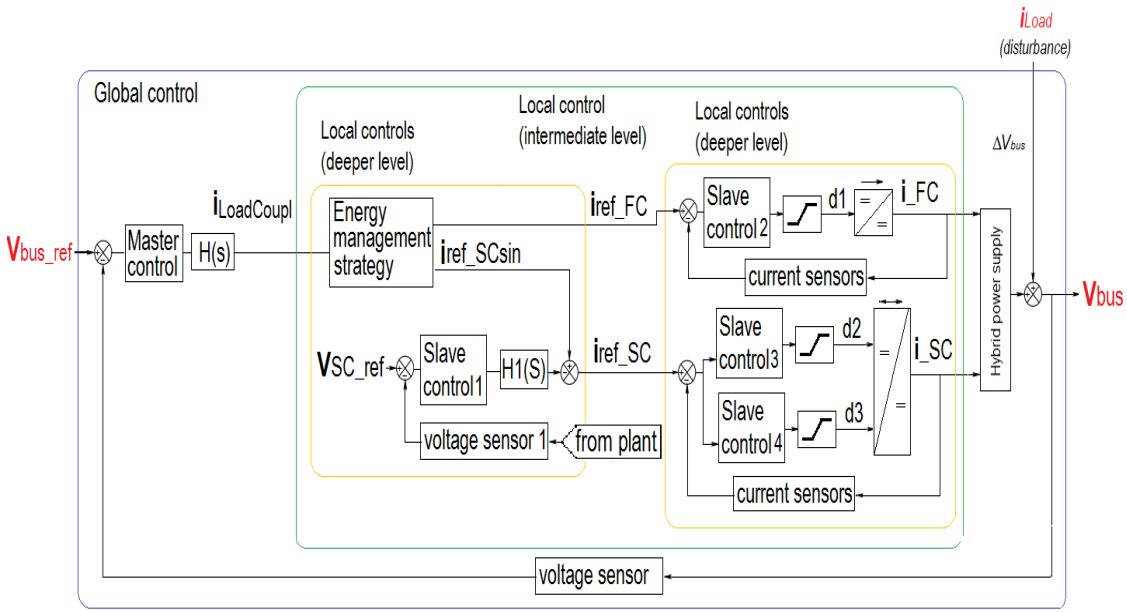


Figure 5.6 Functional control strategy diagram

As it was mentioned before, both cycles are representative inputs for different vehicle related tests under city driving conditions. It is evident that the cycles cover different velocity ranges; hence different power ranges for the same vehicle dimensions and characteristics. Moreover, it is important to remark that the cycles measurements present different frequency properties: consequently, different split of the power between the sources can be expected with respect to the implementation of the proposed energy management strategy.

Negative values of power result whether the velocity diminishes, which indicates dissipated energy due to the vehicle braking. The power profile load was entirely introduced as the system input, including the negative power values; thus, ideal assumption of braking energy recovery for partially charging the SC, was made. The strategy algorithm considers statements aiding to quantify the extra energy obtaining by energy braking recovery.

Considering that the scaled power profile from the driving cycles is demanded to the power hybrid train, the simulation of the system demonstrated that the objectives of the energy administration strategy were achieved. All the internal control loops and the power converters control (third hierarchical level) were performed correctly, but for the sake of simplicity, only the verification of the main objectives of the two principal hierarchical levels of the energy management strategy are presented from now on.

Relating to the global control or demand interpretation, the bus voltage is appropriately regulated, since it fluctuates slightly around the reference specified at 48 V, despite of the sudden changes in the load (Figure 5.7 for ECE-15 and Figure 5.8 for UDDS).

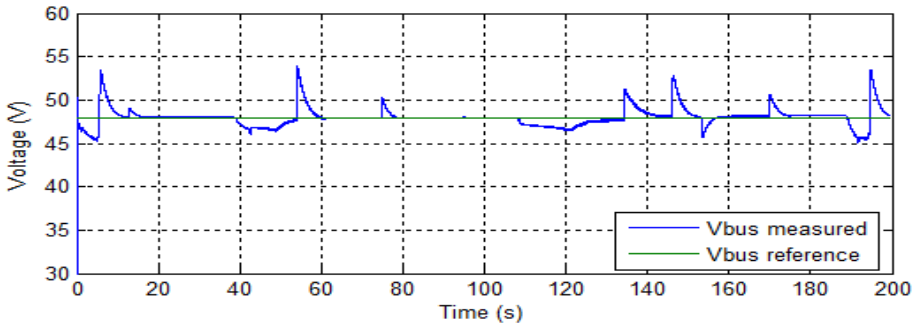


Figure 5.7 Bus voltage ($V_{bus}$) with ECE-15 driving cycle

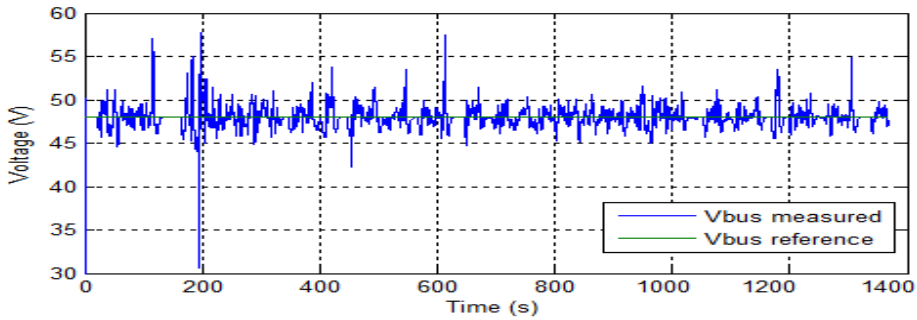


Figure 5.8 Bus voltage ($V_{bus}$) with UDDS driving cycle

The supercapacitor life can be dramatically reduced if the SOC does not remain within certain limits.

Several efficient energy management strategies have been suggested to determine the split of the power sources and to maintain an appropriate supercapacitor SOC, but this last task is not always evident or is simply not considered. The reference [51] presented an energy management strategy that calculates the optimal FC power during a driving cycle, and the supercapacitor power is deduced from the difference between the required power and the fuel cell. However, the supercapacitor SOC goes beyond the safe operating limits, exceeding more than a 100% its capabilities at certain times of the driving cycle.

Concerning the solution to the problem of regulating the SC SOC (second hierarchical level), the following scheme was conceived: the operation of the SC is assumed to initiate at full charge conditions. The objective is to maintain the SC SOC between 70% and 100% during the whole time of the simulations realized with both, the ECE-15 and the UDDS driving cycle profiles. The voltage output of the SC is not an exact measure of the SC SOC, but determines the SOC defined in equation 4.71; therefore, a simple approach is to control the voltage at a level corresponding to a SOC of 90%, with saturation of the controller, corresponding to the SC operating limits (SOC between 70% and 100%). The SOC is continually registered during the simulation and results proved that the SC SOC

remains in the safe operating limits even whether the USD driving cycle is demanded; which conducts to a stronger SC utilization as will be shown later (Figures 5.9 and 5.10).

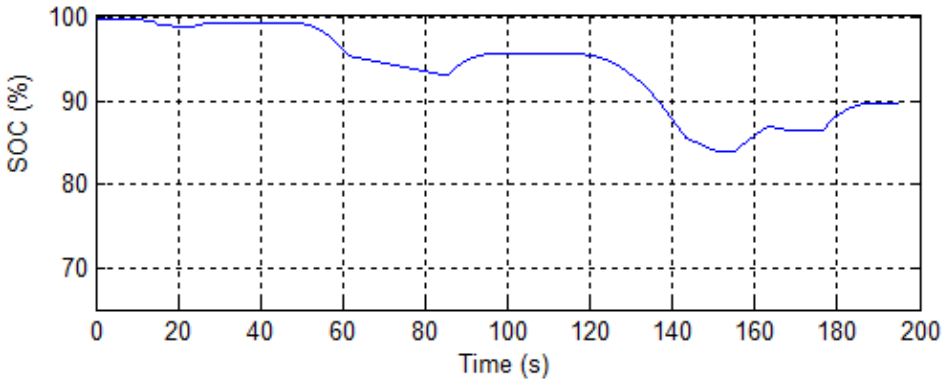


Figure 5.9 Supercapacitor SOC during ECE-15 driving cycle

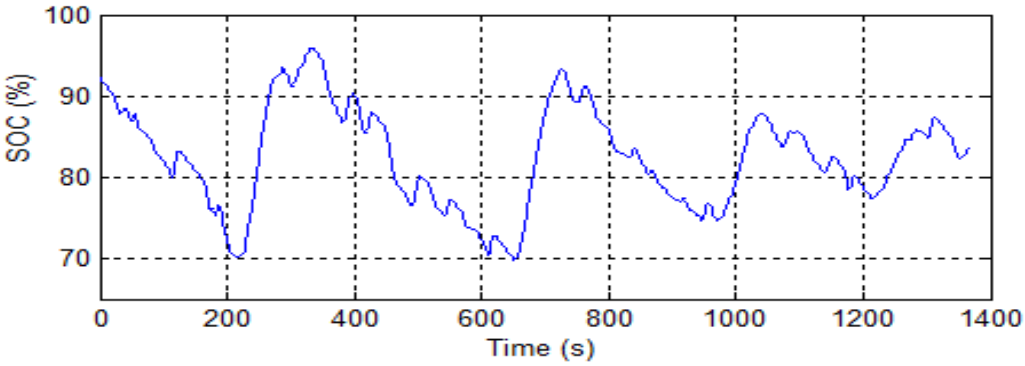


Figure 5.10 Supercapacitor SOC during UDDS driving cycle

It was also verified that the total power necessary to satisfy the vehicle traction requirement for each driving cycle is delivered without problem. The requirement of power matches perfectly with the power delivered by the sources (Figure 5.11). The advantage of the proposed strategy is verified, since very high efficiency is achieved even for the more complex UDDS driving cycle.

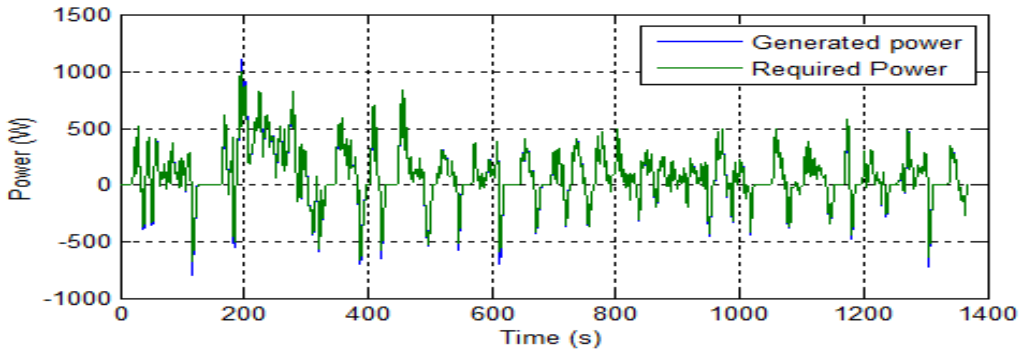


Figure 5.11 Delivered power and required power by the vehicle (scaled to 1 kW).

The proposed power split strategy between the sources (still second hierarchical level) allows the FC to operate only when it is necessary. As a result, it is feasible to reduce expensive fuel consumption and to prevent oxygen starvation problems, causing undesired voltage undershot due to rapid changes of the oxygen demand (Figure 5.11). It can be observed that the fuel cell operation covers the optimal linear performance region of the BAHIA PEMFC module represented in Figure 4.10 (the optimal region covers from 15 to 75 A, or equivalently from 0.285 to 1.178 kW). It is evident that the FC operates under 0.285 kW when the vehicle needs running slowly or is stopping on; but under these conditions, the FC operates safely and with higher efficiency. Therefore, even if the fuel cell does not operates constantly during the whole simulation period, it operates within the whole safe region (ohmic region) and one can conclude that the fuel cell is not overdesigned; instead, it is safely conducted under the maximum limit of its frequency response capabilities.

Furthermore, in Figure 5.12 and 5.13 are observed the periods when the FC charge the SC, since the FC generates more power than it is required to power the vehicle. Summarizing, the fuel cell does correctly the expected deliveries to the load, to the SC and is correctly conducted by the DC converter to maintain the bus voltage at the reference value of 48 V.

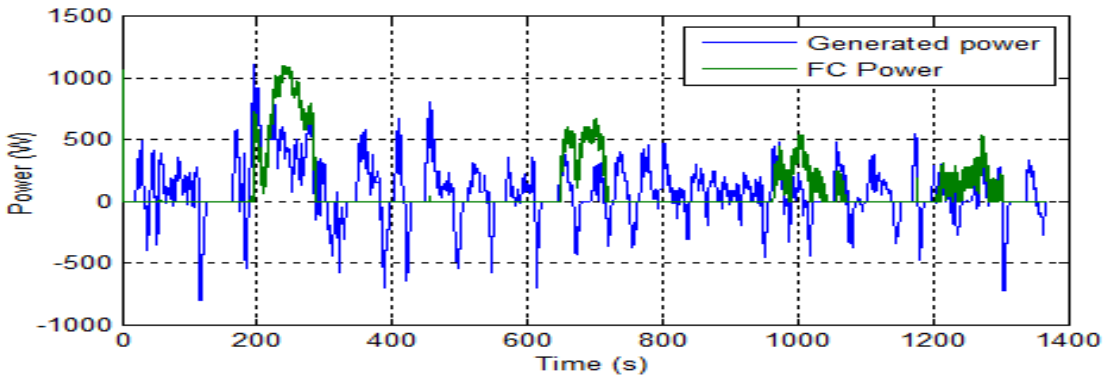


Figure 5.12 Delivered power to the vehicle vs FC power generation (UDDS)

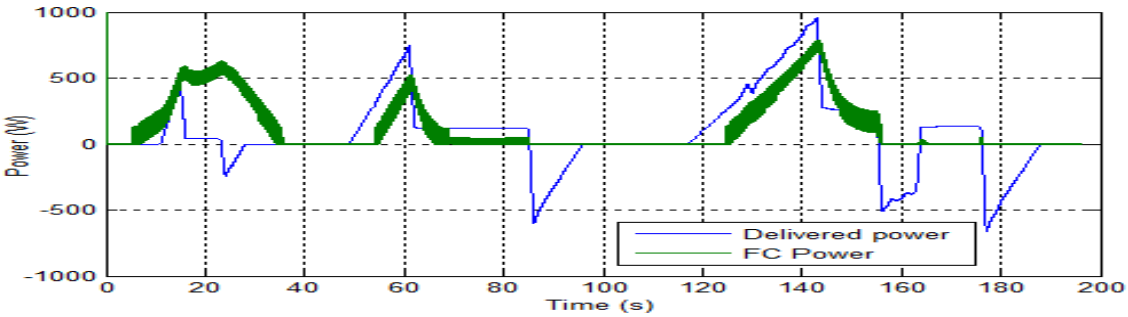


Figure 5.13 Delivered power to the vehicle vs FC power generation (ECE-15)

The SC contribution to the total power demand is shown in Figures 5.14 and 5.15. Given that the UDDS is a cycle with abrupt and sudden power requirements, the SC is active almost all the time, operating in delivery (positive values) or recovery periods (negative values). The SC charge is effectuated by the FC when the vehicle power demand are low frequency signals (green signals in

Figure 5.9), and it is charged with the (ideally) braking recovered energy when the frequency input signals exceed the FC capacities.

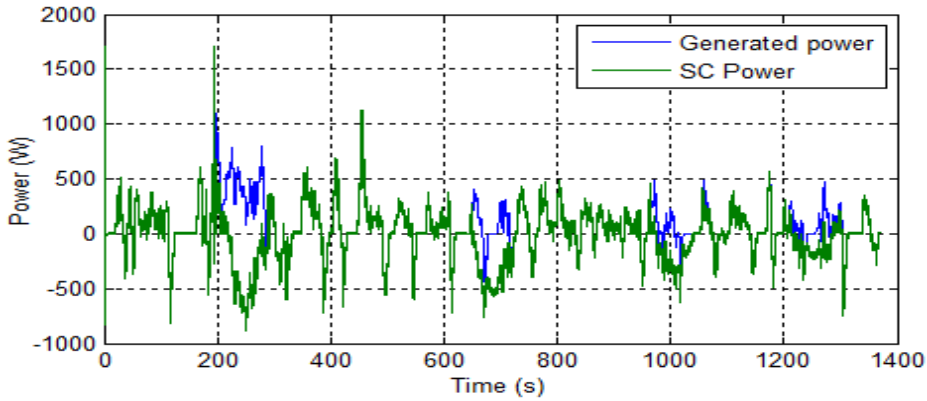


Figure 5.14 Delivered power to the vehicle vs FC power generation (ECE-15)

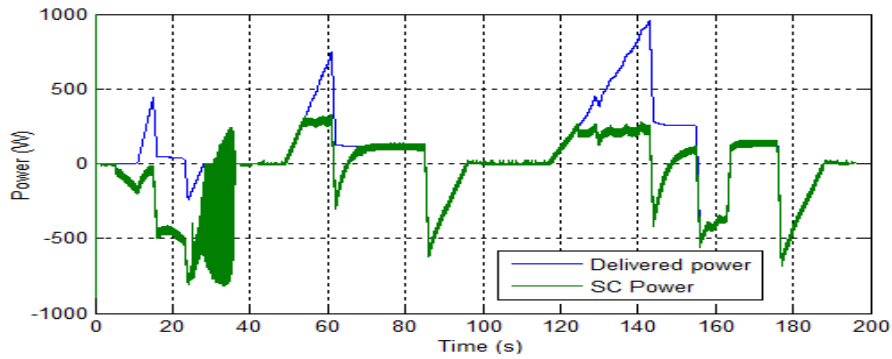


Figure 5.15 Delivered power to the vehicle vs SC power under delivery/recovery conditions (UDDS)

The SC is never exceeding the rated voltage (16 V) and, under the UDDS driving cycle (also applicable to the ECE-15), the FC does not operates when abrupt demand is solicited, saving hydrogen fuel and preventing the voltage undershot phenomenon (Figure 5.16).

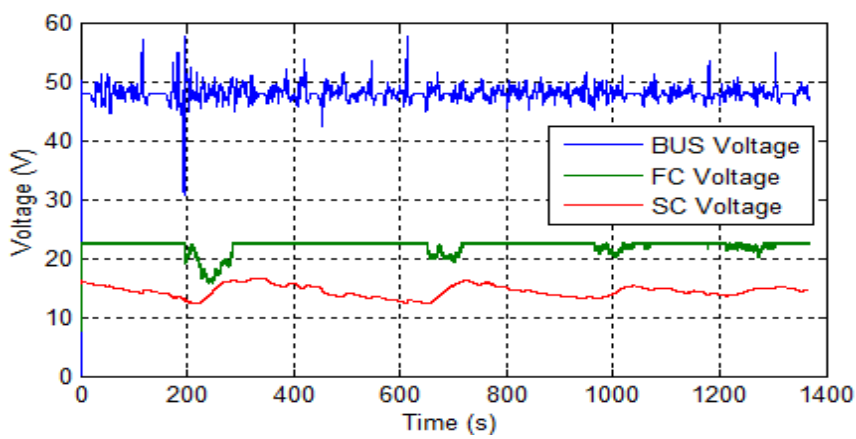


Figure 5.16 $V_{bus}$, FC and SC voltages.

# Chapter 6

## Conclusion

### 6. Conclusion

In this study, an energy management strategy for a hybrid electric system is proposed and proved in the built simulation environment. The hybrid system has a PEM FC as the primary energy source and the SC as energy storage for HF power sourcing. Each power source has a DC/DC converter, which allows the connection between the sources and the traction DC bus.

The main objectives that the proposed strategy adopts for energy management in the hybrid generator are summarized as follows: the fulfillment of the continuous load demand, the optimal power splitting between multiple sources and the enhancement of the sources and the converters operation efficiencies.

The breakthrough of this strategy contributes to dynamically distribute the energy required between the FC and SC and allows operating the FC at its better operating point and the SC under proper SOC conditions, even if the indirect SOC regulation is a straightforward solution. This strategy is based on a frequency division approach, given that the energy sources dynamics do not stand into the same range of frequencies, according to the Ragone plot. The split criterion is simple, but effective. In addition, it is important to note that the cutoff frequency was obtained from the measurements on the experimental module.

Even when the real FC slow dynamics do not allow to respond to abrupt power transitions, there are only few studies attempting to solve the problem. By using this proposed methodology, the FC transient undesired phenomena, such as oxygen starvation or depletion, operation outside the safe limits, or FC degradation, are avoided. The management strategy takes advantage of the real dynamic FC capabilities while reducing the SC charge and contributing to a convenient SOC operation. The definition of the cutoff frequency was made considering as well the PEMFC as the main source and the SC as the backup unit. It was demonstrated that the PEMFC assumes the charging of the SC, the load demand in a wide operating region of the FC and that the shut-on and shoot-down of the FC diminishes, especially for the UDDS solicitations.

Among the advantages of the proposed strategy, the use of switched models for the power converters improved the control response to fast transients, reducing common averaging delays usually present in simplified control modeling solutions. These internal control loops are faster than external control loops; thus, the nested structure of the energy management enables the rapid reaction to disturbance before impacting the output.

UDDS and ECE-15 scaled driving cycles were selected to validate the suggested energy management strategy because those cycles have more accelerations and decelerations than other driving cycles;

moreover, the velocity and the corresponding power signals represent measurements with very different frequency behavior, the ECE-15 driving cycle shows slower dynamics, while the UDDS driving cycle presents abrupt changes in the power demand; in this sense, the performance of the management strategy was tested under different situations, but it conducts, in both cases, the FC behavior over the entire optimal operating region, and allows the FC to provide the necessary energy demanded to power the vehicle and to charge the SC. Furthermore, the DC bus voltage is kept almost constant at 48 V and the SC SOC is always maintained around the desired values. The management objectives are achieved with different level of contribution of the sources, according to the load dynamics characteristics; but, for the two investigated cases, the fuel cell operates over the entire safe region, avoiding the activation and concentration regions. We can conclude that the power train is not oversized or undersized for the selected application. Additionally, the results proved the efficiency of the energy management strategy under load dynamics with a large range of frequencies. Finally, the obtained results proved that the main objectives of the proposed strategy for administrating the energy in the hybrid generator were attained.

Future works includes improving FC modeling by introducing the undershoot dynamic behavior usually present in FCs experimental modules. These and other non-linear phenomena increase with the addition of auxiliary equipment; in this sense, the developed simulator of the PEMFC experimental module cannot be extrapolated directly for real vehicular applications and the model must include the material balance and energy balance for describing the supply manifold system, as well as the temperature and humidity management systems. The supercapacitor model is also simplified, furthermore, this is a relatively new research area because few studies have been published about SC modeling. Nevertheless, it is important to keep in mind that a trade of between simplicity and accuracy is critical for developing adequate power train simulators.

A variety of system architectures and power conditioning topologies are encountered in the literature, herein, only basic topologies were incorporated; then, the analysis of different configurations and structures imposes thorough assessment of different scenarios.

# Bibliography

## Bibliography


[1] M. Winter and R. J. Brodd, “What are batteries, fuel cells, and supercapacitors?,” *Chem. Rev.*, vol. 104, no. 10, pp. 4245–69, Oct. 2004.

[2] T. Yalcinoz and M. Alam, “Improved dynamic performance of hybrid PEM fuel cells and ultracapacitors for portable applications,” *Int. J. Hydrogen Energy*, vol. 33, no. 7, pp. 1932–1940, 2008.

[3] F. Barbir, *PEM Fuel Cells: Theory and Practice*. Academic Press, 2012.

[4] O. Erdinc and M. Uzunoglu, “Recent trends in PEM fuel cell-powered hybrid systems: Investigation of application areas, design architectures and energy management approaches,” *Renew. Sustain. Energy Rev. (RENEW SUST ENERG REV)*, vol. 14, no. 9, pp. 2874–2884, 2010.

[5] M. Ball and M. Wietschel, “The future of hydrogen–opportunities and challenges,” *Int. J. Hydrogen Energy*, vol. 34, pp. 615–627, 2009.

[6] M. H. Nehrir and C. Wang, *Modeling and Control of Fuel Cells: Distributed Generation Applications*. New Jersey: Wiley, IEEE, 2009.

[7] O. C. Onar, O. H. A. Shirazi, and A. Khaligh, “Grid interaction operation of a telecommunications power system with a novel topology for multiple-input buck-boost converter,” *IEEE Trans. Power Deliv.*, vol. 25, no. 4, pp. 2633–2645, 2010.

[8] J. M. Andujar and F. Segura, “Fuel cells: History and updating. A walk along two centuries,” *Renewable and Sustainable Energy Reviews*, vol. 13, no. 9. pp. 2309–2322, 2009.

[9] D. B. Thounthong P, Chunkag V, Sethakul P, “Comparative study of fuel-cell vehicle hybridization with battery or supercapacitor storage device,” *IEEE Trans Veh. Technol*, 2009.

[10] J. H. Wee, *Applications of proton exchange membrane fuel cell systems*, vol. 11, no. 8. 2007.

[11] Honda, “Honda Fuel Cell Power FCX,” *http://world.honda.com/FuelCell/FCX/ FCXPK.pdf*, 2004. .

[12] A. M. Onar OC, Uzunoglu M, “Dynamic modeling, design and simulation of a wind/fuel cell/ultra-capacitor-based hybrid power generation system,” *J. Power Sources*, 2006.

[13] O. C. Onar, M. Uzunoglu, and M. S. Alam, “Dynamic modeling, design and simulation of a wind/fuel cell/ultra-capacitor-based hybrid power generation system,” *J. Power Sources*, vol. 161, p. 707, 2006.

[14] D. R. Jiang Z, Gao L, “Adaptive control strategy for active power sharing in hybrid fuel cell/battery power sources,” *IEEE Trans Energy Convers.*, 2007.

[15] O. M. Xu L, Li J, Hua J, Li X, “Adaptive supervisory control strategy of a fuel cell/battery powered city bus,” *J. Power Sources*, 2009.

[16] P. Fontela, A. Soria, J. Mielgo, J. F. Sierra, J. de Blas, L. Gauchia, and J. M. Mart??nez, “Airport electric vehicle powered by fuel cell,” *J. Power Sources*, vol. 169, no. 1, pp. 184–193, 2007.

[17] a. Payman, S. Pierfederici, and F. Meibody-Tabar, “Energy Management in a Fuel Cell/Supercapacitor Multisource/Multiload Electrical Hybrid System,” *IEEE Trans. Power Electron.*, vol. 24, no. 12, pp. 2681–2691, Dec. 2009.

[18] Q. S. Chen Q, Gao L, Dougal RA, “Multiple model predictive control for a hybrid proton exchange membrane fuel cell system,” *J. Power Sources*, 2009.

[19] X. Zhang, C. C. Mi, A. Masrur, and D. Daniszewski, “Wavelet-transform-based power management of hybrid vehicles with multiple on-board energy sources including fuel cell, battery and ultracapacitor,” *J. Power Sources*, vol. 185, no. 2, pp. 1533–1543, Dec. 2008.

[20] O. Erdinc, B. Vural, M. Uzunoglu, and Y. Ates, “Modeling and analysis of an FC / UC hybrid vehicular power system using a wavelet-fuzzy logic based load sharing and control algorithm,” *Int. J. Hydrogen Energy*, pp. 1–11, 2008.

[21] U. M. Erdinc O, Vural B, “A wavelet-fuzzy logic based energy management strategy for a fuel cell/battery/ultra-capacitor hybrid vehicular power system,” *J. Power Sources*, 2009.

[22] P. Thounthong, S. Raël, and B. Davat, “Energy management of fuel cell/battery/supercapacitor hybrid power source for vehicle applications,” *J. Power Sources*, vol. 193, no. 1, pp. 376–385, Aug. 2009.

[23] D. Feroldi, M. Serra, and J. Riera, “Energy Management Strategies based on efficiency map for Fuel Cell Hybrid Vehicles,” *J. Power Sources*, vol. 190, no. 2, pp. 387–401, May 2009.

[24] D. B. Thounthong P, Rael S, “Control algorithm of fuel cell and batteries for distributed generation system,” *IEEE Trans Energy Convers.*, 2008.

[25] P. Thounthong, S. Raël, and B. Davat, “Control strategy of fuel cell/supercapacitors hybrid power sources for electric vehicle,” *J. Power Sources (J POWER SOURCES)*, vol. 158, no. 1, pp. 806–814, Jul. 2006.

[26] E. M. Stewart, A. E. Lutz, S. Schoenung, M. Chiesa, J. O. Keller, J. Fletcher, G. Ault, J. McDonald, and A. Cruden, “Modeling, analysis and control system development for the Italian hydrogen house,” *Int. J. Hydrogen Energy*, vol. 34, no. 4, pp. 1638–1646, 2009.

[27] I. EG&G Technical Services, “Fuel Cell Handbook,” *Fuel Cell*, vol. 7 Edition, no. November, pp. 1–352, 2004.

[28] D. Liu and H. Li, “A ZVS bi-directional DC-DC converter for multiple energy storage elements,” *IEEE Trans. Power Electron.*, vol. 21, no. 5, pp. 1513–1517, 2006.

[29] P. Thounthong, P. Sethakul, and B. Davat, “Modified 4-phase interleaved fuel cell converter for high-power high-voltage applications,” in *Proceedings of the IEEE International Conference on Industrial Technology*, 2009.

[30] F. H. Khan and L. M. Tolbert, “Multiple-load-source integration in a multilevel modular capacitor-clamped DC-DC converter featuring fault tolerant capability,” *IEEE Trans. Power*

*Electron.*, vol. 24, no. 1, pp. 14–24, 2009.

[31] H. Farzanehfard, D. S. Beyragh, and E. Adib, "A bidirectional soft switched ultracapacitor interface circuit for hybrid electric vehicles," *Energy Convers. Manag.*, vol. 49, no. 12, pp. 3578–3584, 2008.

[32] P. J. Solero L, Lidozzi A, "Design of multiple-input power converter for hybrid vehicles," *IEEE Trans Power Electron*, 2005.

[33] D. Gao, Z. Jin, and Q. Lu, "Energy management strategy based on fuzzy logic for a fuel cell hybrid bus," vol. 185, pp. 311–317, 2008.

[34] L. Q. Gao D, Jin Z, "Energy management strategy based on fuzzy logic for a fuel cell hybrid bus," *J. Power Sources*, 2008.

[35] C.-Y. Li and G.-P. Liu, "Optimal fuzzy power control and management of fuel cell/battery hybrid vehicles," *J. Power Sources*, vol. 192, no. 2, pp. 525–533, Jul. 2009.

[36] L. G. Li CY, "Optimal fuzzy power control and management of fuel cell/ battery hybrid vehicles," *J. Power Sources*, 2009.

[37] V. B. Eren Y, Erdinc O, Gorgun H, Uzunoglu M, "A fuzzy logic based supervisory controller for an FC/UC hybrid vehicular power system," *Hydrog. Energy*, 2009.

[38] P. Rodatz, G. Paganelli, A. Sciarretta, and L. Guzzella, "Optimal power management of an experimental fuel cell/supercapacitor-powered hybrid vehicle," *Control Eng. Pract.*, vol. 13, no. 1, pp. 41–53, 2005.

[39] O. M. Li X, Xu L, Hua J, Lin X, Li J, "Optimal vehicle control strategy of a fuel cell/ battery hybrid city bus," *Int J Hydrog. Energy*, 2009.

[40] V. Paladini, T. Donateo, a Derisi, and D. Laforgia, "Super-capacitors fuel-cell hybrid electric vehicle optimization and control strategy development," *Energy Convers. Manag.*, vol. 48, no. 11, pp. 3001–3008, 2007.

[41] S. Y. Liu G, Zhanga J, "High frequency decoupling strategy for the PEM fuel cell hybrid system.," *Int J Hydrog. Energy*, 2008.

[42] A. M. Uzunoglu M, "Modeling and analysis of an FC/UC hybrid vehicular power system using a novel wavelet based load sharing algorithm," *IEEE Trans Energy Convers.*, 2008.

[43] D. D. Zhang X, Mi CC, Masrur A, "Wavelet-transform-based power management of hybrid vehicles with multiple on board energy sources including fuel cell, battery and ultracapacitor," *J Power Sources*, 2008.

[44] O. Erdinc, B. Vural, and M. Uzunoglu, "A wavelet-fuzzy logic based energy management strategy for a fuel cell/battery/ultra-capacitor hybrid vehicular power system," *J. Power Sources*, vol. 194, no. 1, pp. 369–380, Oct. 2009.

[45] V. B. Ates Y, Erdinc O, Uzunoglu M, "Energy management of an FC/UC hybrid vehicular power system using a combined neural network-wavelet transform based strategy.," *Int J Hydrog. Energy*, 2010.

[46] M. Becherif and M. Ayad, "Advantages of variable DC bus voltage for hybrid electrical

vehicle," *Veh. Power Propuls. Conf. IEEE*, pp. 1–6, 2010.

[47] K. Ettihir, L. Boulon, and K. Agbossou, "Optimization-based energy management strategy for a fuel cell / battery hybrid power system," *Appl. Energy*, vol. 163, pp. 142–153, 2016.

[48] V. Dash and P. Bajpai, "Power Management Control Strategy for a Stand-alone Solar Photovoltaic-Fuel Cell–Battery Hybrid System," *Sustain. Energy Technol. Assessments*, vol. 9, pp. 68–80, 2015.

[49] A. Santucci, A. Sorniotti, and C. Lekakou, "Power split strategies for hybrid energy storage systems for vehicular applications," *J. Power Sources*, vol. 258, pp. 395–407, Jul. 2014.

[50] S. Nasri, B. S. Sami, and A. Cherif, "Power management strategy for hybrid autonomous power system using hydrogen storage," *Int. J. Hydrogen Energy*, pp. 1–9, 2015.

[51] H. Hemi, J. Ghouili, and A. Cheriti, "Combination of Markov chain and optimal control solved by Pontryagin's Minimum Principle for a fuel cell/supercapacitor vehicle," *Energy Convers. Manag.*, vol. 91, pp. 387–393, 2015.

[52] H. Hemi, J. Ghouili, and A. Cheriti, "A real time fuzzy logic power management strategy for a fuel cell vehicle," *Energy Convers. Manag.*, vol. 80, pp. 63–70, 2014.

[53] N. Karami, N. Moubayed, and R. Outbib, "Energy management for a PEMFC – PV hybrid system," vol. 82, pp. 154–168, 2014.

[54] Z. Liu and H. Lee, "LED Driver with Lossless Synchronous Current Control and Floating NMOS-Sensing Scheme," Applied Power Electronics Conference and Exposition (APEC), 2014 Twenty-Ninth Annual IEEE, pp. 1378–1383, 2014.

[55] L. Barelli, G. Bidini, and A. Ottaviano, "Optimization of a PEMFC/battery pack power system for a bus application," *Appl. Energy*, vol. 97, pp. 777–784, Sep. 2012.

[56] E. Q. Guadalupe López, Victor Alvarado, "¿Cómo funcionan las PEMFC?," *Hypatia*, vol. 36, 2014.

[57] J. Larminie and A. Dicks, *Fuel Cell Systems Explained*. West Sussex, England: John Wiley & Sons, Ltd,., 2003.

[58] F. Belhachemi, S. Rael, and B. Davat, "A physical based model of power electric double-layer supercapacitors," *Conf. Rec. 2000 IEEE Ind. Appl. Conf. Thirty-Fifth IAS Annu. Meet. World Conf. Ind. Appl. Electr. Energy (Cat. No.00CH37129)*, vol. 5, no. Upresa 7037, pp. 3069–3076, 2000.

[59] W. Hamann, C, Hamnett, A, Vielstich, *Electrochemistry*. Weinheim Germany, 1998.

[60] Y. Brunet, "*Energy Storage*". J. Sons Editors. 2013.

[61] N. Ramírez Morales, "La Tecnologia De Celdas De Combustible Y Su Interfase Electrónica De Potencia Para Aplicaciones Domésticas E Industriales," 2004.

[62] W.-Y. Chang, "The State of Charge Estimating Methods for Battery: A Review," *ISRN Appl. Math.*, vol. 2013, no. 1, pp. 1–7, 2013.

[63] U. P. Xi, "Contribution à l ' Etude d ' Electro-générateurs à Pile à Combustible Conceptions d ' Architectures et de Leurs Commandes," 2010.

[64] W.-Y. Chang, “The state of charge estimating methods for battery: a review,” *Appl. Math.*, 2013.

[65] M. H. Nehrir, *Modeling and control of fuel cells*. 2009.

[66] M. Ehsani, *Modern Electric , Hybrid Electric , and Fuel Cell Vehicles*. Boca Raton, Florida: CRC Press, 2005.

[67] J. W. Jung, “Modeling and Control of Fuel Cell Based Distributed,” Ohio State University, 2005.

[68] C. Slobodan, “Modelling, analysis and design of switching converters,” California Institute of Technology, 1977.

[69] Helion Hidrogen Power, *Banc Didactique Bahia Type : Bahia V2 . 1-A1*. Aix-en-Provence: Helion Hidrogen Power.

[70] D. C. Delgado, “Experimentos Didácticos en Teoría de Control: Convertidores CD-CD,” Notas del curso. UASLP. Universidad Autónoma de San Luis Potosí, 2003.

[71] N. L. Diaz, T. Dragi, J. C. Vasquez, and J. M. Guerrero, “Fuzzy-Logic-Based Gain-Scheduling Control for State-of-Charge Balance of Distributed Energy Storage Systems for DC Microgrids,” Applied Power Electronics Conference and Exposition (APEC), 2014 Twenty-Ninth Annual IEEE, pp. 2171–2176, 2014.

[72] N. Mohan, T. M. Undeland, and W. P. Robbins, *Power Electronics: Converters, Applications and Design*. 2003.

[73] “Matlab SIMULINK, Reference documents.” The MathWorks, Inc., Natick, Massachusetts, 2014.

[74] Pukrushpan, “Modeling and control for PEM fuel cell stack system,” *Am. Control Conf.*, 2002.

[75] Z. Dai, D. Niemeier, and D. Eisinger, “Driving Cycles : a New Cycle-Building Method That Better Represents Real-World Emissions,” *U.C. Davis-Caltrans Air Qual. Proj. 2008.*, no. 66, 2008.

[76] M. André, “The ARTEMIS European driving cycles for measuring car pollutant emissions,” *Sci. Total Environ. (SCI Total ENVIRON)*, vol. 334–335, no. Science of the total environment, pp. 73–84, 2004.

[77] T. Barlow, S. Latham, I. Mccrae, and P. Boulter, *A reference book of driving cycles for use in the measurement of road vehicle emissions*. 2009.